



National Library
of Canada

Acquisitions and
Bibliographic Services Branch

395 Wellington Street
Ottawa, Ontario
K1A 0N4

Bibliothèque nationale
du Canada

Direction des acquisitions et
des services bibliographiques

395, rue Wellington
Ottawa (Ontario)
K1A 0N4

Your file Votre référence

Our file Notre référence

NOTICE

The quality of this microform is heavily dependent upon the quality of the original thesis submitted for microfilming. Every effort has been made to ensure the highest quality of reproduction possible.

If pages are missing, contact the university which granted the degree.

Some pages may have indistinct print especially if the original pages were typed with a poor typewriter ribbon or if the university sent us an inferior photocopy.

Reproduction in full or in part of this microform is governed by the Canadian Copyright Act, R.S.C. 1970, c. C-30, and subsequent amendments.

AVIS

La qualité de cette microforme dépend grandement de la qualité de la thèse soumise au microfilmage. Nous avons tout fait pour assurer une qualité supérieure de reproduction.

S'il manque des pages, veuillez communiquer avec l'université qui a conféré le grade.

La qualité d'impression de certaines pages peut laisser à désirer, surtout si les pages originales ont été dactylographiées à l'aide d'un ruban usé ou si l'université nous a fait parvenir une photocopie de qualité inférieure.

La reproduction, même partielle, de cette microforme est soumise à la Loi canadienne sur le droit d'auteur, SRC 1970, c. C-30, et ses amendements subséquents.

Canada

University of Alberta

Three Phase Harmonic Analysis of Unbalanced Power Systems

by

Lance Gordon Grainger



**A thesis submitted to the Faculty of Graduate Studies and Research in partial
fulfilment of the requirements for the degree of Doctor of Philosophy**

Department of Electrical Engineering

Edmonton, Alberta

Fall 1995



National Library
of Canada

Acquisitions and
Bibliographic Services Branch

395 Wellington Street
Ottawa, Ontario
K1A 0N4

Bibliothèque nationale
du Canada

Direction des acquisitions et
des services bibliographiques

395, rue Wellington
Ottawa (Ontario)
K1A 0N4

Your file Votre référence

Our file Notre référence

THE AUTHOR HAS GRANTED AN
IRREVOCABLE NON-EXCLUSIVE
LICENCE ALLOWING THE NATIONAL
LIBRARY OF CANADA TO
REPRODUCE, LOAN, DISTRIBUTE OR
SELL COPIES OF HIS/HER THESIS BY
ANY MEANS AND IN ANY FORM OR
FORMAT, MAKING THIS THESIS
AVAILABLE TO INTERESTED
PERSONS.

L'AUTEUR A ACCORDE UNE LICENCE
IRREVOCABLE ET NON EXCLUSIVE
PERMETTANT A LA BIBLIOTHEQUE
NATIONALE DU CANADA DE
REPRODUIRE, PRETER, DISTRIBUER
OU VENDRE DES COPIES DE SA
THESE DE QUELQUE MANIERE ET
SOUS QUELQUE FORME QUE CE SOIT
POUR METTRE DES EXEMPLAIRES DE
CETTE THESE A LA DISPOSITION DES
PERSONNE INTERESSEES.

THE AUTHOR RETAINS OWNERSHIP
OF THE COPYRIGHT IN HIS/HER
THESIS. NEITHER THE THESIS NOR
SUBSTANTIAL EXTRACTS FROM IT
MAY BE PRINTED OR OTHERWISE
REPRODUCED WITHOUT HIS/HER
PERMISSION.

L'AUTEUR CONSERVE LA PROPRIETE
DU DROIT D'AUTEUR QUI PROTEGE
SA THESE. NI LA THESE NI DES
EXTRAITS SUBSTANTIELS DE CELLE-
CI NE DOIVENT ETRE IMPRIMES OU
AUTREMENT REPRODUITS SANS SON
AUTORISATION.

ISBN 0-612-06215-5

Canada

University of Alberta

Library Release Form

Name of Author: Lance G. Grainger

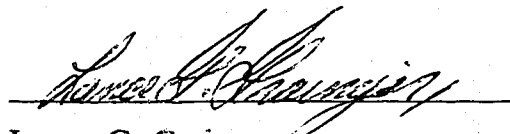
Title of Report: Three Phase Harmonic Analysis of Unbalanced Power Systems

Degree: Doctor of Philosophy

Year This Degree Granted: 1995

Permission is hereby granted to The University of Alberta Library to reproduce single copies of this report and to lend or sell such copies for private, scholarly or scientific research purposes only.

The author reserves all other publication and other rights in association with the copyright in the thesis, and except as hereinbefore provided, neither the thesis nor any substantial portion thereof may be printed or otherwise reproduced in any material form whatever without the author's written permission.



Lance G. Grainger

8603-16 Avenue

Edmonton, Alberta, T6K 2A4

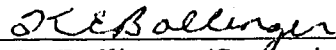
Date:

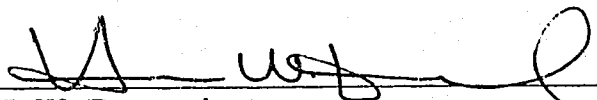
May 24, 95

University of Alberta

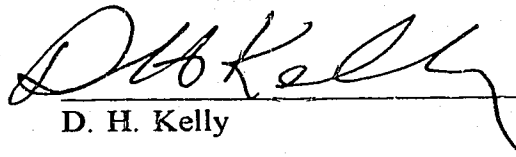
Faculty of Graduate Studies and Research

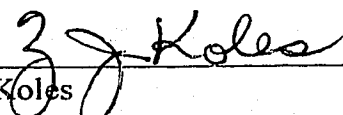
The undersigned certify that they have read, and recommend to the Faculty of Graduate Studies and Research for acceptance, a thesis entitled "Three Phase Harmonic Analysis of Unbalanced Power Systems" submitted by Lance Gordon Grainger in partial fulfilment of the requirements for the degree of Doctor of Philosophy.

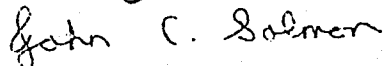

K. E. Bollinger (Supervisor)

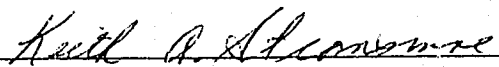

H. W. Dommel


C. G. Englefield


D. H. Kelly


Z. J. Koles


J. C. Salmon


K. A. Stromsmoe

May 24, 1995
Date Approved

Dedication

This thesis is dedicated to my wife Gloria. Her wholehearted encouragement made it possible.

Abstract

This thesis combines linear and nonlinear techniques to analyze harmonics in a three phase frame of reference in unbalanced power systems. The linear and nonlinear portions of the circuit are separated by diakoptic methods at the busses connected to nonlinear loads. The linear portions are solved by applying frequency domain techniques and the nonlinear portions are solved by applying time domain techniques.

The linear portions are solved using linear algebraic methods. A Y Bus loadflow is used to solve for the fundamental current and voltage throughout the network and a Z Bus matrix is used to solve for the harmonic currents and voltages. Sparsity techniques are applied to speed the solution and Zollenkopf's bifactorization is utilized to create the Z Bus matrix one column at a time. Mutual coupling is included in the models for key system components such as transformers, motors, generators, and cables. The nonlinear loads are modelled as current sources with current injected into the linear system at each harmonic frequency. The voltage solutions at each harmonic frequency are superposed to arrive at time domain voltage waveforms at the diakoptic busses. These are applied to solve the nonlinear portions of the network

The nonlinear portions of the network consist primarily of solid state power devices and the magnetizing reactance in transformers, motors, and generators. These are solved in the time domain by the recursive solution of differential equations, and the resulting current waveforms are converted to the frequency domain by Fourier analysis.

The research has led to the extension of transformer and motor models, the development of a frequency measurement technique, and the synthesis of a new computer algorithm to solve harmonics in a multiphase unbalanced power system.

Acknowledgement

The author acknowledges the terrific support and guidance he has received from his two supervisors, Dr. D. H. Kelly, (Emeritus, retired), who supervised the Ph. D. proposal and work leading to the candidacy examination, and Professor K. E. Bollinger who supervised the research project and dissertation.

Table of Contents

Chapter 1	Introduction	1
1.1	Thesis Objectives And Goals	1
1.2	Overview Of The Algorithm Developed In This Thesis	4
1.3	Background To Power System Harmonics	7
1.4	Review Of Harmonic Solution Computer Algorithms	9
1.5	Thesis Outline	11
Chapter 2	Modelling Of Power System Components	13
2.0	Introduction To Chapter 2	13
2.1	Three Phase Transformer Linear Model Derivation	13
2.2	Transformer Magnetizing Branch Nonlinear Model Derivation	21
2.3	Three Phase Transformer Model Verification	29
	2.3.1 Mutual Admittance Measurements	29
	2.3.2 Core Saturation With A Load Having A DC Component	31
2.4	Power Transformer Frequency Response	36
2.5	Three Phase Induction Motor Model Derivation	40
2.6	Cable Model Derivation	47
2.7	Synchronous Generator Model Derivation	54
	2.7.1 Rotor Heating Model	54
	2.7.2 Three Phase Generator Linear Model	67
2.8	Six Pulse Converter Model Derivation	70
2.9	Conclusion To Chapter 2	76

Chapter 3	Measurement Of Nonlinear Loads	77
3.0	Introduction To Chapter 3	77
3.1	The relationship Between The Observed Spectrum And The Continuous Spectrum	78
3.2	Interpolation Method To Recover The Original Signal Spectrum	84
3.3	Error Of The Interpolation Method	85
3.4	Conclusion To Chapter 3	87
Chapter 4	Mathematical Methods For Harmonic Analysis of Power Systems	88
4.0	Introduction To Chapter 4	88
4.1	Symmetrical Components Sequence Frame Of Reference	89
4.2	Applying Zollenkopf's Bifactorization Method	90
4.3	Modified Bifactorization Algorithm	95
4.4	Establishing The Relative Angle For A Harmonic At A Particular Bus	97
4.5	Three Phase Loadflow	104
4.6	Applying Diakoptic Methods	114
4.7	Conclusion To Chapter 4	119
Chapter 5	Synthesis Of A Harmonic Solution Algorithm	120
5.0	Introduction To Chapter 5	120
5.1	Matrix Sparsity Storage Scheme	122
5.2	Bifactorization With Semi-optimal Ordering	126
5.3	Inverting The Matrix One Column At A Time	129
5.4	Three Phase Loadflow Subroutine	133
5.5	Mesh Network Subroutines	137
5.6	Nodal Network Subroutine	139
5.7	Program Validation	141
5.8	Conclusion To Chapter 5	142

6.0	Summary And Recommendations For Further Research	144
6.1	Recommendations For Further Research	144
6.2	Summary	145
	Bibliography	148

List of Tables

Table 2.3.1	Wye-Wye 480/208 Volt 3 kVA Transformer Short Circuit Measurement	30
Table 2.3.2	Delta-Delta 480/208 Volt 3 kVA Transformer Short Circuit Measurement	30
Table 2.3.3	Delta-Wye 480/208 Volt 3 kVA Transformer Short Circuit Measurement	31
Table 2.3.4	Transformer Short Circuit and Mutual Admittances (Siemens) .	31
Table 2.3.5	Comparison of Modelled to Measured Harmonic Current	34
Table 2.4.1	Measured Parameters For 3 kVA Wye-Wye Transformer	38
Table 2.4.2	Frequency Response Data Obtained From Experimental Measurement of a 3 kVA Transformer	39
Table 2.5.1	Typical Locked Rotor Power Factors	45
Table 2.5.2	50 HP Motor Voltage and No Load Current Harmonics	46
Table 2.7.1	Harmonic Impedance of 266 kW Generator	56
Table 2.7.2	Generator Rotor Harmonic Slip	51
Table 2.7.3	Harmonics From Rectifiers And Converters	62
Table 2.7.4	Equivalent Negative Sequence Current For Characteristic Harmonics in Table 2.7.3	65
Table 2.8.1	AC Loads on Unbalanced DC Diode Bridge Supplying VFD	75
Table 2.8.2	AC Voltage In Table 2.8.1 Increased 10% On Each Phase . . .	75
Table 3.3.1	Leakage Harmonics And Associated Error Terms	86
Table 3.3.2	Comparison Between Actual And Interpolated Signal Harmonics	87
Table 4.2.1	Comparison Among Gauss Elimination Methods (n Bus Network)	91
Table 4.2.2	Operations and Storage Requirements For The Modified Bifactorization	92
Table 4.4.1	Fundamental Phase A Current & Voltage (Balanced Conditions)	101
Table 4.4.2	Fourier Analysis of Load Current (No Phase Shift)	101
Table 4.4.3	Harmonic Angles of Currents Injected by SCR 1 and SCR 2 . .	102

Table 4.4.4	Harmonic Angles of Currents at Transformer Primaries	103
Table 4.5.1	Bus Cross Reference Identification For Example	112
Table 4.5.2	Fundamental Load Currents For Loads In Example System	112
Table 4.5.3	Fundamental Voltages For Example System	113
Table 5.7.1	Comparison of Harmonic Voltages For The Balanced Case	142
Table 5.7.2	Harmonic Voltages For The Unbalanced Case	143

List of Figures

Figure 1.1.1	An Example Of A Small Power Network	3
Figure 1.2.1	Network Torn Into Linear and Nonlinear Portions	4
Figure 1.2.2	Flowchart For Harmonic Solution Algorithm	6
Figure 2.1.1	Transformer Nodal Impedance Model	14
Figure 2.1.2	Transformer "Pi" Models For Impedance and Admittance	15
Figure 2.1.3	Magnetizing Branches Removed From Transformer Linear Model	16
Figure 2.1.4	One Core of a 3 Phase Transformer Showing Node And Branch Voltages	17
Figure 2.1.5	Admittance Model of One Core of a 3 Phase Transformer ...	19
Figure 2.1.6	Linear Model of Delta-Wye 3 Phase Transformer	20
Figure 2.2.1	Transformer Flux Offset Due To DC Load Current	21
Figure 2.2.2	Primary Sinusoidal Voltage & Normal Excitation Current	25
Figure 2.2.3	Primary Voltage and Current And Secondary Diode Voltage With Half Wave Rectifier Load on Secondary	26
Figure 2.2.4	Primary Excitation Currents and A Phase Voltage With All Secondaries Open Circuited	27
Figure 2.2.5	Single Phase Half Wave Rectifier on Phase A Causes Distortion In Primary Current of All Phases	28
Figure 2.2.6	Transformer Magnetizing Branch Model	28
Figure 2.3.1	Three Phase Transformer Short Circuit Test	29
Figure 2.3.2	Froelich Hyperbola Fitted To Transformer Magnetizing Curve ..	32
Figure 2.3.3	Test Circuit For Validating Transformer Nonlinear Model	33
Figure 2.3.4	Modelled Magnetizing Current With DC Load	35
Figure 2.3.5	Modelled and Measured Magnetizing Current	35
Figure 2.4.1	Transformer Frequency Response Model	36
Figure 2.4.2	Modelled Frequency Response - 3 kVA Transformer With a 79.34 Ohm Load	39
Figure 2.5.1	50 HP Motor B Phase Voltage (1) and No Load Current (2) ..	46
Figure 2.6.1	Flux Field Surrounding a Conductor Carrying Current	47

Figure 2.6.2	Branch and Nodal Cable Voltages	51
Figure 2.6.3	Admittance Model For Branches Connected To Node a_1	53
Figure 2.7.1	Generator Rotor Harmonic Model	61
Figure 2.7.2	Skin Effect on The Resistance of Generator Amortisseur Bars	63
Figure 2.7.3	Rotor Temperature Rise Due To Negative Sequence Current	66
Figure 2.7.4	Generator Harmonic Model	69
Figure 2.8.1	Three Phase Converter Bridge	70
Figure 2.8.2	Non-Overlap State	72
Figure 2.8.3	Overlap State On The Positive Rail	72
Figure 2.8.4	Overlap State On The Negative Rail	73
Figure 3.1.1	Windowed Signal	78
Figure 3.1.2	Spectrum Leakage With 0.1 Second Window	81
Figure 3.1.3	Spectrum Leakage With 0.33 Second Window	82
Figure 3.1.4	Spectrum Leakage With 1.0 Second Window	83
Figure 3.2.1	Spectrum Leakage In The Vicinity Of The Fundamental	84
Figure 4.4.1	Example Network To Demonstrate Shifted Harmonic Angles	100
Figure 4.4.2	Example Quasi-Square Wave Loads - ψ_h Established When $t_0 = 0$	102
Figure 4.5.1	Transformer Core Matrices Connected in Delta Ungrounded Wye	106
Figure 4.5.2	Transformer Core Matrices Connected In Ungrounded Wye - Wye	108
Figure 4.6.1	Network Torn Into Nodal and Mesh Portions	115
Figure 5.0.1	Flow Chart For Harmonic Solution Algorithm	121
Figure 5.1.1	Typical Pointers and Links In Sparse Storage Lists	124
Figure 5.1.2	Flow Chart For The Add Algorithm In The HYBus Subroutine	125
Figure 5.2.1	Flow Chart For Order Algorithm	127
Figure 5.2.2	Bifactorization Search Scheme For The Factor Subroutine	128
Figure 5.3.1	Flow Chart -Invert Subroutine - a) Reconstructing the Column Factors	130

Figure 5.3.2	Flow Chart -Invert Subroutine -	
	b) Reconstructing the Row Factors	131
Figure 5.4.1	Flow Chart For Three Phase Loadflow Algorithm	134
Figure 5.4.2	Flow Chart For Neutral Bus Loadflow Algorithm	135
Figure 5.5.1	Flow Chart For Six Pulse Converter Algorithm	137
Figure 5.5.2	Flow Chart of Transformer Magnetizing Branch Algorithm . . .	139
Figure 5.6.1	Flow Chart of Nodal Network Harmonic Solution Algorithm .	140
Figure 5.7.1a	"SPS" 1 Line Diagram	141
Figure 5.7.1b	"Solver" 3 Line Diagram	141

Chapter 1

Introduction

1.1 Thesis Objectives And Goals

The primary goal of the work in this thesis is to provide a method for calculating harmonics in an unbalanced multiphase power network. A new computer algorithm is developed which solves for multiphase harmonics. This algorithm combines a three phase loadflow, the inversion of a three phase admittance matrix, sparsity techniques, and state space methods. Multiphase analysis is used because the unbalanced current harmonics flowing in equipment and systems can be determined. Of concern are the residual harmonics¹ due to unbalance as these cause interference on communications circuits. Also of concern is the heating of the generator rotors due to both balanced and unbalanced harmonic currents.

The method of diakoptics² [12] is used to tear the network into linear and nonlinear portions, which then permits solving each portion with appropriate methods. The diakoptic equations are modified and extended to describe the nonlinear portion of the network in the time domain and to describe the linear portion of the network in the frequency domain. Many power system components can be practically treated as linear impedances, thus the linear portion of the network is by far the largest portion. This linear portion is solved by applying linear algebraic techniques in the frequency domain. The Zollonkopf bifactorization method [11] is used to invert the nodal admittance matrix.

¹ Residual harmonics are defined as those harmonics which can be measured by placing a window style zero sequence current transformer around all three phases of a feeder, or alternatively, as those harmonic which flow in system neutrals.

² "Diakoptics" from the Greek "*dia*" meaning "through" and "*koptic*" meaning "to tear", was the term invented by Gabriel Kron for his method [34] of subdividing large networks. Harmonic terminology used in this thesis can be found in the paper by Emanuel, Orr, and Cyganski [17].

This method is extended and modified to minimize the required computational effort.

The components of the power system which are treated as nonlinear are few in number and consist of small sub-systems in the network. These sub-systems are solved by applying differential equation solution techniques in the time domain. Examples of the nonlinear sub-systems are harmonic loads such as DC rectifiers, and nonlinear impedances such as transformer magnetizing branches.

New work is done to create models in the three phase frame of reference for power system components. Linear models are developed for transformers, cables, induction motors and generators. These models are required in order to build the admittance matrices needed to implement a three phase solution. Laboratory work to validate the models for transformers and motors confirms that transformers and motors can be treated as linear devices with small error. As the regulatory standards are only concerned with the first 80 harmonics in a power system, the system models need to be appropriate for frequencies in the 50 to 5000 Hertz range. This range permits the application of the models to both North American and European power system studies.

Nonlinear models are developed for the transformer magnetizing branches and for a DC six pulse converter. The six pulse converter is only one of several kinds of nonlinear loads, but it provides a good example of how harmonics are created when transformers are supplying nonlinear loads. Laboratory measurements confirm that the magnetizing branches of transformers contribute harmonic currents, particularly when the transformer loads draw a DC current component. A secondary objective of the thesis is to determine generator rotor heating due to harmonic loads. A model is developed which estimates the amount of harmonic current flowing in the amortisseur bars, and this current is used to estimate rotor temperature rise. During model validation some signals are measured asynchronously. When asynchronous sampling occurs, the period assumed by the analyzer does not match the period of the measured signal. This "smears" the results due to leakage between the spectral bins. A tertiary objective is to establish an interpolation method to recover correct harmonic data from smeared data.

An example of a power network is shown in Figure 1.1.1. Harmonics are produced by the nonlinear loads and absorbed by the generators. Harmonic currents flow through transformers and cables, and if the system is unbalanced, residual harmonics flow through the neutral wires. This thesis brings together a number of models and mathematical methods to formulate solutions for such power systems.

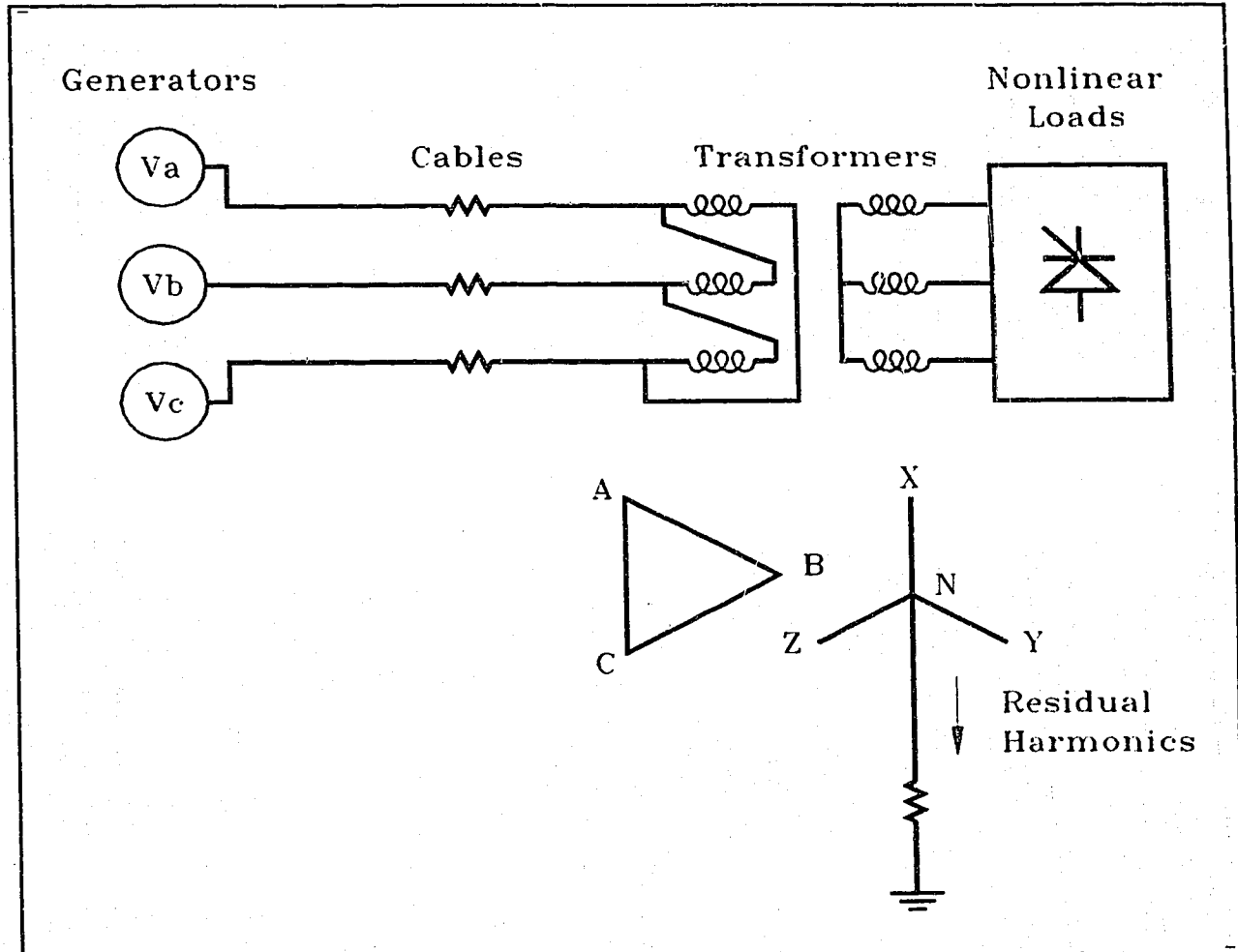


Figure 1.1.1 - An Example Of A Small Power Network

1.2 Overview Of The Algorithm Developed In This Thesis

As shown in figure 1.2.1, a power system network can be torn into linear and nonlinear portions connected together at specified busses, referred to hereafter as "diakoptic" busses. The linear and nonlinear portions of the circuit are solved separately and connected with diakoptic techniques. The linear part of the network is described by nodal equations in the frequency domain while the nonlinear part is described by mesh differential equations in the time domain.

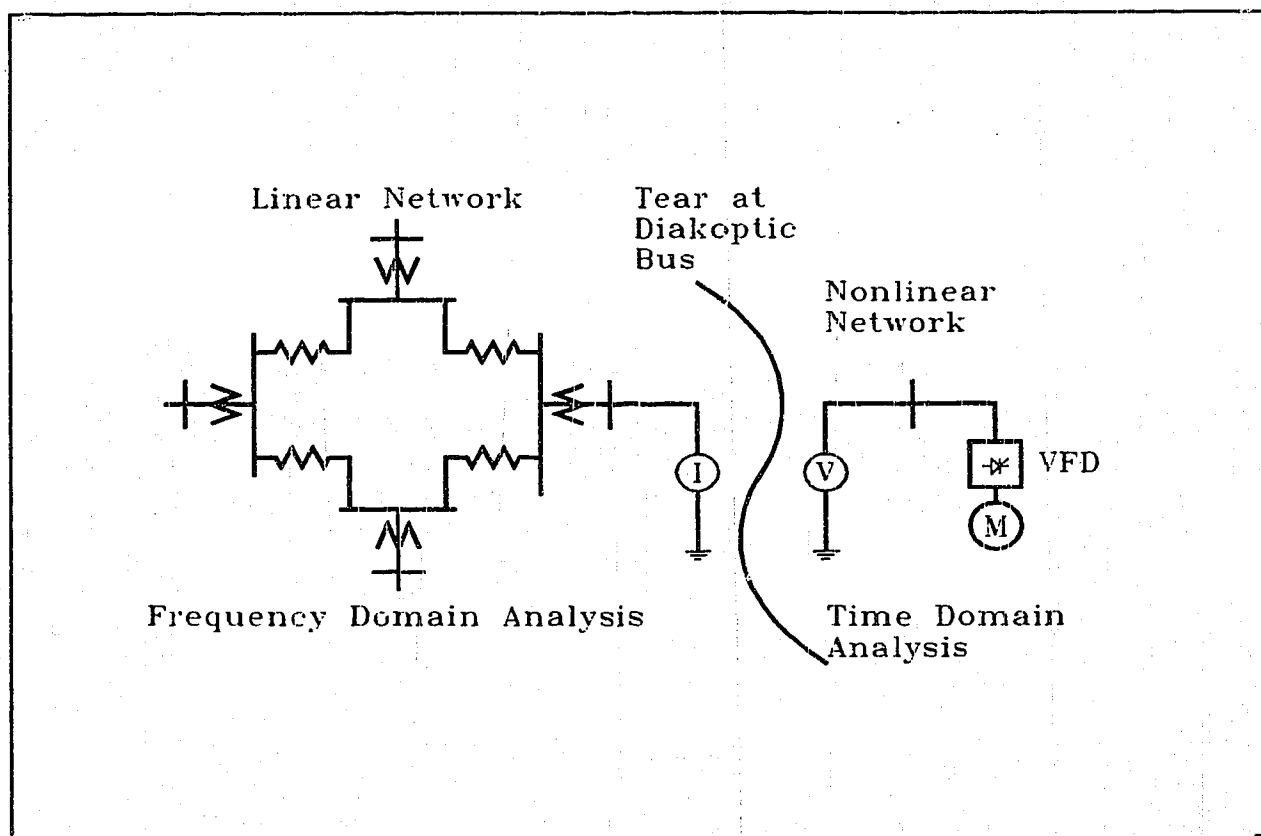


Figure 1.2.1 - Network Torn Into Linear and Nonlinear Portions

The flow chart in figure 1.2.2 gives the basic algorithm. In the linear portion of the network, a fundamental frequency multiphase loadflow is used to establish initial fundamental voltage and current conditions, then a multiphase nodal admittance (Y Bus) matrix is reformulated for each harmonic order. The inverse of the nodal admittance matrix (hereafter referred to as a Z Bus) is obtained for each harmonic order. The idea is similar to that developed to invert a single phase network [58], but with important conceptual differences. The Z Bus is formed one column at a time by Zollonkoff's bifactorization technique and only for those busses where harmonic current is injected by nonlinear loads or magnetizing branches. In the linear network the nonsinusoidal loads and nonlinear impedances are represented by harmonic current sources. The currents are injected into the diakoptic busses for each harmonic to calculate the harmonic voltages. These steps are referred to in the figure as the "Nodal Network Frequency Domain Solution".

After calculating all harmonic orders these voltages are stored and recombined to establish the distorted time domain waveforms. This is the "Inverse Fourier Transform" step in the figure.

In the nonlinear portion of the network, the solid-state devices and nonlinear impedances are defined by differential equations. The linear network is represented by distorted voltage waveforms and characteristic impedances connected to the diakoptic busses. The distorted voltage waveform is applied to the nonlinear network differential equations to calculate the unbalanced current waveforms. Similarly the DC load current component and distorted voltage waveform is applied to the magnetizing branches of converter transformers, utilizing an iterative solution of differential equations to solve for the magnetizing current waveforms. This is referred to in the figure as the "Mesh Network Time Domain Solution".

The current waveforms thus determined are then subjected to Fourier analysis to obtain the harmonic currents to be injected back into the linear portion of the network. This allows the harmonics to be solved independently of one another.

This new method was conceived by the author in his Ph. D. proposal and was subsequently published in the IEEE Transactions on Industry Applications [19].

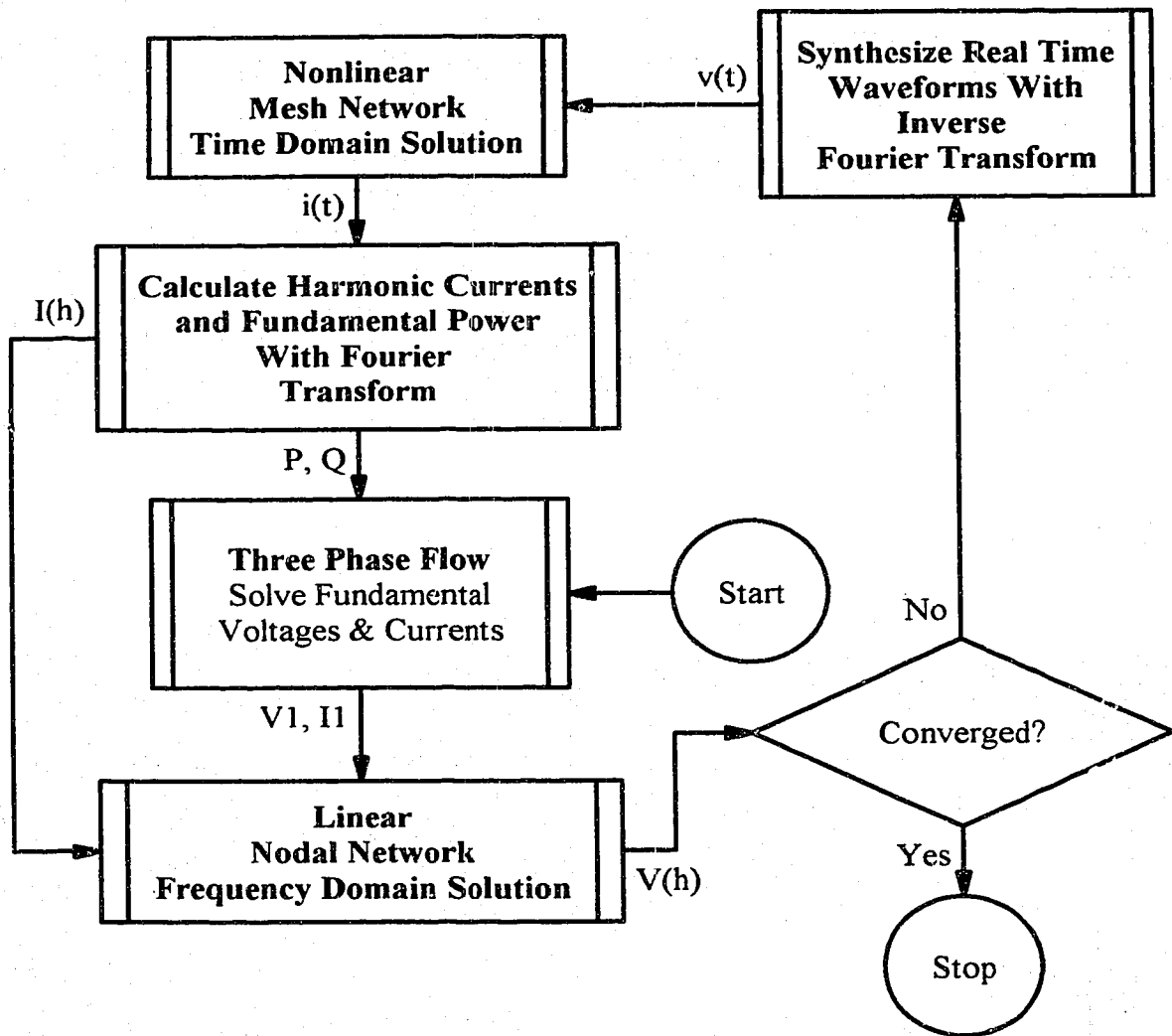


Figure 1.2.2 - Flowchart For Harmonic Solution Algorithm

1.3 Background To Power System Harmonics

Harmonics sometimes create severe problems for an industrial plant's power distribution system or the utility's power grid. Harmonics created by industrial nonsinusoidal loads may be separated into two categories, balanced harmonics and residual harmonics. The second category is due to unbalanced conditions in the power network. Limits for residual harmonics are not defined in the IEEE Standard 519 "Guide for Harmonic Control and Reactive Compensation of Static Power Converters" [26], which is the generally accepted standard in North America, but limits are defined in Alberta utilities' harmonic regulations [2] [59] which are among the most stringent in the world.

Problems arising from balanced harmonics are well documented by the Institute of Electrical and Electronics Engineers (IEEE) Power System Harmonics Working Group, [29] [30]. Two common results of system harmonics are the heating of rotors in motors and generators, and the creation of resonance overvoltages [44]. The most common industrial load which creates harmonics is the DC rectifier. Excellent case studies for harmonics and associated problems have been documented for these devices [49] [52] [53] [55]. Lighting ballasts may generate excessive third harmonic currents [35] causing neutral wiring to overheat, and harmonics created by the AC to DC converters in high voltage DC transmission systems may cause system resonance problems [32].

Problems arising from residual harmonics usually involve noise on data and communications circuits [57]. A common measure of such noise is the root sum square of the products of harmonic current (I_h) and a telephone harmonic weighting factor (T_h). This is referred to in the standards as the "I*T Product", given by,

$$I*T = \sqrt{\sum_{h=1}^N [I_h * T_h]^2} \quad (1.1.1)$$

The Alberta regulatory bodies have imposed more rigorous acceptance criteria on

unbalanced harmonics than they have on balanced harmonics because harmonics flowing in the earth result in much greater noise being induced in communication circuits. They require the residual $I \cdot T$ product to be less than 100 as opposed to the balanced $I \cdot T$ product which is to be less than 1500 on systems with voltages smaller than 25 kV. The utilities also require this level to be met with an assumed voltage unbalance equivalent to a 2% negative sequence component. IEEE Standard 519 is silent upon the subject of residual harmonic $I \cdot T$ limits, nor were limits considered for residuals by the working committee [16] during the recent updating of the standard.

When a system is unbalanced, troublesome "triplen" harmonics (ie. harmonics with orders that are odd integer multiples of three) and the unbalanced portions of other harmonic orders invade the power system and travel in the neutral and earth paths in addition to the power conducting paths. As well, system voltage unbalance can affect the firing angles in thyristor rectifiers. This may cause the generation of D. C. bias current which in turn cause displacement of the magnetizing flux of transformer cores with attendant generation of even harmonics due to saturation occurring on half the voltage cycle [69] [70]. These various problems, together with the stringent requirements of the Alberta utilities have resulted in the need for analytical techniques which use a three phase model that includes the earth and neutral conducting paths. As pointed out by the author in a recent paper [14] harmonic problems are best solved at the design stage of a project.

1.4 Review Of Harmonic Solution Computer Algorithms

Harmonic analysis of power systems has been used for several years to design harmonic filters and to pinpoint system problems under balanced operating conditions. A majority of the techniques in commercially available software utilize the balanced system approach because of its simplicity, ease of implementation, and ability to solve a considerable number of harmonic problems. While not an exhaustive list, the following companies offer single phase harmonic analysis programs on a commercial basis:

- a) Cooper Power Systems - "V Harm"
- b) Fichtner - "DigSilent"
- c) Micromatrix Research Ltd. - "SPS"
- d) Operation Technology Inc. - "ETAP"
- e) Power Technologies Inc. - "PSS/U"

AC/DC loadflow algorithms were developed by Hassan and Stanek [24] in 1981. In 1982 Mahmoud and Shultz [36] formulated a single phase Z Bus at each harmonic order and solved for harmonic voltages by injecting known harmonic currents. That same year, Xia and Heydt [62] [63] formulated a single phase Y Bus at each harmonic order and solved for harmonic voltages using a Newton-Raphson loadflow and Jacobian. The harmonic loads were calculated using the closed form solutions proposed by Yacamini and de Oliveira [71] in 1980. Other single phase harmonic loadflow algorithms have been developed since by various authors [23][48][64][65][73]. The Tamby and John approach [58] was to use a fundamental loadflow to establish initial conditions, then to reformulate the Y Bus matrix for each harmonic order and create a Z Bus using Gauss elimination methods. Their concept is adapted and extended to the three phase frame of reference in this thesis.

In 1981 Pillegi, Chandra, and Emanuel [40] used symmetrical components to formulate the sequence admittance matrix at each harmonic order, which they inverted and injected with sequence currents to solve for unbalanced harmonic voltages. The converter currents were calculated by a closed form method based on a quasi-square wave using the

fundamental unbalanced voltages. This method accommodated voltage unbalance, but only for networks with balanced impedances on each phase. That same year Kitchin [33] devised a state space method to solve differential equations describing the three phase network. He tore the network into linear and nonlinear systems, modelling the AC and DC networks as linear systems and the converters as nonlinear systems. The converter currents were used as state variables in the linear systems. A fundamental three phase loadflow was used to establish initial conditions. Kitchin's concept of network tearing is similar to the network tearing used in this thesis.

In 1983 Arrillaga, Bradley, Bodger and Arnold [4] [5] [6] developed a method which formulated an admittance matrix for each harmonic order, then reduced the network to contain only the current injected busses. The voltages and currents were solved with an iterative loadflow algorithm. The early program was not interactive with the converter, but in 1989 Arrillaga and Callaghan [7] incorporated the converter. The same year Acha, Arrillaga, Medina and Semlyn [1] developed a Y Bus "harmonic space" admittance matrix which contained all harmonic orders and hence was very large. They modelled nonlinear impedances, such as the magnetizing branches of rotating machines, as matrix linear off-diagonal elements coupling the harmonic orders. The network is solved by a Newton loadflow algorithm, but with the Jacobian only partially inverted. The solution is initialized by a three phase flow. In 1991 Xu, Marti and Dommel [66] formulated a multiphase admittance matrix for each harmonic order, and solved it using a Newton-Raphson loadflow and Jacobian. They modelled the nonlinear loads as Norton equivalent circuits and the motors and generators at harmonic frequencies as constant impedances, hence the problem was linearized at the harmonic frequencies and a solution was obtained with one iteration. They also presented a unique method of initializing the voltages to maintain the stability of the Newton-Raphson method. In 1994 Marinos, Periera and Carneiro [37] used parallel processing to speed the harmonic loadflow solution of the admittance matrix.

1.5 Thesis Outline

Before a multiphase power network can be represented mathematically as an admittance matrix, it is necessary to develop multiphase models for the more common power system components. Linear three phase models are developed for cable, motors, generators and transformers. Similarly, prior to establishing the differential equations describing the nonlinear components of the network it is necessary to develop models for them. Nonlinear models are developed for the transformer magnetizing branches and for a six pulse converter. Refer to Chapter 2 which describes the modelling of power system components in the three phase reference frame.

During rotor heating model validation, it is required to measure the voltage and current harmonics of generators which are operating when not synchronized to the power system. Due to the measurement techniques used some of the data is sampled asynchronously. A method is developed in Chapter 3 for recovering accurate Fourier coefficients from the measurement of a nonsinusoidal signal when the fundamental frequency is not precisely known, and the sampling was performed asynchronously.

Various mathematical methods, which were combined to accomplish the harmonic analysis of the system, are described in Chapter 4. Firstly, the rationale is presented for using a three phase frame of reference as opposed to the symmetrical components sequence frame of reference. A rationale is also developed for using the Zollonkopf bifactorization for the Gauss elimination technique. The method of creating Z Bus one column at a time is developed. A technique which ascertains the correct phase angle for currents injected at the diakoptic busses is described. The three phase loadflow equations are developed and demonstrated, and an example system is solved for 2% unbalanced supply voltages. Finally, the diakoptic equations are developed and modified to solve the nonlinear portions of the network in the time domain, and the linear portions of the network in the frequency domain.

The various mathematical techniques are programmed as computer algorithms. The matrix sparse storage scheme is integral to the bifactorization of the admittance matrix. The factors are created in a semi-optimal order and recombined to create the inverse of the admittance matrix one column at a time. The loadflow algorithm is developed utilizing the sparse storage scheme, but with the admittance matrix modified to omit the motors and generators. The six pulse converter is selected as a typical nonlinear load, and is modelled from the differential equations describing the operating states of the semiconductors and the associated circuit impedances. The magnetizing branches of transformers are modelled from the differential equations describing the flux linkages in the core. For the flowcharts for these algorithms, refer to Chapter 5.

The conclusions and recommendations for further research are presented in Chapter 6.

Chapter 2

Modelling Of Power System Components

2.0 Introduction To Chapter 2

When a power system with nonlinear loads operates under voltage unbalanced conditions residual harmonics appear in the system neutrals. Utility regulations state that the residual harmonics must be in compliance with the prescribed limits when the supply voltage contains a 2% negative sequence unbalance. For an engineer to meet this regulation requires the use of a design tool which can model all three phases and the neutrals of power systems and their components. This chapter describes computer models developed for the cables, motors, generators, transformers, and six pulse converters. Models are presented which can be incorporated into a linear Y Bus matrix. A nonlinear model is also developed for transformers supplying loads which draw a substantial direct current component. The six pulse converter is described in the time domain with differential equations.

2.1 Three Phase Transformer Linear Model Derivation

The three phase transformer is well described by others [21] [22] [20] [6] [60] [69] [70]. To establish a matrix topology which will correctly handle the frequency domain phase shifts for a delta-wye transformer requires the development of a transformer model which retains its winding terminals. It therefore requires four nodes for each high voltage/low voltage winding pair associated with a particular core. The magnetizing branches are separated from the linear admittance model and treated as injected harmonic current sources. The harmonic currents are divided in half and injected equally into either end of the leakage admittance branches [1]. This is better understood if the basic transformer equations are developed in admittance "Pi" model form. figure 2.1.1 shows a transformer model with assumed directions of current, and defines the variables for the

following derivation.

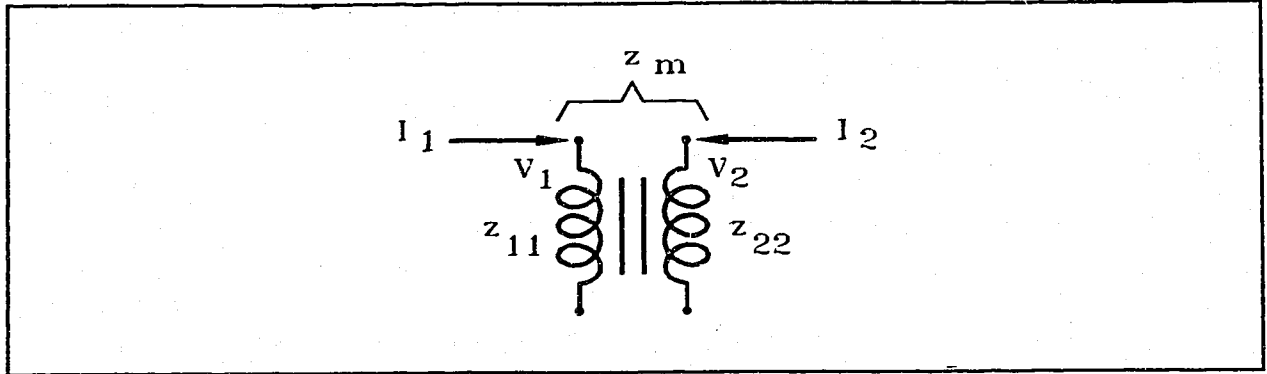


Figure 2.1.1 - Transformer Nodal Impedance Model

Assuming per unit (normalized) quantities, the circuit is described in matrix notation by:

$$\begin{bmatrix} V_1 \\ V_2 \end{bmatrix} = \begin{bmatrix} z_{11} & z_m \\ z_m & z_{22} \end{bmatrix} \begin{bmatrix} I_1 \\ I_2 \end{bmatrix} \quad (2.1.1)$$

Solving the determinant and inverting the impedance matrix places the equations in the form needed for the short circuit test on the transformer. This is given by,

$$\begin{bmatrix} I_1 \\ I_2 \end{bmatrix} = \frac{1}{\Delta} \begin{bmatrix} z_{22} & -z_m \\ -z_m & z_{11} \end{bmatrix} \begin{bmatrix} V_1 \\ 0 \end{bmatrix} \quad (2.1.2)$$

where

$$\Delta = z_{11} z_{22} - z_m^2 \quad (2.1.3)$$

The short circuit admittance is defined as;

$$y_{sc} = \frac{I_1}{V_1} \bigg|_{V_2=0} = \frac{z_{22}}{z_{11} z_{22} - z_m^2} \quad (2.1.4)$$

The leakage impedance is related to the branch impedances as follows:

$$z_1 = z_2 = \frac{z_{leak}}{2} \quad (2.1.5)$$

$$z_{11} = z_1 + z_m \quad (2.1.6)$$

$$z_{22} = z_2 + z_m \quad (2.1.7)$$

Substituting (2.1.6) and (2.1.7) into (2.1.4) results in an impedance definition for short circuit admittance,

$$y_{sc} = \frac{z_m + z_2}{z_1 z_2 + z_1 z_m + z_2 z_m} \quad (2.1.8)$$

Neglecting the very small $z_1 z_2$ product and substituting for z_{leak} yields;

$$y_{sc} \approx \left[\frac{z_m}{z_m z_{leak}} + \frac{z_{leak}}{2 z_m z_{leak}} \right] \quad (2.1.9)$$

and finally the admittance,

$$y_{sc} \approx \left[\frac{1}{z_{leak}} + \frac{1}{2 z_m} \right] = \left[y_{leak} + \frac{y_m}{2} \right] \quad (2.1.10)$$

can be expressed in the "Pi" format illustrated in figure 2.1.2.

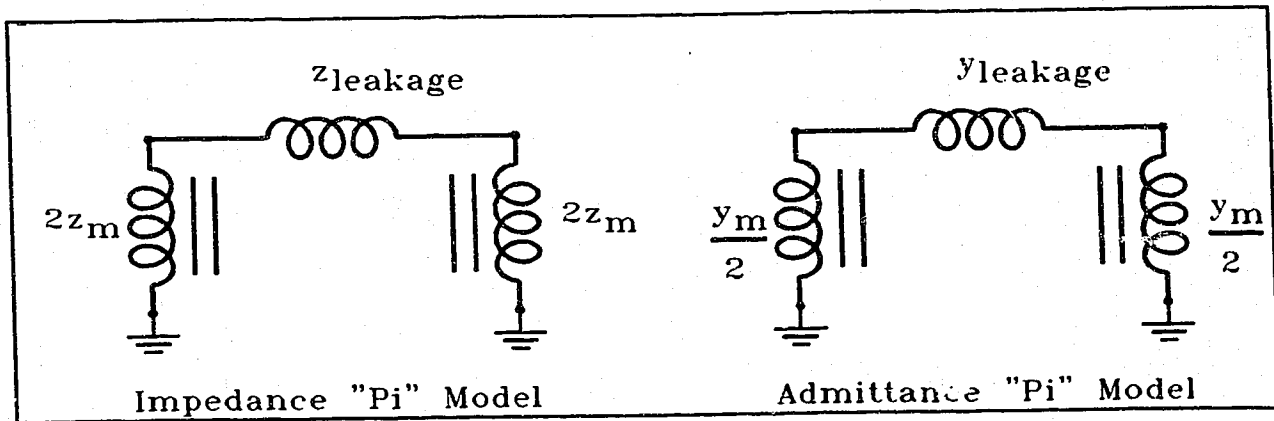


Figure 2.1.2 - Transformer "Pi" Models For Impedance and Admittance

The pi admittance format is particularly suited to matrix nodal analysis, as it permits the magnetizing branches to be associated with the busses on either side of the transformer as opposed to an internal transformer connection as is the case for the traditional "tee" model. Since the magnetizing branches are nonlinear, and linear

algebraic matrix manipulations require the use of linear elements, the magnetizing branches should be separated from the linear model during matrix operations. The magnetizing branches are replaced by harmonic current sources which inject current into the network at the points where the magnetizing branches are removed. This is a form of diakoptic tearing of the network. The branch removal is shown in figure 2.1.3. The leakage admittance, y_{leak} , for brevity of notation will be referenced hereafter as y .

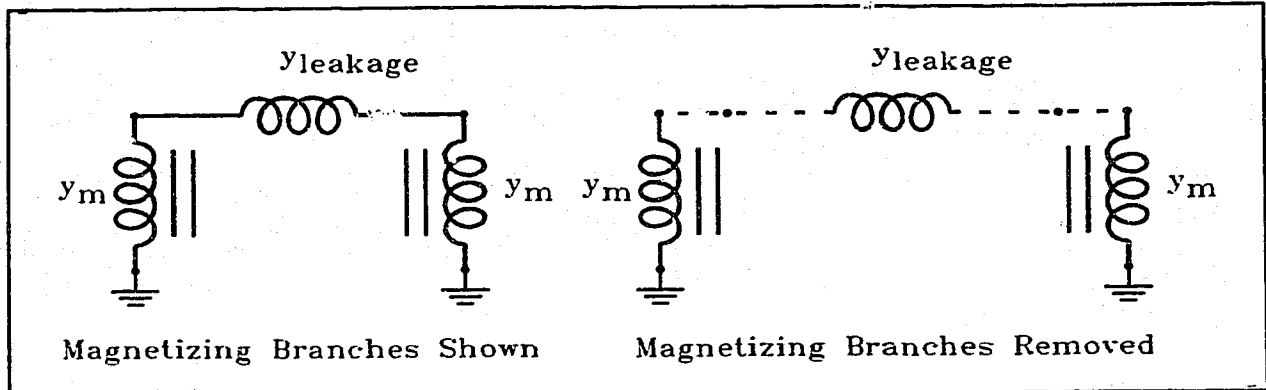


Figure 2.1.3 - Magnetizing Branches Removed From Transformer Linear Model

The leakage admittance is readily obtained from equipment ratings by taking the inverse of the transformer nameplate impedance. The nomenclature is illustrated in figure 2.1.4. The driving-point admittance on a matrix diagonal is the sum of all branch admittances attached to a node, and the transfer admittances on the off diagonals are the negative of the branch admittances connecting the node to another node [51].

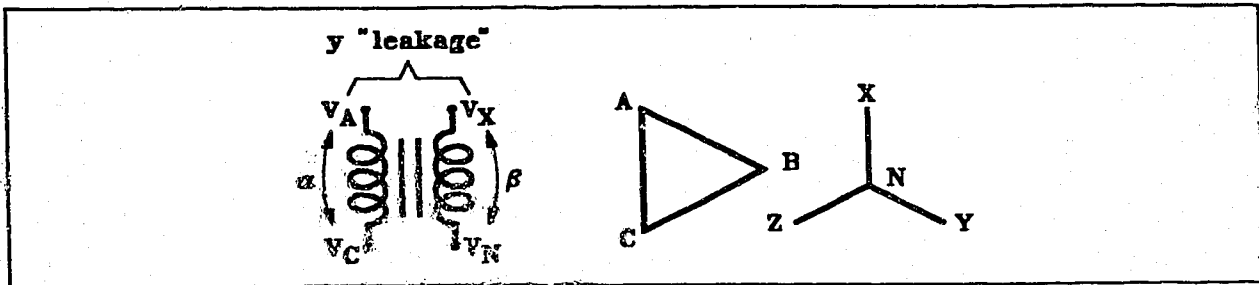


Figure 2.1.4 - One Core of a 3 Phase Transformer Showing Node And Branch Voltages

From this definition the primitive admittance is defined in terms of the leakage admittances as ,

$$Y_{PRIM}' = \begin{bmatrix} y & -y \\ -y & y \end{bmatrix} \quad (2.1.11)$$

It is necessary to modify this primitive matrix to accommodate the fact that the primary per unit voltage α and the secondary per unit voltage β may differ from line to neutral voltage. Incorporating the per unit voltages, the primitive admittance becomes,

$$Y_{PRIM} = \begin{bmatrix} \frac{1}{\alpha} & 0 \\ 0 & \frac{1}{\beta} \end{bmatrix} \begin{bmatrix} y & -y \\ -y & y \end{bmatrix} \begin{bmatrix} \frac{1}{\alpha} & 0 \\ 0 & \frac{1}{\beta} \end{bmatrix} = \begin{bmatrix} \frac{y}{\alpha^2} & -\frac{y}{\alpha \beta} \\ -\frac{y}{\alpha \beta} & \frac{y}{\beta^2} \end{bmatrix} \quad (2.1.12)$$

This primitive matrix may be thought of as representing the two terminals of a single phase transformer, one on the primary and one on the secondary, with the voltages being between the terminals and reference. These voltages are similar to the branch voltages across the primary and secondary windings of a two winding transformer. To develop a connection matrix showing the relationship between the branch and nodal voltages, consider the voltages shown in figure 2.1.4. By inspection, the voltage across the branch

is related to the voltage at a node by

$$\begin{aligned}\alpha &= V_A - V_C \\ \beta &= V_X - V_N\end{aligned}\tag{2.1.13}$$

or in matrix form,

$$\begin{bmatrix} \alpha \\ \beta \end{bmatrix} = \begin{bmatrix} 1 & -1 & 0 & 0 \\ 0 & 0 & 1 & -1 \end{bmatrix} \begin{bmatrix} V_A \\ V_C \\ V_X \\ V_N \end{bmatrix}\tag{2.1.14}$$

thus creating the connection matrix;

$$C = \begin{bmatrix} 1 & -1 & 0 & 0 \\ 0 & 0 & 1 & -1 \end{bmatrix}\tag{2.1.15}$$

By applying topological considerations [54], the nodal admittance,

$$Y_{NODE} = C^T Y_{PRIM} C\tag{2.1.16}$$

is formulated and expanded to,

$$Y_{NODE} = \begin{bmatrix} \frac{y}{\alpha^2} & -\frac{y}{\alpha^2} & -\frac{y}{\alpha\beta} & \frac{y}{\alpha\beta} \\ -\frac{y}{\alpha^2} & \frac{y}{\alpha^2} & \frac{y}{\alpha\beta} & -\frac{y}{\alpha\beta} \\ -\frac{y}{\alpha\beta} & \frac{y}{\alpha\beta} & \frac{y}{\beta^2} & -\frac{y}{\beta^2} \\ \frac{y}{\alpha\beta} & -\frac{y}{\alpha\beta} & -\frac{y}{\beta^2} & \frac{y}{\beta^2} \end{bmatrix}\tag{2.1.17}$$

By recalling that the off-diagonal elements of an admittance matrix are the negative values of the branch admittances of a circuit, a network model for one core of a transformer, shown in figure 2.1.5, is "reverse engineered" by inspection of the above matrix.

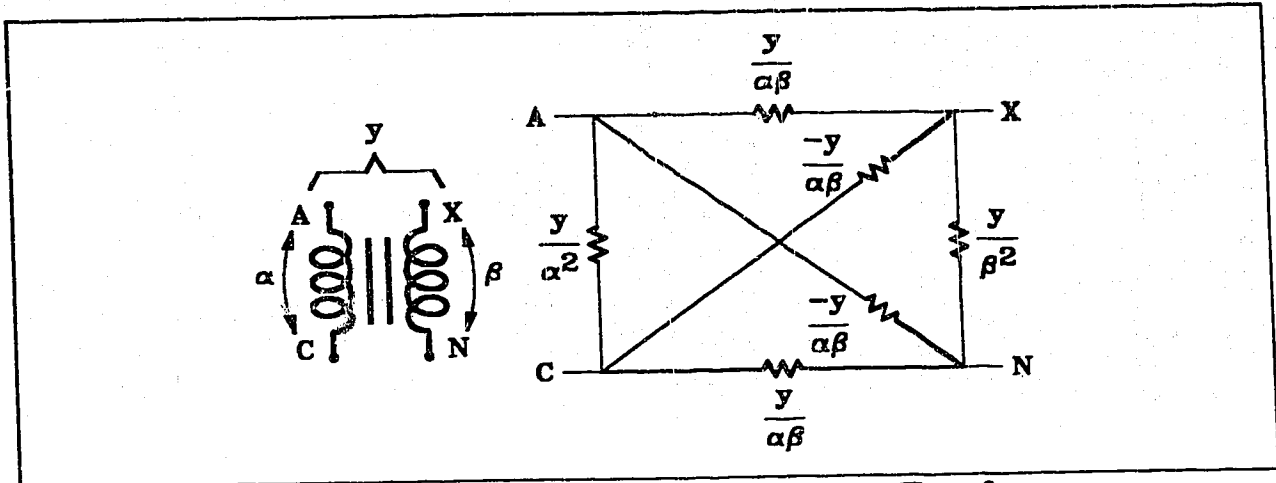


Figure 2.1.5 - Admittance Model of One Core of a 3 Phase Transformer

This model contains negative circuit elements with no physical parallel, but it has the virtue that it can be connected in the same manner as any pair of physical transformer windings to obtain wye-wye, delta-wye or delta-delta configurations. As an example, figure 2.1.6 shows the delta-wye connection where the delta side voltage leads the wye side voltage under balanced conditions. The model also permits the inclusion of single phase transformers or open delta transformers, since the data is entered on a core by core basis.

The advantages of the model are that the four terminals of the windings are preserved, which allows the delta windings to be correctly represented, and that the phase shift in voltage and current across a delta-wye transformer is correct. The limitation when using the model is that both sides of transformer must be connected with a shunt admittance to reference to solve a network as the model matrix is otherwise singular (or alternatively at least one nodal voltage on each side of the model must known). Despite this limitation the model is useful for depicting three phase networks because it contains no mutually coupled admittances. The equivalence to mutual coupling has been handled by the interconnection of linear elements.

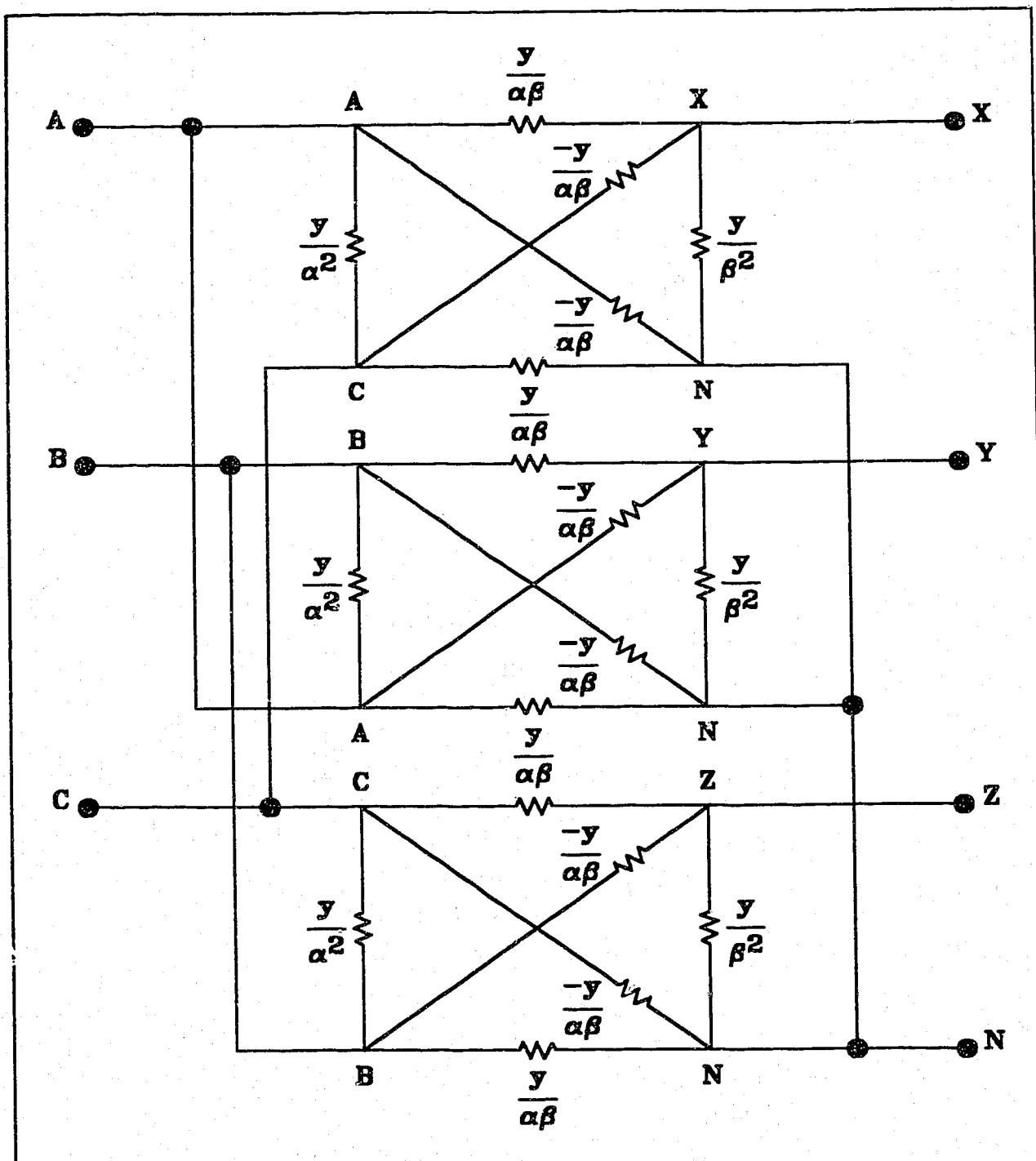


Figure 2.1.6 - Linear Model of Delta-Wye 3 Phase Transformer

2.2 Transformer Magnetizing Branch Nonlinear Model Derivation

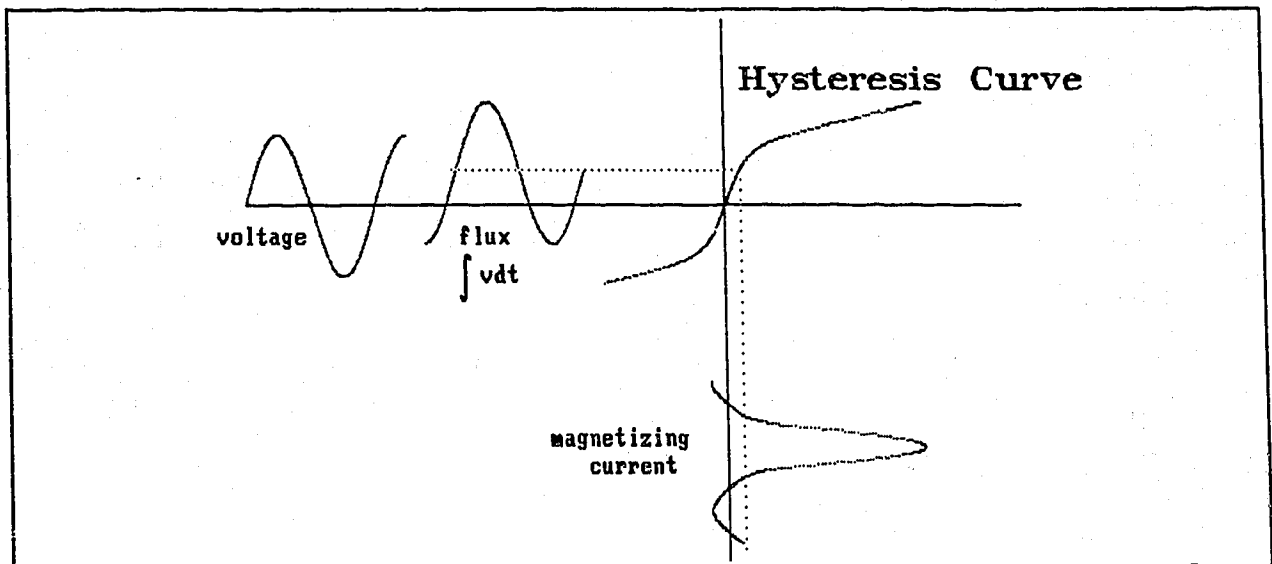


Figure 2.2.1 - Transformer Flux Offset Due To DC Load Current

The linear element approach described in the previous section includes inter-phase coupling in the transformer model and is sufficient for units supplying loads which are free of harmonics; however, it neglects the magnetization branches which are nonlinear. As shown later in this chapter these branches contribute harmonics when transformers are connected to rectifiers. Two factors are of concern. The first is the significance of the nonlinearity - that is, can it be ignored? If not, then the second factor is that of modelling. Considering this second factor, a distinction has to be made between those portions of the circuit which can be considered to behave linearly and those portions of the circuit which need to account for second order saturation effects. The method of diakoptics [12] [34] is used to tear the network into linear and nonlinear portions, with the current and voltage interactions between the two portions represented by voltage sources and current sources. In this thesis the networks are torn into linear and nonlinear parts at the secondaries of those transformers connected directly to harmonic producing loads. The magnetizing currents and the load currents are represented in the linear portion of the network by means of current sources. The current sources are developed from a

Fourier transform of the time domain analysis of the nonlinear portions of the torn network, with the intention that each harmonic frequency of interest is injected into the linearly modeled network.

A nonlinear model may be needed for the magnetic branches of those transformers supplying loads with a DC component as they may contribute significant harmonics under certain conditions of circuit overvoltage. For other transformers the harmonic currents contributed by the magnetizing branches can be neglected. The reason for this is that the magnetizing current for transformers supplying linear loads is usually less than 1% of the transformer's rated load current. When a load has a DC component the direct current creates an offset in the flux pattern which tends to drive the transformer into saturation on one half of the cycle while allowing it to be non-saturated on the other half of the cycle. Under these conditions the harmonics produced by the magnetizing branches may become significant. In addition, the DC component of flux created in one core divides and links the other cores of a three phase transformer, thus a DC load on only one phase of a three phase transformer will cause the other cores to also saturate. As a result, the mutual coupling between phases, which could be neglected in the linear model, cannot be ignored in the case for the transformer supplying loads with a DC current component.

The magnetizing branch of the transformer is nonlinear and can be modelled by injected current harmonics. Some authors use a polynomial curve fitting method to predict the saturation curve from RMS measurements [20] [41]. Other authors describe a curve modelling technique based on the open circuit test of a transformer [38]. The magnetizing branch may also be described by a harmonic Norton equivalent [1] [46], which presents an accurate model of the magnetization curve, provided that it includes the core saturation effects due to the DC component of load current. The behaviour when the core is saturated due to a DC component in the load current is to create even harmonic magnetizing currents [69] [70]. A small DC offset in flux linkage results in a large increase in the peak of the magnetizing current. An estimate can be made of the DC component of flux linkage by examining the slope of the saturation curve in the vicinity of the peak current.

To calculate the harmonics in the magnetizing current requires a Fourier analysis of the magnetizing current predicted by a model developed as follows: Firstly, the saturation curve is obtained from the transformer open circuit test by recording the instantaneous magnetizing current and excitation voltage across one cycle. Secondly, the AC voltage is integrated to obtain AC excitation flux linkage. Thirdly, this flux linkage is plotted against the current to obtain the transformer magnetization curve. Next the DC current component is reflected against the saturation curve at the peak value of magnetizing current to obtain the DC flux linkage. To calculate the magnetizing current curve resulting from a given DC load component, the AC and DC fluxes are added at each instant in time and reflected against the saturation curve. This is shown in figure 2.2.1. In other words, the magnetization curve is given a DC bias based upon the DC load current, the transformer turns ratio, and the slope of the magnetization curve where the magnetizing current is at peak value. Subsequent projection of the integrated AC voltage against the biased curve estimates a plot of the magnetization current present when a transformer feeds a DC load. This work is simplified if one uses a digital oscilloscope which has the capability to download real time data to a computer.

Two forcing functions, the AC voltage, v , and the DC flux, λ_{DC} , created by the DC load current define the magnetizing flux,

$$\lambda = \int v dt + \lambda_{DC} \quad (2.2.1)$$

The saturation curve can be modeled as a hyperbolic curve based on Froelich's equation, given by,

$$\lambda = \frac{k_1 i_M}{k_2 + i_M} \quad (2.2.2)$$

which uses magnetizing current i_M to define flux linkage, where k_1 , k_2 are derived constants. Equation (2.2.2) only defines the curve in the upper right-hand quadrant for positive λ and positive i_M . For negative λ and i_M the curve must be transposed to the lower left quadrant by using the negative of k_1 and k_2 . The hyperbolic approximation is created by selecting two points from the measured data from the open circuit test, one

near the knee and one where the flux linkage peaks. Differentiating,

$$\frac{d\lambda}{di_M} = \frac{k_1 k_2}{(k_2 + i_M)^2} \quad (2.2.3)$$

and recalling that across a coil the voltage,

$$v = \frac{d\lambda}{dt} = \frac{d\lambda}{di_M} \cdot \frac{di_M}{dt} \quad (2.2.4)$$

we rearrange equation (2.2.4) and substitute (2.2.3) to obtain an expression for differentiating current,

$$\frac{di_M}{dt} = \frac{v}{\left(\frac{d\lambda}{di_M}\right)} = \frac{v(k_2 + i_M)^2}{k_1 k_2} \quad (2.2.5)$$

For small time increments the step change in current is,

$$\Delta i_M = \frac{di_M}{dt} \cdot \Delta t \quad (2.2.6)$$

and the step change in flux linkage is,

$$\Delta \lambda = \frac{d\lambda}{dt} \cdot \Delta t = v \cdot \Delta t \quad (2.2.7)$$

The magnetizing current at any step $k+1$

$$i_{M(k+1)} = i_{M(k)} + \Delta i_{M(k)} \quad (2.2.8)$$

and the flux linkage at any step $k+1$

$$\lambda_{(k+1)} = \lambda_{(k)} + \Delta \lambda_{(k)} \quad (2.2.9)$$

are solved recursively from the values obtained by the preceding step k .

The resulting curves are in the time domain and must be converted to the frequency domain by a Fourier method to obtain the current harmonics which are used to model the magnetizing branches of the transformer.

When considering the DC component of the load it is necessary to consider the

inter-core DC coupling. Whereas the AC inter-core coupling is considered negligible the DC inter-core coupling is quite strong. This is because DC flux in one core will complete a magnetic loop in the iron core of the transformer. Should a DC load be connected between any two secondary lines, the DC flux will circulate in the two affected cores, being positive in sign in one core and negative in sign in the other core. However, should the DC load be connected between one line and neutral, the DC flux created in that core will divide approximately equally between the other two cores. Thus a single phase DC load creates harmonics in the primary currents of all three phases of a three phase transformer.

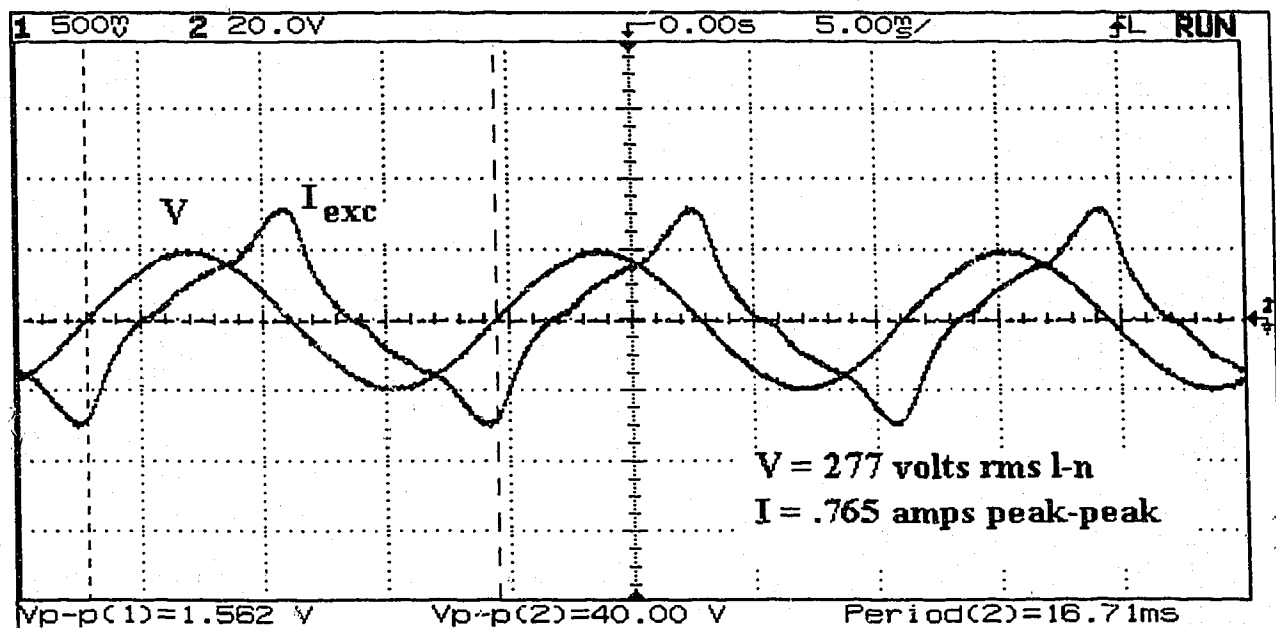


Figure 2.2.2 - Primary Sinusoidal Voltage & Normal Excitation Current

Measurements taken on a three phase core type transformer give the waveform in figure 2.2.2 for a three phase transformer with the secondary open circuited. With no load the excitation current is approximately symmetrical in its positive and negative lobes. However, when a half-wave rectifier is supplied, as shown in figure 2.2.3, the DC flux drives the transformer into saturation during one half of the cycle, while tending to let it operate in a more linear region during the opposite half cycle.

This behaviour is incorporated into the model by reflecting the DC current through the magnetization curve to obtain DC flux. It is, however, important to reflect it through the slope that exists where the AC excitation current would have peaked had no DC been present. It was found by experimentation that the more the AC voltage drives the peak of the excitation flux linkage into saturation, the less is the offset produced by the DC flux component. It was also found that the DC offset calculated in this fashion applies when operating in a more linear portion of the hysteresis curve.

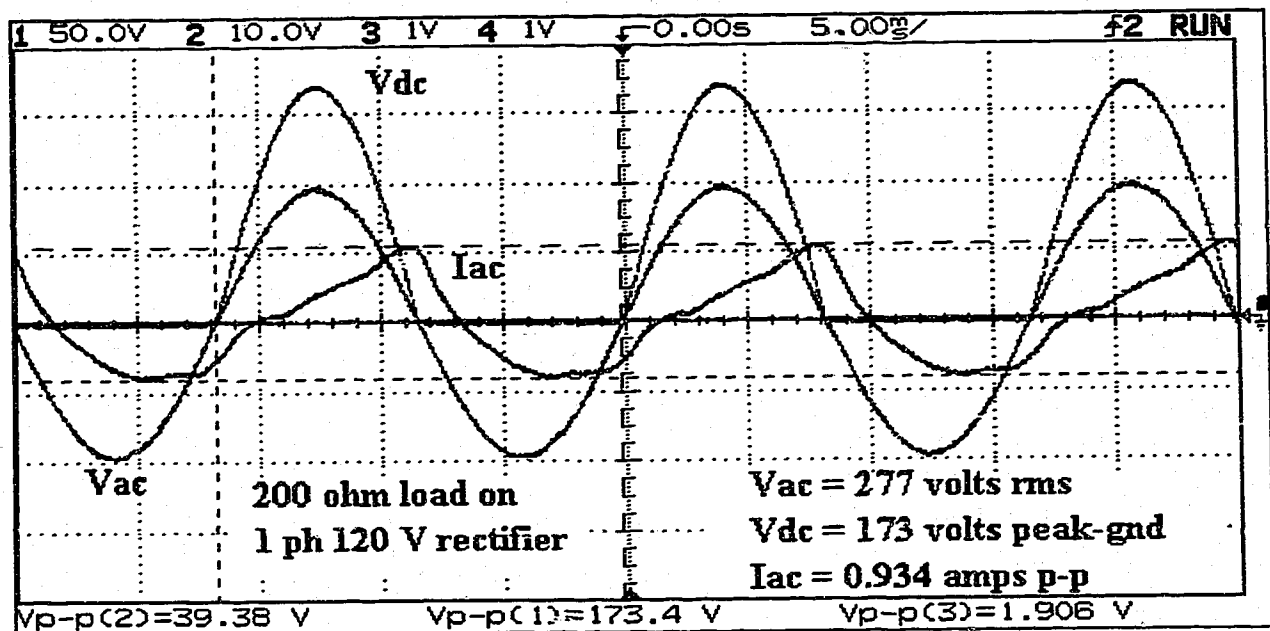


Figure 2.2.3 - Primary Voltage and Current And Secondary Diode Voltage With Half Wave Rectifier Load on Secondary

Since the DC load cannot be "transformed" its net effect is to appear as even harmonics in the transformer primary excitation current. This will show up for single phase loads such as the switch-mode power supplies on computers, printers, photocopiers, televisions, and fax machines, and it will also appear on controlled rectifiers where the firing angle controller permits the positive lobe duration of current to be of a different duration than the negative lobe duration. This latter phenomenon will usually affect two input line currents to the rectifier which creates a positive DC current component in one line current and a negative DC component in the other. These DC components create DC

flux in the rectifier transformers' secondaries which creates even harmonics on the primary side. In figure 2.2.3, the load current is purposeily made small to permit measurement of the magnetizing current in the negative half cycle where the load current normally is dominant. It is seen that very little distortion is present in the negative half cycle.

Figures 2.2.4 and 2.2.5 compare the excitation in a transformer with an open circuited secondary and a transformer supplying a single phase load with a large DC component in the load current. As can be seen in the figures, the excitation current under open circuit conditions is small. This excitation current is typical for balanced loads containing no DC component. It may be neglected for power system analysis. The excitation current is somewhat larger when a DC component is present in the load. While excitation current may usually be neglected, there are certain conditions where it may be a significant factor. One of these is when the system is subjected to overvoltages, driving the transformers into saturation.

To reduce the amount of computational effort, only transformers supplying loads with a DC component should have the magnetizing branches modeled as harmonic current sources. For other transformers the magnetizing branches may be neglected.

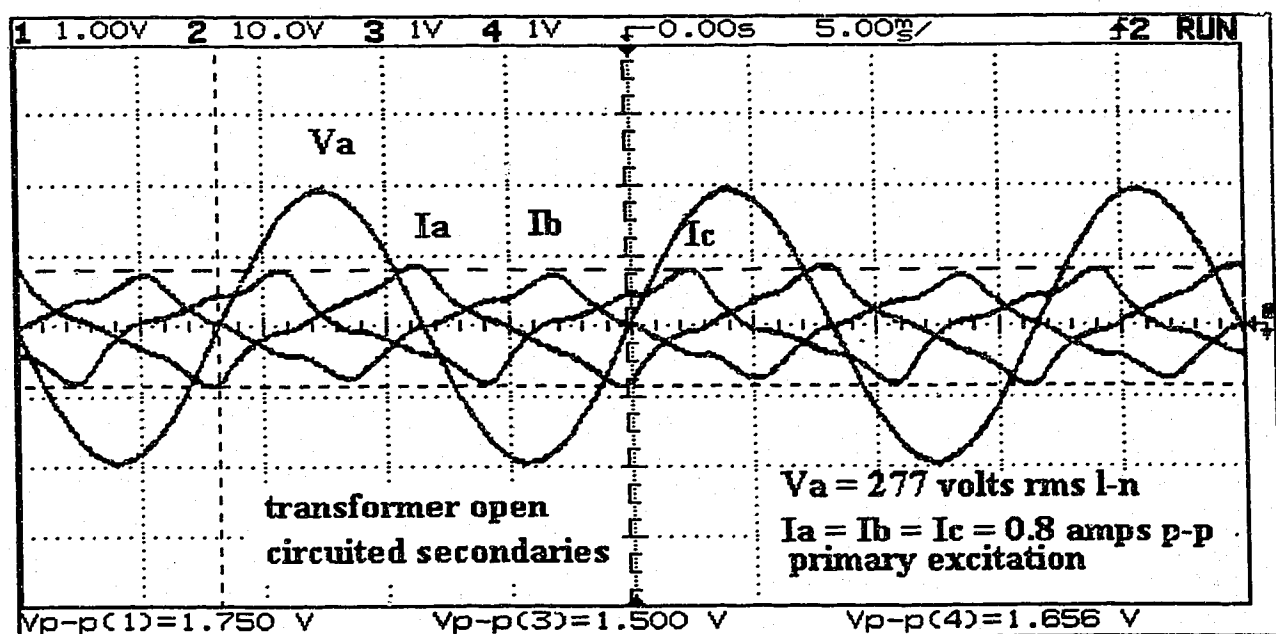


Figure 2.2.4 - Primary Excitation Currents and A Phase Voltage With All Secondaries Open Circuited

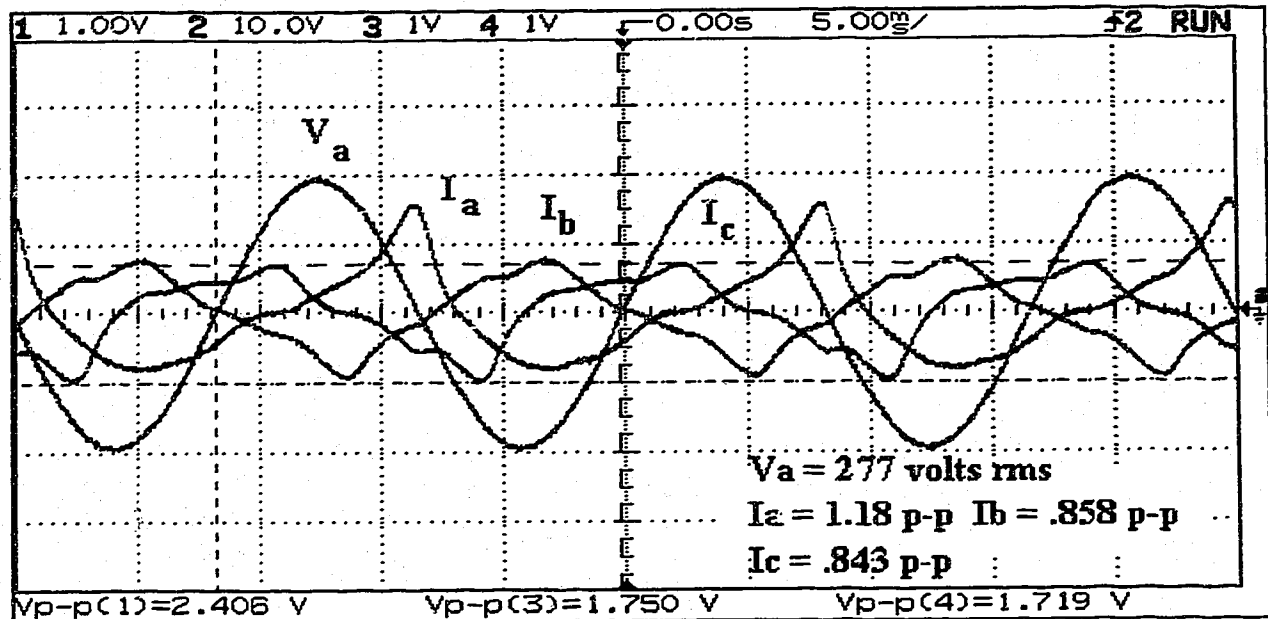


Figure 2.2.5 - Single Phase Half Wave Rectifier on Phase A Causes Distortion In Primary Current of All Phases

The model for the magnetizing current is shown in figure 2.2.6. The harmonic branches are modelled by current sources which are derived from the spectrum analysis of the magnetizing current waveform resulting from reflecting the AC flux linkage, offset by a DC component, against the saturation curve. These injected currents are readily incorporated into the nodal admittance network model. As is shown in the next section, the magnitudes of these harmonics are small and may usually be neglected.

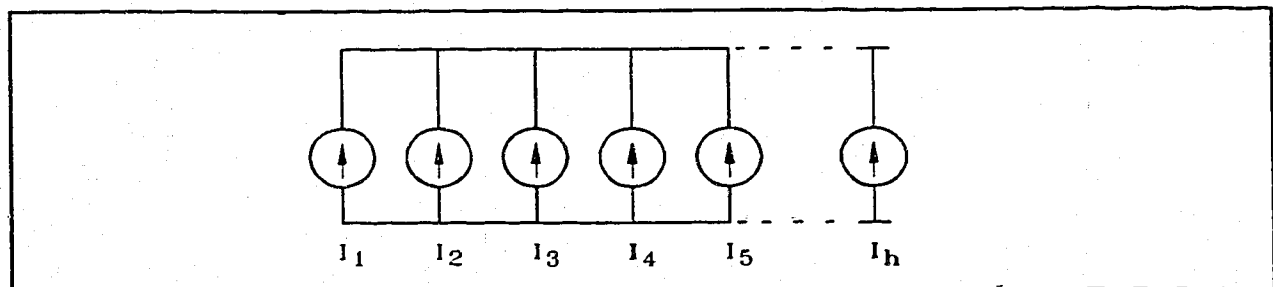


Figure 2.2.6 - Transformer Magnetizing Branch Model

2.3 Three Phase Transformer Model Verification

To validate the theoretical models, tests are performed on laboratory scale three phase core-type transformers. The core consists of laminated iron plates with a primary and a secondary winding on each of three limbs. The tests are performed on Delta-Delta, Delta-Wye, and Wye-Wye transformers. The tests consist of the following measurements:

- Mutual admittance between windings
- Core saturation with a load having a large DC component

2.3.1 Mutual Admittance Measurements

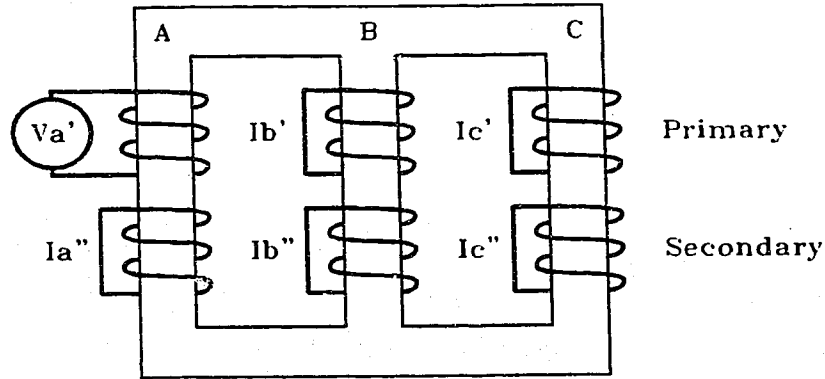


Figure 2.3.1 Three Phase Transformer Short Circuit Test

The theoretical models assume the mutual admittances between windings wound on different cores can be neglected. To verify the error limits associated with this assumption, a low voltage is applied to the primary winding of one core with all other windings short circuited, as depicted in figure 2.3.1. The short circuit admittance is

$$y_{sc} = \frac{I_A'}{V_A'} \cdot \frac{N''}{N'} \quad (2.3.1)$$

where $\frac{N''}{N'}$ is the transformer secondary to primary turns ratio.

The mutual admittances are:

$$y'_{ab} = \frac{I'_B}{V'_A} \quad (2.3.2)$$

$$y''_{ab} = \frac{I''_B}{V'_A} \cdot \frac{N''}{N'} \quad (2.3.3)$$

$$y'_{ac} = \frac{I'_C}{V'_A} \quad (2.3.4)$$

$$y''_{ac} = \frac{I''_C}{V'_A} \cdot \frac{N''}{N'} \quad (2.3.5)$$

Measurements are taken with readings in RMS volts and amps.

Table 2.3.1 - Wye-Wye 480/208 Volt 3 kVA Transformer Short Circuit Measurement

N''/N'	V_a'	I_a'	I_b'	I_c'	I_a''	I_b''	I_c''
120/277	8.93	3.75	.120	.122	8.41	.281	.263

Table 2.3.2 - Delta-Delta 480/208 Volt 3 kVA Transformer Short Circuit Measurement

N''/N'	V_a'	I_a'	I_b'	I_c'	I_a''	I_b''	I_c''
208/480	14.94	2.16	.050	.052	4.86	.154	.144

Table 2.3.3 - Delta-Wye 480/208 Volt 3 kVA Transformer Short Circuit Measurement

N''/N'	V_a'	I_a'	I_b'	I_c'	I_a''	I_b''	I_c''
120/480	16.2	2.21	.043	.040	8.40	.188	.169

The resulting admittances are shown in table 2.3.4. The mutual admittance ranges between 2% and 4% of the short circuit admittance, justifying the decision to neglect mutual admittances in the linear model of the transformer.

Table 2.3.4 - Transformer Short Circuit and Mutual Admittances (units in Siemens)

Transformer Winding	y_{SC}	y_{ab}'	y_{ab}''	y_{ac}'	y_{ac}''
Wye-Wye	.408	.013	.014	.014	.013
Delta-Delta	.141	.0033	.0045	.0035	.0042
Delta-Wye	.130	.0027	.0029	.0025	.0026

2.3.2 Core Saturation With A Load Having A DC Component

To verify this model requires the following steps:

- 1) Determine a magnetization curve model from the open circuit data, incorporating a resistor to model hysteresis in the curve;
- 2) Analyze the load current for its DC component and reflect it against the magnetization curve in the vicinity of the peak current to obtain the DC flux linkage;
- 3) Integrate the AC voltage to obtain the AC component of flux linkage;
- 4) Offset the AC flux linkage by the DC flux linkages and reflect it against the magnetization curve to obtain a corrected magnetization current;

- 5) Add the load current reflected to the primary to the magnetization current to derive the primary current.
- 6) Compare the derived primary current to the measured primary current.

The voltage in figure 2.2.2 of the previous section is integrated and plotted against the current in the same figure to develop the saturation curve of figure 2.3.2. An hyperbola is fitted to the mean of the hysteresis waveform to model the saturation curve.

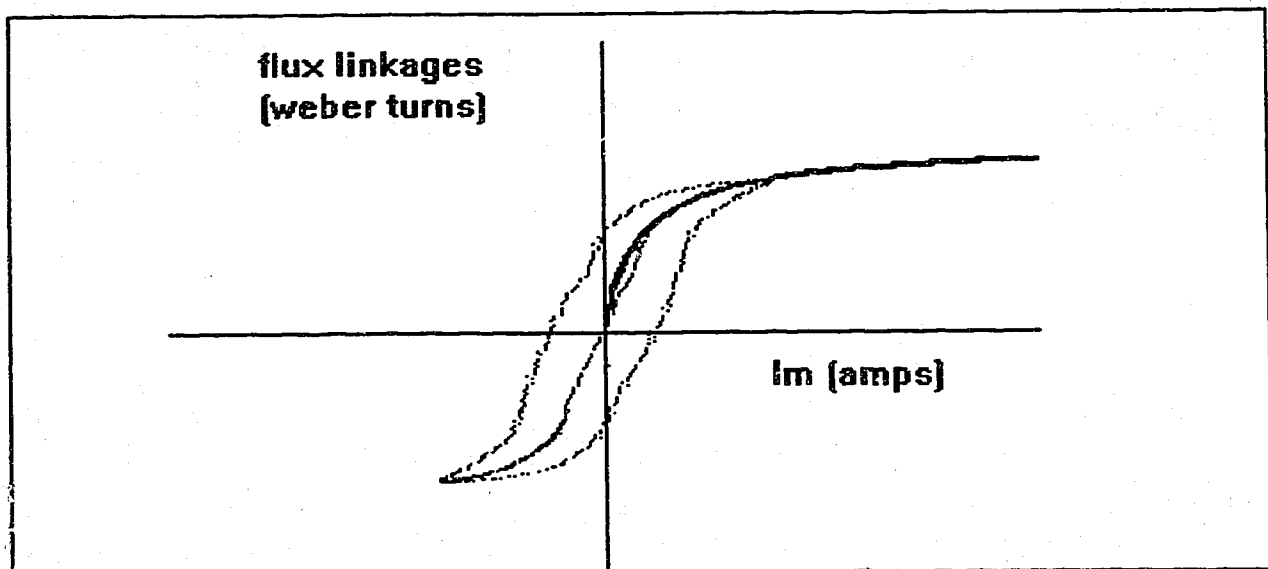


Figure 2.3.2 - Froelich Hyperbola Fitted To Transformer Magnetizing Curve

This portion of the model construction requires a measurement of the transformer primary current with the secondary open circuited. The load current is both calculated from the circuit parameters and measured on the secondary side of the transformer. Both methods result in a half-wave DC current with a peak value of 0.86 amps. A load of 200 Ohms is chosen to obtain a small load current so it doesn't obscure the magnetizing current results. The test circuit is shown in figure 2.3.3.

The modelled magnetizing current when a DC load is present is shown in figure 2.3.4. The measured magnetizing current is overlaid onto the modelled current in figure 2.3.5. By inspection the two waveforms are similar in magnitude and shape, however a

Fourier analysis of both the measured and the modelled waveform indicates the model overestimates harmonics below the fifth and underestimates the higher harmonics.

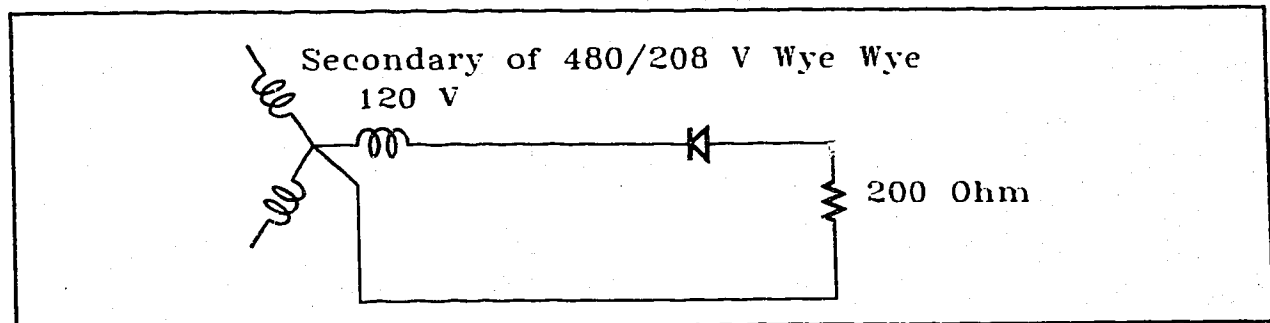


Figure 2.3.3 - Test Circuit For Validating Transformer Nonlinear Model

Table 2.3.5 indicates that the magnitudes of the magnetizing harmonics are small. The fundamental is only 0.2 amps and the other harmonics are smaller. When compared to the rated load current of 3.6 amps, this is only 5%. This percentage would be even lower for larger power transformers, which draw a magnetizing current which is relatively smaller as a percentage of full load. The magnetizing harmonic currents are negligible in their overall effect. In fact the nonlinearity of the magnetizing branch can be ignored for most system studies.

Table 2.3.5 - Comparison of Modelled to Measured Harmonic Current

Harmonic Order	Measured Harmonic Current	Modelled Harmonic Current
1	0.19791	0.22643
2	0.05924	0.07550
3	0.06690	0.08019
4	0.02793	0.03098
5	0.03745	0.02405
6	0.01546	0.01355
7	0.01460	0.00934
8	0.00831	0.00432
9	0.00565	0.00292
10	0.00487	0.00200
11	0.00439	0.00099

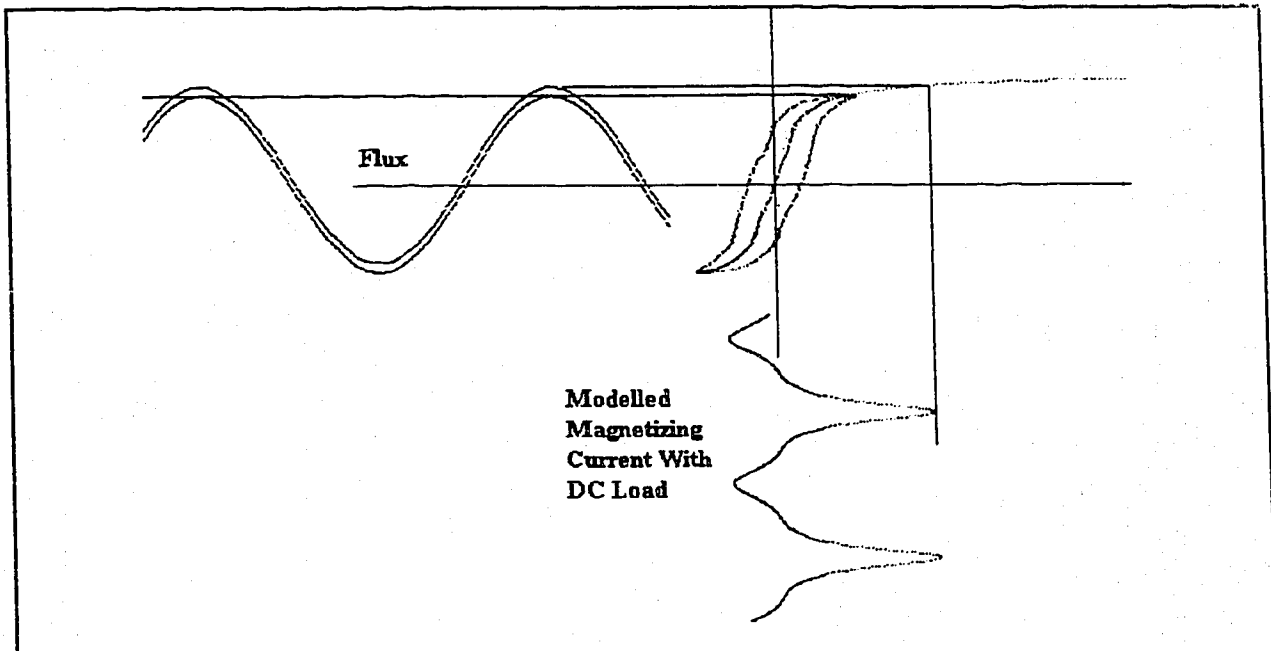


Figure 2.3.4 - Modelled Magnetizing Current With DC Load

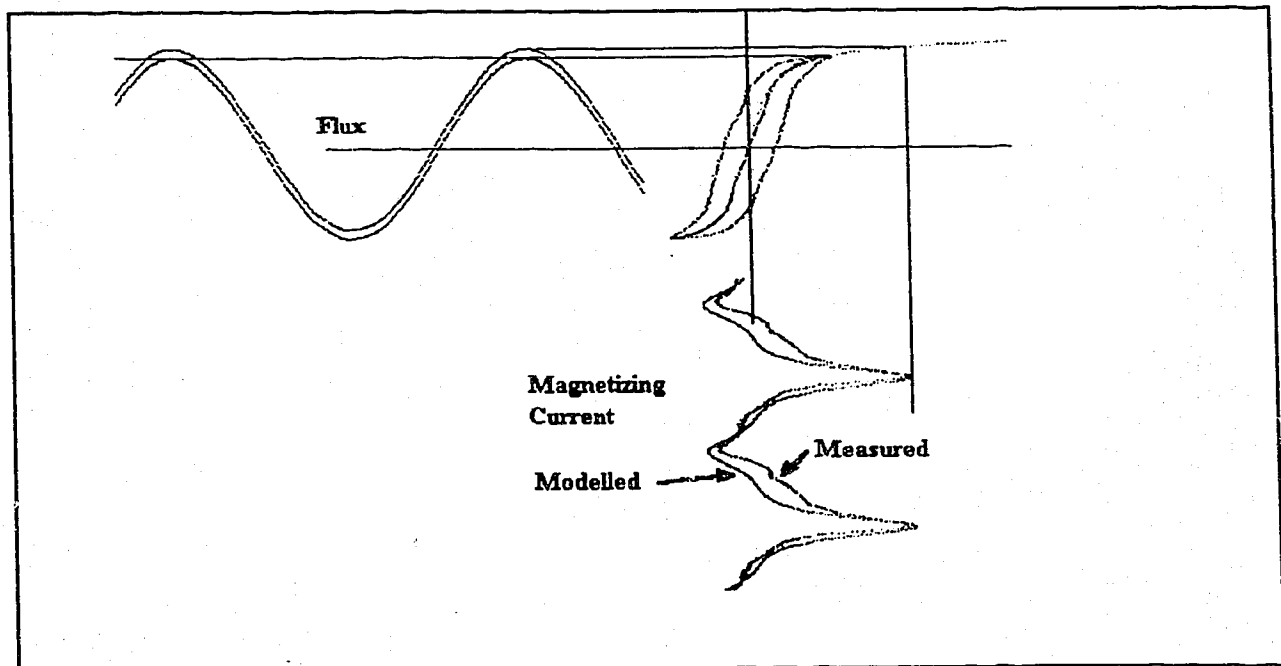


Figure 2.3.5 - Modelled and Measured Magnetizing Current

2.4 Power Transformer Frequency Response

It is of interest to determine how well harmonics generated by nonsinusoidal loads flow through transformers and into the power system. The transformer model developed in Section 2.1 is based solely on leakage reactance and passes harmonics without attenuation. To determine if this is a sufficiently accurate model it is necessary to examine a more detailed model and to measure the frequency response of a power transformer and then analyze the results. The flux leakage model has a unity current gain (the ratio of primary per unit current to secondary per unit current). Should the more detailed model and the measurements show a similar gain, then the use of the flux leakage model is justified. The range from 50 to 5000 Hz is specified in the IEEE standards [25] [26] [27] [28], and in the regulations invoked by power utilities [2] [59].

Figure 2.4.1 shows a more detailed single phase transformer model supplying a resistive load. The frequency response of such a model can be defined by the ratio of load current divided by primary current.

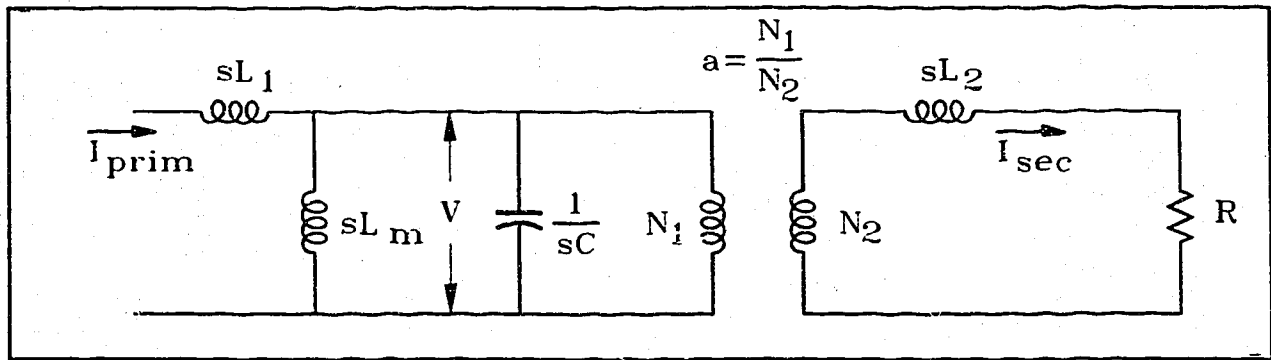


Figure 2.4.1 - Transformer Frequency Response Model

Defining the parallel combination of L_m and C as the magnetizing branch impedance results in,

$$Z_m = \frac{s L_m \left[\frac{1}{s C} \right]}{s L_m + \frac{1}{s C}} = \frac{\frac{L_m}{C}}{s L_m + \frac{1}{s C}} \quad (2.4.1)$$

Defining the series combination of L_2 and R reflected to the primary side by the turns ratio a as the load impedance results in,

$$Z_L = a^2 s L_2 + a^2 R \quad (2.4.2)$$

(where s is the Laplace operator). Reflecting the secondary current to the primary side defines a gain ratio,

$$\frac{I_{sec}'}{I_{prim}} = \frac{Z_m}{Z_m + Z_L} \quad (2.4.3)$$

where I_{sec}' is the secondary current reflected to the primary side.

Substituting and simplifying results in equation (2.4.4):

$$\frac{I_{sec}'}{I_{prim}} = \frac{s L_m}{s^3 a^2 L_2 L_m C + s^2 a^2 R L_m C + s [a^2 L_2 + L_m] + a^2 R} \quad (2.4.4)$$

The frequency response is,

$$\frac{I_{sec}'}{I_{prim}} = \frac{j\omega L_m}{(j\omega)^3 a^2 L_2 L_m C + (j\omega)^2 a^2 R L_m C + j\omega [a^2 L_2 + L_m] + a^2 R} \quad (2.4.5)$$

The transformer parameters shown in Table 2.4.1 were obtained from laboratory measurements on a Wye-Wye transformer with a 277/120 turns ratio.

Table 2.4.1 - Measured Parameters For 3 kVA Wye-Wye Transformer

R (load)	L_m	$C_{\text{prim-gnd}}$	L_2
79.34 Ohm	3.4 Henry	2×10^{-9} Farads	0.00169 Henry

The frequency response model was validated in the laboratory by supplying one leg of a 3 kVA transformer with varying frequency voltage from a Radio Frequency Laboratory Model 250 RC Oscillator. A load of 79.34 Ohms was placed on the secondary. This simulated the lightly loaded condition, which exaggerated the effect of magnetizing current on the current gain. Measurements were taken as the frequency was varied from 60 Hz to 3000 Hz (the range of the Model 250 RC Oscillator) and documented in Table 2.4.2. The primary voltage was maintained at 100 Volts.

The modelled and measured frequency responses are shown in figure 2.4.2. The Model shows near unity gain (0 dB) is not achieved until the frequency reaches approximately 300 rad/sec (48 Hz). Unity gain is, of course, never reached due to the current drawn by the magnetizing branch. The measured gain approaches unity (0 dB) and the gain curve lies within 0.5 dB of the modelled results once the frequency exceeds 1000 Hz. The modeled gain is flat up to 100,000 rad/sec (16,000 Hz).

The conclusion from this is that a power transformer passes current harmonics with negligible attenuation. It is therefore reasonable to neglect winding capacitance and the magnetizing branch admittance when developing the linear transformer model provided the frequency is restricted to a range of 50 to 5000 Hz.

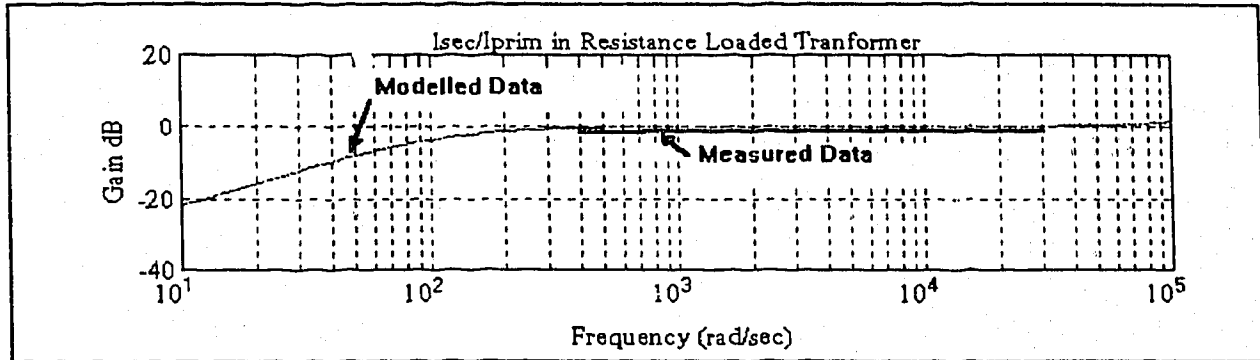


Figure 2.4.2 Modelled Frequency Response - 3 kVA Transformer With a 79.34 Ohm Load

Table 2.4.2 - Frequency Response Data Obtained From Experimental Measurement of a 3 kVA Transformer ($a = 480 / 208$)

Hz	I_p	I_s	$I_s' = I_s/a$	$20 \log_{10}(I_s'/I_p)$
60	.2847	.5429	.2352	-1.65
120	.2742	.5288	.2291	-1.56
240	.2645	.5408	.2343	-1.05
480	.2494	.5299	.2296	-0.72
960	.2553	.5534	.2398	-0.54
1920	.2446	.5375	.2329	-0.42
3000	.2391	.5256	.2278	-0.42

2.5 Three Phase Induction Motor Model Derivation

The three phase admittance model for an induction motor developed in this section is based upon a symmetrical components approach as historically the sequence parameters are readily available for induction motors. The following assumptions are made:

- a) The stator is a delta or an ungrounded wye configuration
- b) Each phase has a symmetrical construction with $Z_a = Z_b = Z_c$
- c) The air gap in the magnetizing path permits the nonlinear effects to be considered negligible [9].

With these assumptions, symmetrical components can be applied to develop a coupled three phase admittance matrix of the motor. This approach is used as the sequence components are orthogonal and lead to a diagonal matrix which is easy to invert. Once the sequence admittance matrix is obtained, the phase admittance matrix can be realized by means of the transformation matrices which relate the phase and sequence quantities.

The phase to sequence transformation is given by,

$$A = \begin{bmatrix} 1 & 1 & 1 \\ a^2 & a & 1 \\ a & a^2 & 1 \end{bmatrix} \quad (2.5.1)$$

where $a = e^{j\frac{2\pi}{3}}$ (2.5.2)

The sequence to phase transformation is given by

$$A^{-1} = \frac{1}{3} \begin{bmatrix} 1 & a^2 & a \\ 1 & a & 1 \\ 1 & 1 & 1 \end{bmatrix} \quad (2.5.3)$$

In the phase frame of reference the expression for voltage is given by,

$$|V_{ph}| = |Z_{ph}| |I_{ph}| \quad (2.5.4)$$

and the inverse of phase impedance is phase admittance,

$$|Y_{ph}| = |Z_{ph}|^{-1} \quad (2.5.5)$$

In the sequence frame of reference the expression for voltage is given by,

$$|V_{seq}| = |Z_{seq}| |I_{seq}| \quad (2.5.6)$$

and the inverse of sequence impedance is sequence admittance,

$$|Y_{seq}| = |Z_{seq}|^{-1} \quad (2.5.7)$$

The positive, negative and zero sequence networks are uncoupled if the impedance network elements are balanced hence the sequence impedance,

$$|Z_{seq}| = \begin{bmatrix} Z_p & 0 & 0 \\ 0 & Z_n & 0 \\ 0 & 0 & Z_0 \end{bmatrix} \quad (2.5.8)$$

is readily inverted by taking the inverse of each diagonal element, yielding,

$$|Z_{seq}|^{-1} = \begin{bmatrix} \frac{1}{Z_p} & 0 & 0 \\ 0 & \frac{1}{Z_n} & 0 \\ 0 & 0 & \frac{1}{Z_0} \end{bmatrix} = \begin{bmatrix} Y_p & 0 & 0 \\ 0 & Y_n & 0 \\ 0 & 0 & 0 \end{bmatrix} \quad (2.5.9)$$

(Note that $\frac{1}{Z_0} \rightarrow 0$ in an ungrounded machine)

where Z_p , Z_n , and Z_0 are the positive, negative, and zero sequence impedances respectively as described by Wagner and Evans in [61].

The following equations develop the transformation relationship between phase admittance and sequence admittance. Rearranging equation (2.5.6) obtains the sequence current,

$$|I_{seq}| = |Z_{seq}^{-1}| |V_{seq}| \quad (2.5.10)$$

The sequence and phase voltages are related by equation (2.5.11)

$$|V_{seq}| = A^{-1} |V_{ph}| \quad (2.5.11)$$

and the sequence and phase currents are related by equation (2.5.12)

$$|I_{seq}| = A^{-1} |I_{ph}| \quad (2.5.12)$$

Substituting equation (2.5.11) and equation (2.5.12) into equation (2.5.10) yields,

$$A^{-1} |I_{ph}| = |Z_{seq}|^{-1} A^{-1} |V_{ph}| \quad (2.5.13)$$

Pre-multiplying both sides by **A** obtains phase current,

$$|I_{ph}| = A |Z_{seq}|^{-1} A^{-1} |V_{ph}| \quad (2.5.14)$$

and rearranging equation (2.5.4) yields equation (2.5.15),

$$|I_{ph}| = |Z_{ph}^{-1}| |V_{ph}| \quad (2.5.15)$$

Substituting equation (2.5.5) admittance into equation (2.5.15) yields,

$$|I_{ph}| = |Y_{ph}| |V_{ph}| \quad (2.5.16)$$

Comparing equation (2.5.14) with equation (2.5.16) gives equation (2.5.17)

$$|Y_{ph}| = A |Z_{seq}|^{-1} A^{-1} \quad (2.5.17)$$

and substituting equation (2.5.7) into (2.5.17) results in phase admittance,

$$|Y_{ph}| = A |Y_{seq}| A^{-1} \quad (2.5.18)$$

expressed in terms of sequence admittance. This important result is used to build a phase quantity admittance matrix from a sequence quantity admittance matrix. Expanding the phase admittance,

$$|Y_{ph}| = \begin{bmatrix} 1 & 1 & 1 \\ a^2 & a & 1 \\ a & a^2 & 1 \end{bmatrix} \begin{bmatrix} Y_p & 0 & 0 \\ 0 & Y_n & 0 \\ 0 & 0 & 0 \end{bmatrix} \frac{1}{3} \begin{bmatrix} 1 & a & a^2 \\ 1 & a^2 & a \\ 1 & 1 & 1 \end{bmatrix} \quad (2.5.19)$$

and collecting the products results in equation (2.5.20)

$$|Y_{ph}| = \frac{1}{3} \begin{bmatrix} Y_p + Y_n & a Y_p + a^2 Y_n & a^2 Y_p + a Y_n \\ a^2 Y_p + a Y_n & Y_p + Y_n & a Y_p + a^2 Y_n \\ a Y_p + a^2 Y_n & a^2 Y_p + a Y_n & Y_p + Y_n \end{bmatrix} \quad (2.5.20)$$

This formulation of the matrix permits a motor admittance matrix to be constructed from its sequence component impedances. These are readily available from manufacturers for larger machines and can be estimated for smaller machines using the following method. The positive sequence impedance,

$$Z_p \approx \frac{V_{rated}}{I_{fl}} \angle \cos^{-1}(pf_{fl}) \quad (2.5.21)$$

is obtained from the motor full load current, I_{fl} , and power factor, pf_{fl} , at rated voltage, V_{rated} , and the negative sequence impedance,

$$Z_n \approx \frac{V_{rated}}{I_{lr}} \angle \cos^{-1}(pf_{lr}) \quad (2.5.22)$$

is approximately obtained from the motor locked rotor current, I_{lr} , and the locked rotor power factor, pf_{lr} , at rated voltage. This is due to the similarity between the motor starting equivalent circuit and the negative sequence equivalent circuit [10]. In the absence of manufacturer's data the starting power factors can be estimated from Table 2.5.1.

Table 2.5.1 Typical Locked Rotor Power Factors

Motor	LV Induction	MV Induction	MV Synchronous
PF	.25	.2	.15

In order to determine if the magnetizing current of an induction motor contains significant harmonic content, measurements were taken on a no load test of a 50 HP 460 volt 6 pole NEMA design B induction motor. The no load test was selected as under this operating condition almost all of the current drawn by the motor is magnetizing current. The voltage (trace 1) and no load current (trace 2) in figure 2.5.1 were subjected to a Fourier analysis and the results are tabulated in table 2.5.2. Note the voltage probe was set for a 600 volt system and this has been corrected for 480 volts. As shown in Table 2.5.2 the higher order harmonics are negligible (less than 4%). This analysis indicates that the motor magnetizing branch is reasonably linear and can be approximated by representing it with an inductance and a resistance.

For the first fifty harmonic orders, a reasonable harmonic model for the motor is arrived at by multiplying the inductive reactive components of equation (2.5.8) by the harmonic order, and by dividing the rotor equivalent resistance by harmonic slip. As is shown in Section 2.7 the harmonic slip on the rotor of a rotating machine is near unity and this makes the reflected rotor resistance small. As a result the harmonic current flow into a motor is governed by the leakage inductance.

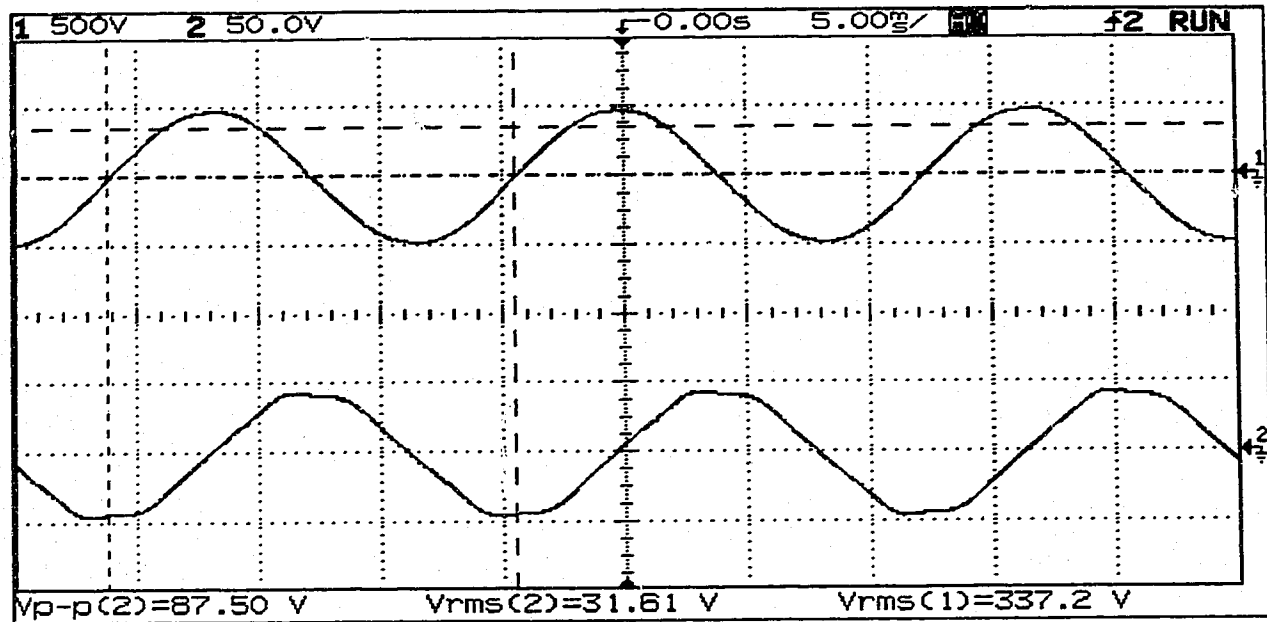


Figure 2.5.1 - 50 HP Motor B Phase Voltage (1) and No Load Current (2)

Table 2.5.2 - 50 HP Motor Voltage and No Load Current Harmonics

Harmonic Order	Harmonic Voltage	Harmonic Current
1	272.4 Volts at 0 degrees	31.5 Amps at -86.2 degrees
3	3.7	0.2
5	2.6	1.0
7	1.4	0.5
9	0.4	0.1
11	0.7	0.0
13	0.2	0.1

2.6 Cable Model Derivation

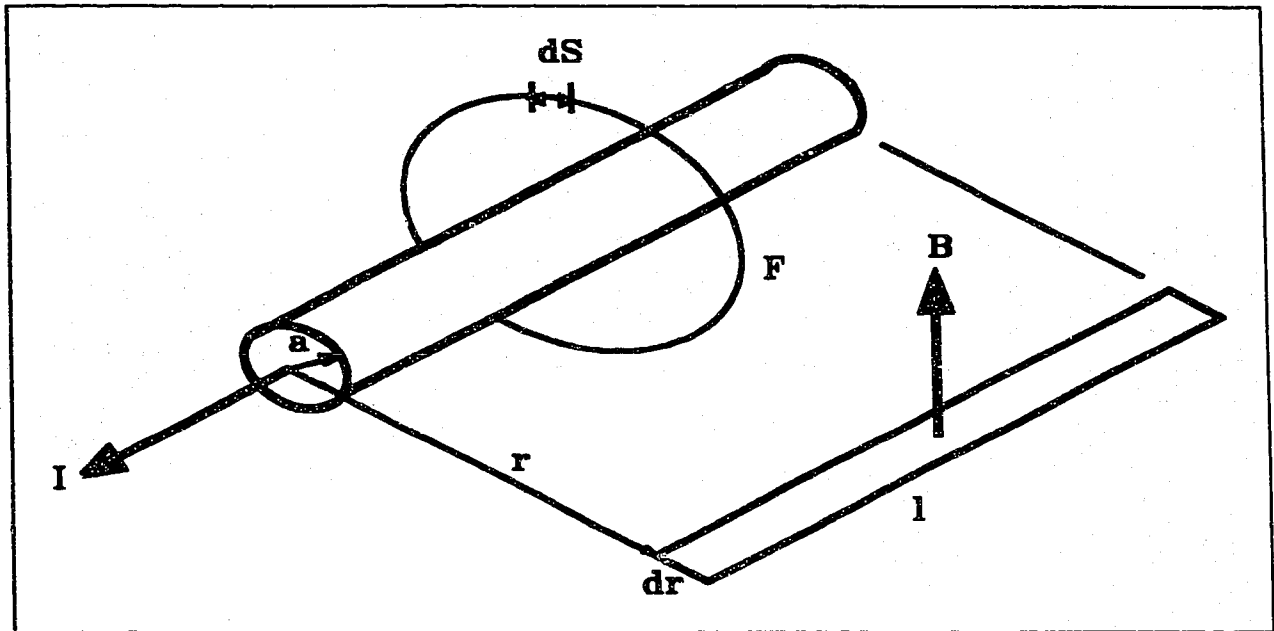


Figure 2.6.1 - Flux Field Surrounding a Conductor Carrying Current

The inductance in a cable is related to its physical geometry and the skin effect at higher frequencies. Stranded and solid conductors behave in a similar fashion [53]. Figure 2.6.1 shows the geometry of a single cylindrical conductor.

The starting point to obtain a nodal admittance model is to review the basic conductor equations. If current I flows through a conductor of radius a and length l , the number of turns, N , ($N=1$ in figure 2.6.1) and the magnetic field intensity, H , is related to the current, I by the magnetomotive force,

$$F = \oint H dS = NI = 2 \pi r H \quad (2.6.1)$$

Therefore the magnetic field intensity,

$$H = \frac{NI}{2 \pi r} \quad (2.6.2)$$

and flux density, B is;

$$B = \mu H = \frac{\mu N I}{2 \pi r} \quad (2.6.3)$$

where μ is the magnetic permeability. To obtain the flux linkage we integrate the area through which the flux density applies to obtain flux, ϕ , and multiply by N to obtain flux linkages, λ , yielding equation (2.6.4)

$$\lambda = N \phi = N \int_0^{\infty} B l dr = \frac{\mu l I}{2 \pi} \int_0^{\infty} \frac{N^2}{r} dr \quad (2.6.4)$$

In free space the inductance due to flux, L , is linear, and is expressed by,

$$L = \frac{\lambda}{I} = L_{internal} + L_{external} = \frac{\mu l}{2 \pi} \int_0^a \left(\frac{2 \pi r^2}{2 \pi a^2} \right)^2 \frac{N^2}{r} dr + \frac{\mu l}{2 \pi} \int_a^{\infty} \frac{N^2}{r} dr \quad (2.6.5)$$

For inductance due to flux linkage internal to the conductor the current density is assumed to be uniform, $N=1$ for a single conductor and the current is assumed to be partially linked by the ratio of conductor cross-sectional areas yielding,

$$L_{internal} = \frac{\mu l}{2 \pi} \left[\frac{1}{4} \right] \quad (2.6.6)$$

This internal flux linkage and inductance decreases as frequency increases due to skin effect. This decrease is noticeable in cables as the conductors are close together making the internal inductance a significant fraction of the total. Equation (2.6.6) is therefore modified to account for frequency effects as follows:

$$L_{internal} = \frac{\mu l}{2 \pi} \left[\frac{1}{4} \right] [K_{skin\ effect}] \quad (2.6.7)$$

The skin effect factor is calculated by the use of Bessel functions. A frequency dependent factor, m is defined by equation (2.6.8) as,

$$m = \sqrt{\frac{2 \pi f \mu}{\rho}} \quad (2.6.8)$$

where ρ is the conductivity in Ohm-metres of the conductor.

With reference to figure 2.6.1, the conductor radius, a , is used to define the skin effect factor,

$$K_{\text{skin effect}} = \left[\frac{4}{m a} \right] \left[\frac{\text{ber}(m a) \text{ber}'(m a) + \text{bei}(m a) \text{bei}'(m a)}{[\text{ber}'(m a)]^2 + [\text{bei}'(m a)]^2} \right] \quad (2.6.9)$$

where the real (**ber**) and imaginary (**bei**) components of the Bessel function and their first derivatives are defined by equations (2.6.10) through (2.6.13)

$$\text{ber}(m a) = 1 - \frac{[m a]^4}{(2)^2 (4)^2} + \frac{[m a]^8}{(2)^2 (4)^2 (6)^2 (8)^2} - \dots \quad (2.6.10)$$

$$\text{ber}'(m a) = \frac{d}{d(m a)} \text{ber}(m a) = - \frac{[m a]^3}{(2)^2 (4)} + \frac{[m a]^7}{(2)^2 (4)^2 (6)^2 (8)} - \dots \quad (2.6.11)$$

$$\text{bei}(m a) = \frac{[m a]^2}{(2)^2} - \frac{[m a]^6}{(2)^2 (4)^2 (6)^2} + \frac{[m a]^{10}}{(2)^2 (4)^2 (6)^2 (8)^2 (10)^2} - \dots \quad (2.6.12)$$

$$\text{bei}'(m a) = \frac{m a}{2} - \frac{[m a]^5}{(2)^2 (4)^2 (6)} + \frac{[m a]^9}{(2)^2 (4)^2 (6)^2 (8)^2 (10)} - \dots \quad (2.6.13)$$

The flux linkage between two points "a" and "D" external to an isolated conductor is used to redefine the external inductance for a two conductor line with spacing "D" between the

conductors. This development is given in [53]. The result is

$$L_{external} = \frac{\mu l}{2 \pi} \left[\ln \left(\frac{D}{a} \right) \right] \text{ (per conductor)} \quad (2.6.14)$$

Combining equations (2.6.7) for internal inductance and equation (2.6.14) for external inductance for a single phase, two conductor cable, with spacing **D** between conductors yields the total inductance,

$$L = \frac{\mu l}{2 \pi} \left[\frac{K_{skin \ effect}}{4} + \ln \left(\frac{D}{a} \right) \right] \text{ (per conductor)} \quad (2.6.15)$$

For a three phase, three wire cable the flux linkage equations can be written to include mutual effects. Assuming the sum of the currents in the three phases is zero, the "D" terms cancel and the "a" phase flux linkage is given by,

$$\lambda_a = \frac{\mu l}{2 \pi} \left[I_a \left(\frac{K_{skin \ effect}}{4} + \ln \frac{1}{D_{aa}} \right) + I_b \left(\ln \frac{1}{D_{ab}} \right) + I_c \left(\ln \frac{1}{D_{ac}} \right) \right] \quad (2.6.16)$$

where,

D_{aa} = radius of conductor a

D_{ab}, D_{ac}, D_{bc} = distance between the conductors

Ignoring resistance for the moment, the voltage drop across conductor "a" is determined by the frequency ω as follows:

$$\Delta V_a = j \omega \lambda_a = j \omega L_{aa} I_a + j \omega L_{ab} I_b + j \omega L_{ac} I_c \quad (2.6.17)$$

where L_{aa} , L_{ab} , and L_{ac} are self and mutual inductances as defined by the constant coefficients of equation (2.6.16).

Skin effect also increases conductor resistance as frequency increases. The ratio of effective A.C. resistance to D.C. resistance as a function of ma is given by,

$$\frac{R_{AC}}{R_{DC}} = \left[\frac{m a}{2} \right] \left[\frac{\text{ber}(m a) \text{bei}'(m a) - \text{bei}(m a) \text{ber}'(m a)}{[\text{ber}'(m a)]^2 + [\text{ber}'(m a)]^2} \right] \quad (2.6.18)$$

Combining resistance with reactance to form impedance obtains the primitive impedance,

$$Z_{PRIM} = \begin{bmatrix} Z_{aa} & Z_{ab} & Z_{ac} \\ Z_{ba} & Z_{bb} & Z_{bc} \\ Z_{ca} & Z_{cb} & Z_{cc} \end{bmatrix} \quad (2.6.19)$$

Inverting the primitive impedance matrix forms the primitive admittance matrix resulting in,

$$Y_{PRIM} = Z_{PRIM}^{-1} = \begin{bmatrix} Y_{aa} & Y_{ab} & Y_{ac} \\ Y_{ba} & Y_{bb} & Y_{bc} \\ Y_{ca} & Y_{cb} & Y_{cc} \end{bmatrix} \quad (2.6.20)$$

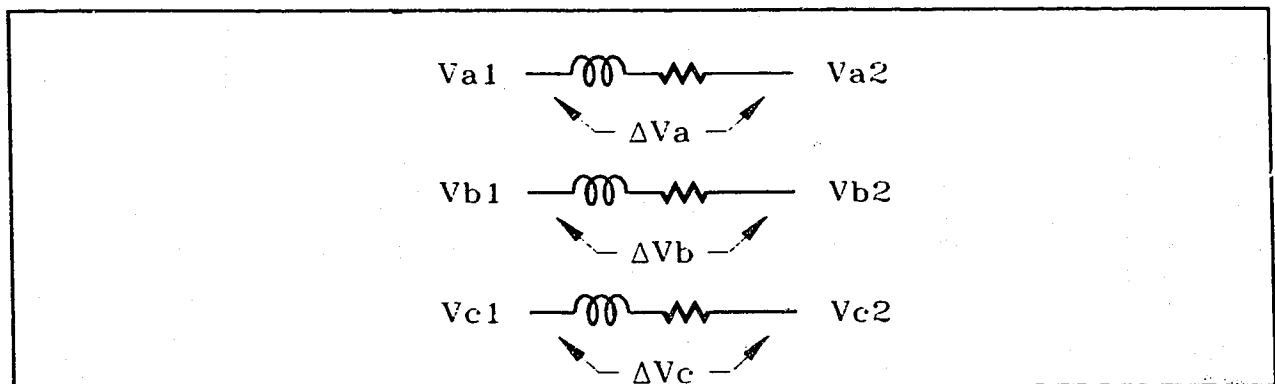


Figure 2.6.2 - Branch and Nodal Cable Voltages

With reference to figure 2.6.2 the primitive admittance can be converted to a nodal admittance for inclusion in the Y_{BUS} admittance matrix. The branch and nodal voltages are related by a connection matrix, shown in equation (2.6.21),

$$\begin{bmatrix} \Delta V_a \\ \Delta V_b \\ \Delta V_c \end{bmatrix} = \begin{bmatrix} 1 & -1 & 0 & 0 & 0 & 0 \\ 0 & 0 & 1 & -1 & 0 & 0 \\ 0 & 0 & 0 & 0 & 1 & -1 \end{bmatrix} \begin{bmatrix} V_{a1} \\ V_{a2} \\ V_{b1} \\ V_{b2} \\ V_{c1} \\ V_{c2} \end{bmatrix} \quad (2.6.21)$$

and this connection matrix is used to relate the primitive admittances to the nodal admittances,

$$Y_{NODAL} = C^T Y_{PRIM} C \quad (2.6.22)$$

Expanding equation (2.6.22) yields the nodal admittance matrix,

$$Y_{NODAL} = \begin{bmatrix} y_{aa} & -y_{aa} & y_{ab} & -y_{ab} & y_{ac} & -y_{ac} \\ -y_{aa} & y_{aa} & -y_{ab} & y_{ab} & -y_{ac} & y_{ac} \\ y_{ba} & -y_{ba} & y_{bb} & -y_{bb} & y_{bc} & -y_{bc} \\ -y_{ba} & y_{ba} & -y_{bb} & y_{bb} & -y_{bc} & y_{bc} \\ y_{ca} & -y_{ca} & y_{cb} & -y_{cb} & y_{cc} & -y_{cc} \\ -y_{ca} & y_{ca} & -y_{cb} & y_{cb} & -y_{cc} & y_{cc} \end{bmatrix} \quad (2.6.23)$$

By inspection of the nodal admittance matrix in equation (2.6.23) and recalling that the off-diagonal elements of an admittance matrix are the negative values of the branch admittances of a circuit, one can create a model to assist in the implementation of a computer program. In essence, the mutually coupled elements are reduced to a grouping of linear elements with no mutual coupling as depicted in figure 2.6.3. The method uses a three conductor example, but it applies equally well to cables with any number of conductors.

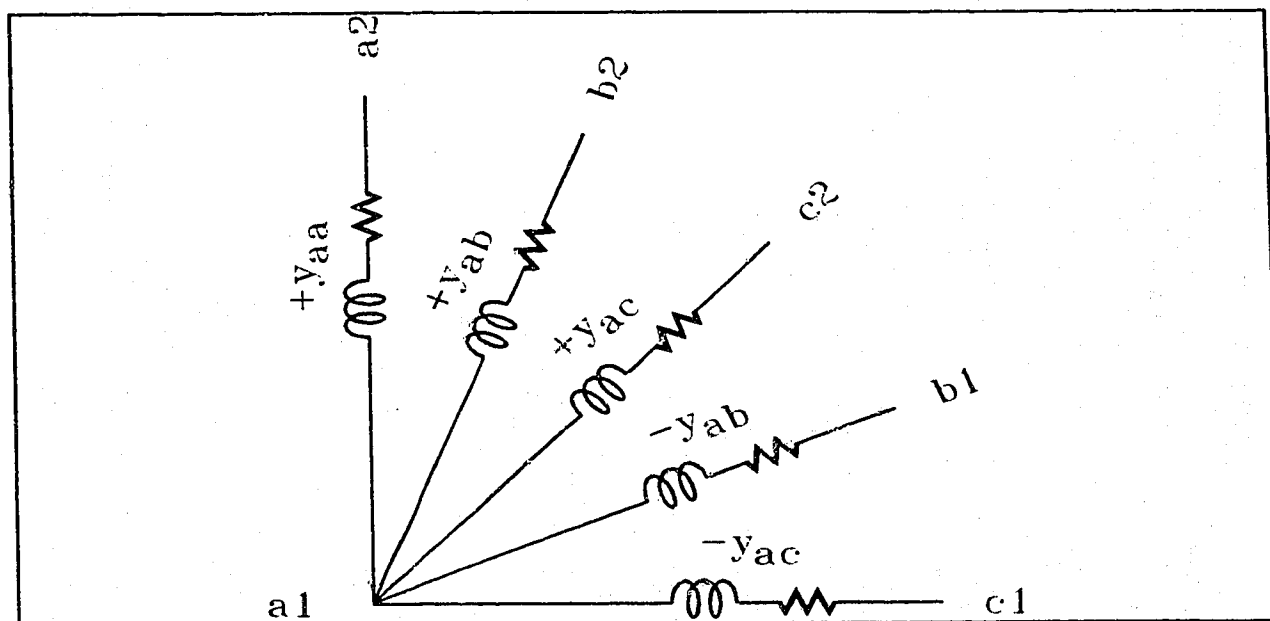


Figure 2.6.3 - Admittance Model For Branches Connected To Node a1

The computer algorithm requires cable geometry data to construct the model. Steel armoured designs would require some modification to the above equations, and are not included in this model. Cable capacitance is modeled by adding capacitors to the cables at the nodes. Should cables exceed 4 kilometres in length this model becomes inaccurate and the cable has to be broken into segments. The hyperbolic long line equations would be required for very long power cables but have not been incorporated as the "modal analysis" technique for doing so is well documented [5].

2.7 Synchronous Generator Model Derivation

The study of generators in unbalanced power systems requires two models. A phase coupled model is required for system analysis, and a rotor heating model is required to assess generator derating. A simplified three phase generator model is developed later in this section. This model is based on previous work [37] and is sufficient for the purpose of analyzing a power network. It can incorporate second order effects of the nonlinear magnetizing reactance which are well described by others [47] [68]. These second order effects are less than 3%. To analyze rotor heating requires a separate detailed model of the rotor circuit and analysis of its empirical thermal behaviour.

2.7.1 Rotor Heating Model

In industrial power systems, and particularly in those which are isolated from a major utility, the generation is provided by small local units. An example of this situation occurs in off shore oil production platforms, where the generator sizes range from 500 kVA to 4 MVA. Modern oil production is achieved by down-hole motors driven by variable frequency drives. The harmonic loading on these generators is much more severe than has been historically experienced by large utility generators. There have been instances³ where the generators have burned out from harmonic heating in situations where the total kVA loading is only 75% of the generator rating.

The synchronous generator neutral connection is sometimes connected to a neutral resistor or to a neutral inductor. The model of the generator under balanced and unbalanced fundamental frequency conditions has been described by utilizing Park's transformation to derive what has come to be known as the "d-q" model [3]. When the generator is subjected to frequencies which are integer multiples of the fundamental, the

³ Pemex Oil in their oil field in the Bay of Campeche 200 kilometres east of Ciudad del Carmen, Mexico lost two generators in 1993, both supplying VFDs.

"d-q" model (which is based on a rotor frame of reference) can be replaced by a much simpler model based on the stator frame of reference and which is an adaptation of the induction motor model. To describe a behaviour for the generator when it is subjected to harmonics, the braking behaviour of the amortisseur bars to negative sequence current provides an appropriate starting point.

The negative sequence component associated with unbalanced conditions induces a current of twice rated frequency in the rotor circuits. This keeps the flux linkages of the rotor near zero, and as a result of this the flux of the armature current is forced into paths of low permeance in the tips of the rotor poles; hence, this flux links the amortisseur bars and little else [31]. Since the negative sequence magnetomotive force (mmf) wave moves at twice the rotor speed it alternately sees two rotor permeances corresponding to the subtransient direct and quadrature reactances x_d'' and x_q'' . The negative sequence reactance, x_2 , is therefore approximately equal to the average of the two, as shown by,

$$x_2 = \frac{x_d'' + x_q''}{2} \quad (2.7.1)$$

Equation (2.7.1) defines the fundamental frequency harmonic reactance of the generator. It can be used for other harmonic orders by multiplying the reactances by the harmonic order. Converting the negative sequence reactance to inductance by dividing by fundamental frequency, ω_0 , yields,

$$L_2 = \frac{x_d'' + x_q''}{2 \omega_0} \quad (2.7.2)$$

which can be determined from standard machine parameters. By similar reasoning, the mmf associated with higher frequencies will also see the average of the two rotor permeances corresponding to the subtransient direct and quadrature reactances x_d'' and x_q'' , hence the harmonic impedance is given by,

$$x_h = \omega L_2 = h \left[\frac{x_d'' + x_q''}{2} \right] \quad (2.7.3)$$

Thus the negative sequence inductance provides a reasonable model for the generator for harmonics higher than the fundamental. This method is used in IEEE Std. 519 and is verified by field measurement of a 266 kW generator with a 150 kW VFD six pulse load, as recorded in Table 2.7.1. The observed values for the 5th, 7th, 11th, and 13th harmonics agree with the machine parameters and equation (2.7.3). The machine parameters were $x_q'' = 0.092$ per unit and $x_d'' = 0.10$ per unit. The 5th, 7th, 11th, and 13th harmonics validate the approximation as shown by the impedances in the final column of the table. The values for the 3rd and 9th zero sequence harmonics are much larger than the harmonic order multiplied by the negative sequence impedance. This is an indication that the generator ground connection circuit may have contained some impedance. The measured results for the triplens are not otherwise explainable.

Table 2.7.1- Harmonic Impedance of 266 kW Generator ⁴

h	V _h	I _h	Z _h	Z _h /h
3	.0320	.0160	2.00	.667
5	.1450	.2720	.533	.107
7	.0624	.0992	.630	.090
9	.0180	.0040	4.50	.500
11	.0722	.0730	.989	.090
13	.0598	.0460	1.30	.100

⁴

The data was made available by Mr. M. Sieberg, Principal Electrical Engineer, Kato Engineering Division of Reliance Electric, Mankato, Minnesota.

Harmonic current is induced into the amortisseur bars of the generator rotor. These bars slip with respect to the harmonic current in the stator. Ignoring the even harmonics, the following considerations must be allowed for the odd harmonics:

Firstly all "triples" harmonics behave similarly to zero sequence current. They create flux on each phase of the stator which is stationary in space, hence induce into the rotor a frequency which is the same as the stator harmonic frequency. These "triples" see an inductance equivalent to the zero sequence of the generator which is usually less than the subtransient inductance. In addition, if there is any impedance, Z_g , in the neutral connection three times the value of this impedance must be included in the model.

Applying Park's transformation to stator harmonic phase current yields the stator current **d-q-0** components. While an AC current at the fundamental frequency on the stator implies a DC current in the rotor, this is not true for harmonic currents. Harmonic currents on the stator create harmonic currents on the rotor. These rotor currents are functions of the stator **d-q-0** currents [3], hence harmonics appearing in the stator direct axis currents will be present in the rotor currents. The **d-q-0** stator currents for zero sequence stator harmonics are given by,

$$\begin{bmatrix} I_d \\ I_q \\ I_o \end{bmatrix} = \sqrt{\frac{2}{3}} \begin{bmatrix} \cos(\omega t) & \cos(\omega t - \frac{2\pi}{3}) & \cos(\omega t - \frac{4\pi}{3}) \\ \sin(\omega t) & \sin(\omega t - \frac{2\pi}{3}) & \sin(\omega t - \frac{4\pi}{3}) \\ \frac{1}{\sqrt{2}} & \frac{1}{\sqrt{2}} & \frac{1}{\sqrt{2}} \end{bmatrix} \begin{bmatrix} I \cdot \sin(h \omega t) \\ I \cdot \sin(h \omega t) \\ I \cdot \sin(h \omega t) \end{bmatrix} \quad (2.7.4)$$

Solving equation (2.7.4) yields,

$$\begin{bmatrix} I_d \\ I_q \\ I_o \end{bmatrix} = \sqrt{3} \cdot I \begin{bmatrix} 0 \\ 0 \\ \sin(h \cdot \omega t) \end{bmatrix} \quad (2.7.5)$$

which indicates the rotor currents are unaffected by the zero sequence component of the stator phase currents since I_d is zero.

Secondly, all odd harmonic pairs which lie on either side of integer multiples of the sixth harmonic create stator flux fields which rotate at multiples of six times the rotor speed, as shown in Table 2.7.1. For example consider the 5th and 7th harmonics. The 5th stator harmonic opposes the direction of the rotor, hence the rotor rotational speed must be added to the 5th harmonic's rotational speed. The result is that the rotor harmonic is $5 + 1 = 6$ for the 5th stator harmonic. The 7th stator harmonic rotates in the same direction as the rotor, hence the rotor harmonic is the difference between them, or $7 - 1 = 6$. Thus the 5th and 7th stator harmonics both appear to the rotor as a 6th harmonic. While the 5th harmonic creates a negative torque and the 7th harmonic creates a positive torque, these and higher order torque effects can be neglected since they are small and tend to cancel one another in terms of net steady state generator torque. The frequency conversion is demonstrated for positive sequence stator current by,

$$\begin{bmatrix} I_d \\ I_q \\ I_o \end{bmatrix} = \sqrt{\frac{2}{3}} \begin{bmatrix} \cos(\omega t) & \cos(\omega t - \frac{2\pi}{3}) & \cos(\omega t - \frac{4\pi}{3}) \\ \sin(\omega t) & \sin(\omega t - \frac{2\pi}{3}) & \sin(\omega t - \frac{4\pi}{3}) \\ \frac{1}{\sqrt{2}} & \frac{1}{\sqrt{2}} & \frac{1}{\sqrt{2}} \end{bmatrix} \begin{bmatrix} I \cdot \sin(h \omega t) \\ I \cdot \sin(h \omega t - \frac{2\pi}{3}) \\ I \cdot \sin(h \omega t + \frac{2\pi}{3}) \end{bmatrix} \quad (2.7.6)$$

Simplifying equation (2.7.6) gives the form,

$$\begin{bmatrix} I_d \\ I_q \\ I_o \end{bmatrix} = \sqrt{\frac{3}{2}} \cdot I \begin{bmatrix} \cos(\omega t) \cos(h \cdot \omega t) + \sin(\omega t) \sin(h \cdot \omega t) \\ \sin(\omega t) \cos(h \cdot \omega t) - \cos(\omega t) \sin(h \cdot \omega t) \\ 0 \end{bmatrix} \quad (2.7.7)$$

Using the trigonometric identities,

$$\begin{aligned} -\sin(a-b) &= \sin(b) \cos(a) - \sin(a) \cos(b) \\ \cos(a-b) &= \cos(a) \cos(b) + \sin(b) \sin(a) \end{aligned} \quad (2.7.8)$$

equation (2.7.7) yields **d-q-0** stator current,

$$\begin{bmatrix} I_d \\ I_q \\ I_o \end{bmatrix} = \sqrt{\frac{3}{2}} \cdot I \begin{bmatrix} \cos([h-1] \cdot \omega t) \\ -\sin([h-1] \cdot \omega t) \\ 0 \end{bmatrix} \quad (2.7.9)$$

The I_d component of (2.7.9) demonstrates that the rotor current frequency is one harmonic order less than the stator phase current when the stator phase current is positive sequence.

Similarly the **d-q-0** stator currents for negative sequence stator harmonics are given by,

$$\begin{bmatrix} I_d \\ I_q \\ I_o \end{bmatrix} = \sqrt{\frac{2}{3}} \begin{bmatrix} \cos(\omega t) & \cos(\omega t - \frac{2\pi}{3}) & \cos(\omega t - \frac{4\pi}{3}) \\ \sin(\omega t) & \sin(\omega t - \frac{2\pi}{3}) & \sin(\omega t - \frac{4\pi}{3}) \\ \frac{1}{\sqrt{2}} & \frac{1}{\sqrt{2}} & \frac{1}{\sqrt{2}} \end{bmatrix} \begin{bmatrix} I \cdot \sin(h \omega t) \\ I \cdot \sin(h \omega t + \frac{2\pi}{3}) \\ I \cdot \sin(h \omega t - \frac{2\pi}{3}) \end{bmatrix} \quad (2.7.10)$$

Simplifying equation (2.7.10) gives the form,

$$\begin{bmatrix} I_d \\ I_q \\ I_o \end{bmatrix} = \sqrt{\frac{3}{2}} \cdot I \begin{bmatrix} \cos(\omega t) \sin(h \cdot \omega t) + \sin(\omega t) \cos(h \cdot \omega t) \\ \sin(\omega t) \sin(h \cdot \omega t) - \cos(\omega t) \cos(h \cdot \omega t) \\ 0 \end{bmatrix} \quad (2.7.11)$$

Rearranging the trigonometric identities of equation (2.7.8) gives,

$$\begin{aligned}\sin(a+b) &= \sin(a)\cos(b) + \sin(b)\cos(a) \\ \cos(a+b) &= \cos(a)\cos(b) - \sin(b)\sin(a)\end{aligned}\tag{2.7.12}$$

which when substituted into equation (2.7.11) yields stator **d-q-0** current,

$$\begin{bmatrix} I_d \\ I_q \\ I_o \end{bmatrix} = \sqrt{\frac{3}{2}} \cdot I \begin{bmatrix} \sin([h+1] \cdot \omega t) \\ -\cos([h+1] \cdot \omega t) \\ 0 \end{bmatrix}\tag{2.7.13}$$

The I_d component of (2.7.13) demonstrates that the rotor current frequency is one harmonic order greater than the stator phase current when the stator phase current is negative sequence. The simplified consequence of these equations is that the rotor heating is a function of the odd zero sequence harmonics (3,9,15, etc.) as well as odd harmonic pairs lying on either side of the converter pulse number (5&7, 11&13, 17&19, etc.). Non-characteristic even harmonics are usually neglected due to them being small in magnitude, but if they are present they may be handled in the same way.

A simple generator model which includes the amortisseur bars can be constructed from R_s , the stator resistance, R_R , the rotor resistance reflected to the stator, L_m , the magnetizing inductance, s , the rotor slip as shown in Table 2.7.2, and the negative sequence inductance, L_2 , to arrive at the circuit in figure 2.7.1. The model is only useful for balanced harmonics and it suppresses triplen harmonic current in the rotor branch. If the harmonics were unbalanced the **d-q-0** current expressions would be more complex, and unbalanced triplen harmonics in the stator would give rise to harmonic currents in the rotor.

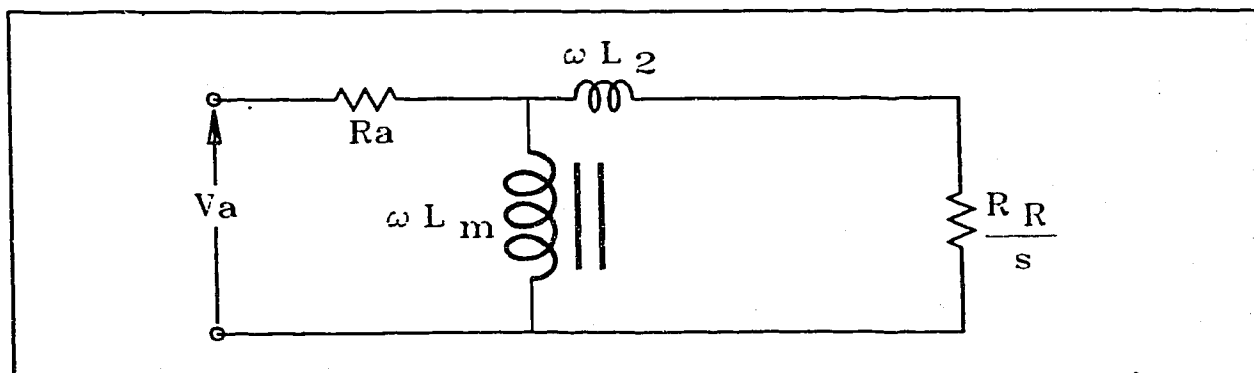


Figure 2.7.1 - Generator Rotor Harmonic Model

Table 2.7.2 - Generator Rotor Harmonics And Slip

Stator Harmonic	Rotor Harmonic	Rotor Slip
3	3	0
5,7	6	1.20, .857
9	9	0
11,13	12	1.09, .923
15	15	0
17,19	18	1.06, .947
21	21	0
23,25	24	1.04, .960
etc.	etc	etc.

When power generators are applied to an industrial power system which has a high percentage of solid state switched loads such as diode rectifiers or SCR converters, the rotors of the generators are subjected to harmonic heating. The harmonics created by a

diode rectifier or SCR converter are shown in Table 2.7.3 The characteristic harmonics are shown in bold type. In 12 pulse and 24 pulse systems the harmonic cancellation is not perfect, hence some of the six pulse harmonics exist. The characteristic harmonics exist as pairs (one positive and one negative) on either side of the pulse number.

For 6 pulse **characteristic $h = 6k \pm 1$**

For 12 pulse **characteristic $h = 12k \pm 1$**

For 24 pulse **characteristic $h = 24k \pm 1$** **$k = 1, 2, 3, \dots$ etc.**

Table 2.7.3 - Harmonics From Rectifiers And Converters

6 Pulse		12 Pulse		24 Pulse	
h	Typical Mag	h	Typical Mag	h	Typical Mag
1	100%	1	100%	1	100%
5	30%	5	3.0%	5	3%
7	14.3%	7	1.4%	7	1.4%
11	9.1%	11	9.1%	11	0.9%
13	7.7%	13	7.7%	13	0.7%
17	5.9%	17	0.5%	17	0.5%
19	5.2%	19	0.5%	19	0.5%
23	4.3%	23	4.3%	23	4%
25	4.0%	25	4.0%	25	4%
29	3.4%	29	0.3%	29	0.3%
31	3.2%	31	0.3%	31	0.3%
35	2.8%	35	2.8%	35	0.3%
37	2.7%	37	2.7%	37	0.3%

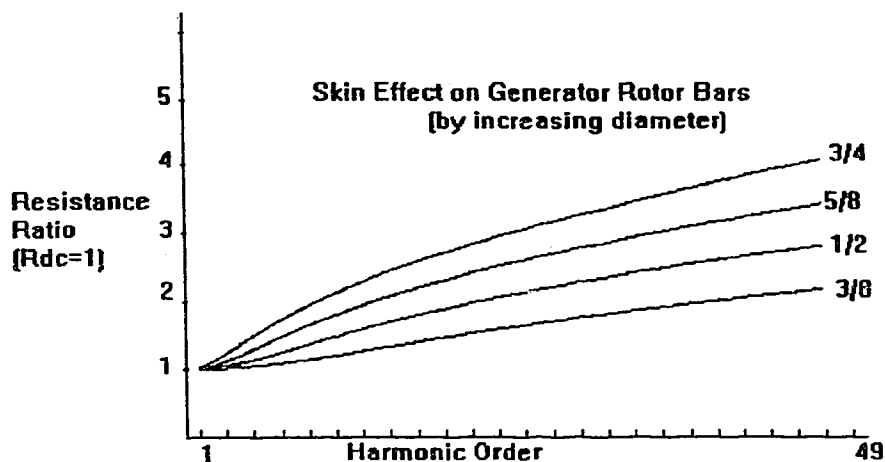


Figure 2.7.2 - Skin Effect on The Resistance of Generator Amortisseur Bars

Other harmonic orders may be generated by these loads under voltage unbalanced conditions, but provided the voltage unbalance is less than 2%, these other harmonics (often referred to as "non-characteristic") will be less than 0.2% of the fundamental magnitude and may be neglected when calculating generator rotor heating. The magnitudes shown are for waveforms supplying variable frequency Pulse Width Modulated (PWM) type drives which have large capacitors connected across the DC rails. Manufacturers' designs may vary from these magnitudes, but the table can be used for a "first approximation" calculation of the anticipated heating effects on a generator rotor.

Since each pair of harmonics above and below the integer multiples of 6 appear on the rotor at different frequencies, the rotor resistance must be adjusted for skin effect. Generators are commonly constructed with solid round copper damping bars built in the form of a "squirrel cage" or amortisseur winding. Bessel functions of the first kind, zero order were solved to obtain the resistance of the bars, as shown in figure 2.7.2. The heating in the rotor is then calculated from the heating due to each harmonic pair, given by,

$$Q = R_{6th} [I_5 + I_7]^2 + R_{12th} [I_{11} + I_{13}]^2 + \dots \quad (2.7.14)$$

This can be converted to an equivalent per unit negative sequence current from the expression,

$$I_{nequiv} = \sqrt{\frac{\frac{R \text{ Ratio}_{6th}}{R \text{ Ratio}_{2nd}} [I_5 + I_7]^2 + \frac{R \text{ Ratio}_{12th}}{R \text{ Ratio}_{2nd}} [I_{11} + I_{13}]^2 + \dots}{\dots + \frac{R \text{ Ratio}_{3rd}}{R \text{ Ratio}_{2nd}} [I_3]^2 + \frac{R \text{ Ratio}_{9th}}{R \text{ Ratio}_{2nd}} [I_9]^2 + \dots}} \quad (2.7.15)$$

where,

$$R \text{ Ratio}_h = \frac{R_h}{R_1} \quad (2.7.16)$$

and the harmonic current components in equation (2.7.15) are similarly expressed in per unit.

The reason for this latter equivalent is that most industrial generators are designed to withstand 10% negative sequence heating. It is possible for a generator manufacturer to increase this 10% limit by using a thicker than standard copper cage bar connector and larger diameter bars to form a low resistance squirrel cage, and by derating the generator by about 5%. With these modifications, a machine that can withstand up to 17% negative sequence heating, or its harmonic equivalent can be manufactured. In the 4 MVA to 10 MVA size range this has a cost impact of 3% to 5%.⁵

In certain cylindrical rotor designs, the generator has no amortisseur winding and the harmonic current will be primarily carried in the stainless steel slot wedges. In these

⁵ Cost and derating figures made available by Mr. T. Hammer, Chief Electrical Engineer, Ideal Generator Company.

designs the skin effect determines penetration into the wedge and the usual assumption is that the depth of penetration varies inversely as the square root of frequency [44]. For these machines equation (2.7.15) changes to,

$$I_{nequiv} = \sqrt{\sqrt{\frac{6f}{120}} [I_5 + I_7]^2 + \sqrt{\frac{12f}{120}} [I_{11} + I_{13}]^2 + \dots} \quad (2.7.17)$$

where f is the fundamental frequency.

Each term may be multiplied by a correction factor to convert from maximum rotor surface loss intensity to average surface loss. These factors are in the range of 0.4 to 0.5. For a conservative calculation equation (2.7.17) assumes them to be 1.0. The foregoing equations permit a designer to calculate the effect of harmonic loading on a generator. The equivalent percentage negative sequence current resulting from the characteristic harmonic currents in Table 2.7.3 are calculated in Table 2.7.4 for different diameters of round copper amortisseur bars, assuming the bars are carrying the same current density (Amps per square metre). In practice, generators designed to supply harmonic producing loads are equipped with larger bars to reduce the current density and lower the heating effect of the harmonics on the rotor.

Table 2.7.4 - Equivalent Negative Sequence Current For Characteristic Harmonics in Table 2.7.3

Diameter (inches)	3/16	1/4	3/8	1/2	5/8	3/4
6 Pulse	50%	51%	54%	58%	63%	68%
12 Pulse	20%	21%	23%	26%	28%	31%
24 Pulse	6%	9%	11%	12%	13%	14%

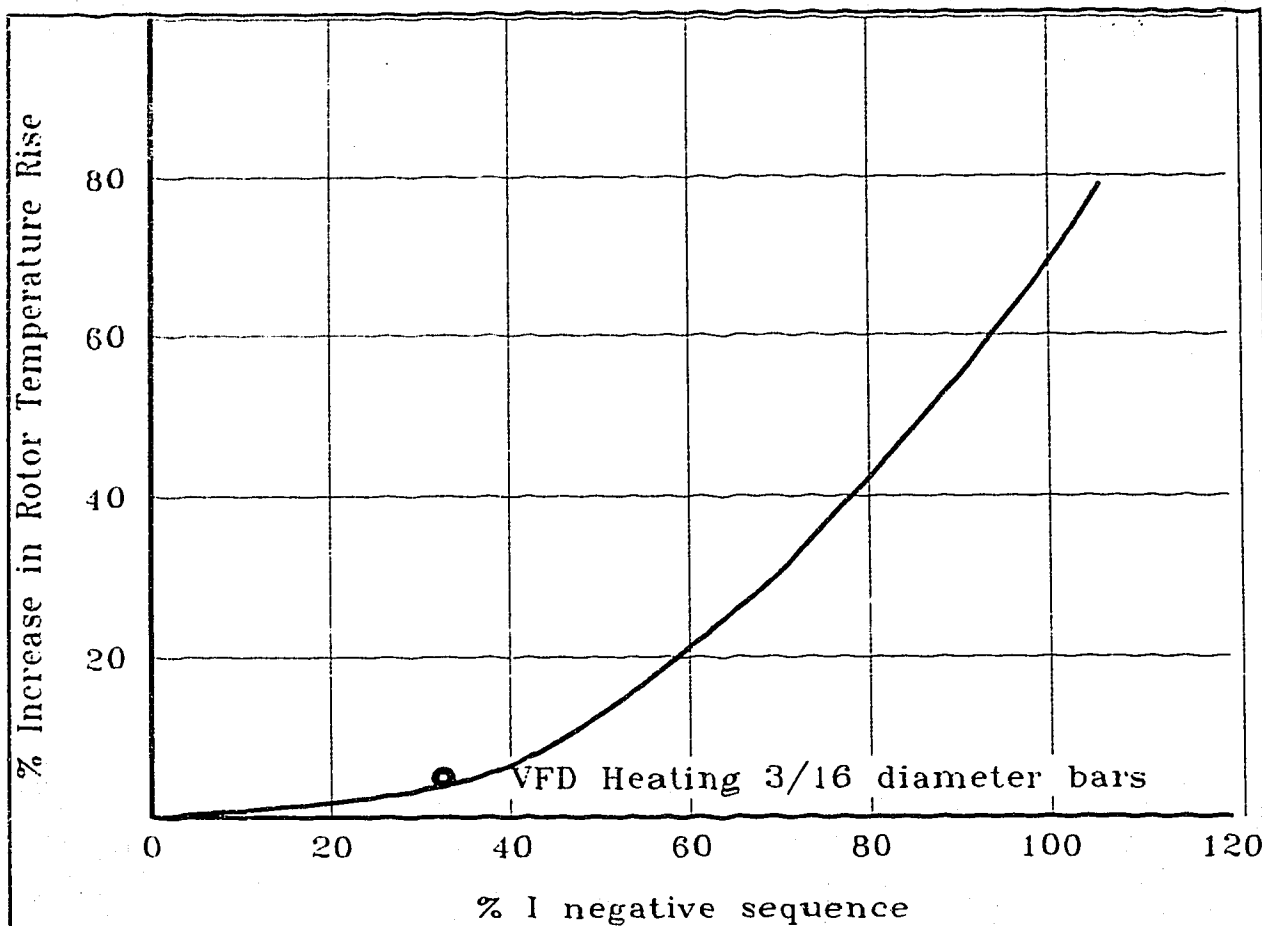


Figure 2.7.3 - Rotor Temperature Rise Due To Negative Sequence Current

The negative sequence rotor temperature rises of several generators with copper amortisseur cages utilizing round copper bars with fixed field excitation are shown in figure 2.7.3. The negative sequence current is in per cent of the full load rated current of the generator. The measurement on each generator is made by placing a single phase load on the generator, with the phases of the stator winding connected in series, to create an unbalanced stator current. A heat run is made and the rotor temperature is measured by stopping the machine once temperatures have stabilized and immediately taking resistance measurements of the rotor windings.

The harmonic currents and the associated percentage temperature rise is available

for a 150 kW six pulse variable frequency drive load applied to a 200 kW generator ⁶. Applying equation (2.7.14) to this data, the equivalent heating negative sequence current for the drive is plotted as a single point in figure 2.7.3. This point lies on the equivalent negative sequence curve, giving promising indication that the method may be valid. Validation would require more measurements with VFD loads be taken and compared to the negative sequence heating curve. The calculation clearly shows that the harmonic equivalent negative sequence current is well above the typical generator standard of a 10% allowance for negative sequence current. Particularly in islanded power systems where a large percentage of the load consists of converters, the generator manufacturer should be apprised of the harmonic loadings so he can include adequate design modifications in the machine's rotor.

2.7.2 Three Phase Generator Linear Model

The linear model of the generator is developed in a manner similar to the model for the induction motor. The approach is to develop a model which uses sequence components to couple the three phases [37], but which otherwise assumes linear behaviour in the generator. The three phase synchronous generator model is based upon the following assumptions:

- a) The stator is a grounded wye configuration
- b) Each phase has a symmetrical construction with $Z_a = Z_b = Z_c$
- c) The magnetizing impedance can be modelled in a manner similar to that used for the transformer magnetizing branch.

The symmetrical components sequence impedance matrix is formulated and inverted to form the sequence admittance matrix. This is given by,

⁶

The data was made available by Mr. M. Sieberg, Principal Electrical Engineer, Kato Engineering Division of Reliance Electric, Mankato, Minnesota.

$$|Z_{seq}|^{-1} = \begin{bmatrix} \frac{1}{Z_p} & 0 & 0 \\ 0 & \frac{1}{Z_n} & 0 \\ 0 & 0 & \frac{1}{Z_0} \end{bmatrix} = \begin{bmatrix} Y_p & 0 & 0 \\ 0 & Y_n & 0 \\ 0 & 0 & Y_o \end{bmatrix} \quad (2.7.17)$$

and then transformed back to a phase frame of reference by,

$$|Y_{ph}| = A |Y_{seq}| A^{-1} \quad (2.7.18)$$

Expanding the phase admittance gives,

$$|Y_{ph}| = \begin{bmatrix} 1 & 1 & 1 \\ a^2 & a & 1 \\ a & a^2 & 1 \end{bmatrix} \begin{bmatrix} Y_p & 0 & 0 \\ 0 & Y_n & 0 \\ 0 & 0 & Y_o \end{bmatrix} \frac{1}{3} \begin{bmatrix} 1 & a & a^2 \\ 1 & a^2 & a \\ 1 & 1 & 1 \end{bmatrix} \quad (2.7.19)$$

and collecting the products results in the form,

$$|Y_{ph}| = \frac{1}{3} \begin{bmatrix} Y_p + Y_n + Y_o & a Y_p + a^2 Y_n + Y_o & a^2 Y_p + a Y_n + Y_o \\ a^2 Y_p + a Y_n + Y_o & Y_p + Y_n + Y_o & a Y_p + a^2 Y_n + Y_o \\ a Y_p + a^2 Y_n + Y_o & a^2 Y_p + a Y_n + Y_o & Y_p + Y_n + Y_o \end{bmatrix} \quad (2.7.20)$$

Neglecting the generator resistance the sequence impedance at each harmonic frequency is given by equations (2.7.21) and (2.7.22) as follows:

$$Z_p = Z_n = j\omega_h L_2 \quad (2.7.21)$$

$$Z_o = 3R_G + j\omega_h L_0 \quad (2.7.22)$$

Generators of the 1 to 10 MVA range also do not supply perfectly sinusoidal voltage. The no load voltage waveform can be obtained from the generator manufacturer in the form of line to line harmonic voltages, and these can be converted to Norton equivalent current sources on the generator bus, which are added in parallel to the magnetizing branch as shown in figure 2.7.4. While this permits the generator to be accurately modelled, it is worth noting that the flow of current through the magnetizing branch for frequencies higher than the fundamental is small and can be neglected. The harmonic slip makes the reflected rotor resistance small and it can likewise be neglected. The net result is that only the negative sequence inductance need be included in the model. This simplified approach is adequate for most system studies.

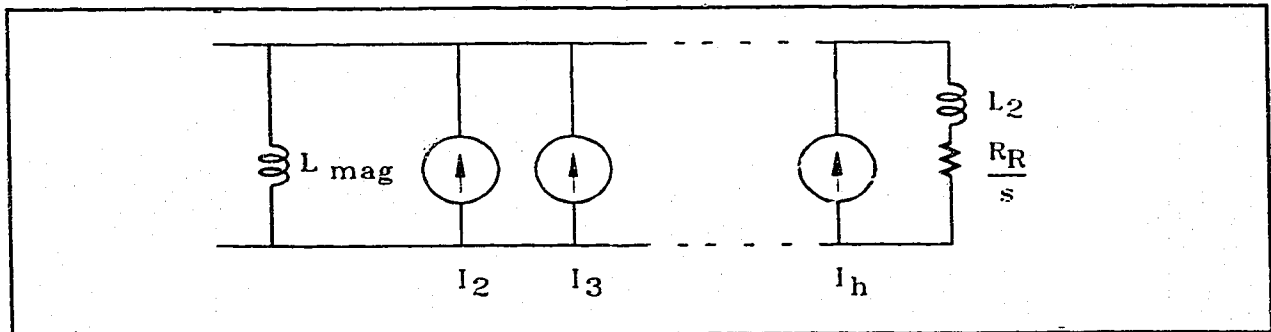


Figure 2.7.4 - Generator Harmonic Model

To conclude, for the first fifty harmonic orders, the generator can be modeled with a sequence component method similar to that used for the induction motor. The harmonic impedance can be approximated by using the negative sequence inductance at the appropriate frequency. If it is desired, second order effects can be included by modelling the magnetizing branch as a Norton equivalent current source at each harmonic of interest. The rotor resistance is small compared to the inductance seen by the harmonic, hence can

be neglected when formulating the admittance matrix for network harmonic solutions. When examining the harmonic heating effects on the rotor; however, the rotor resistance is of paramount importance and the rotor amortisseur skin effect needs to be included in the rotor resistance model.

2.8 Six Pulse Converter Model Derivation

A typical industrial nonsinusoidal load is the six pulse converter. Converters use either silicon controlled rectifiers (SCR) or diodes as rectifying devices. The balanced behaviour of the three phase bridge has been described in closed form analysis by several authors [18] [62] [63] [64] [65] [71] [72] [45]. These analyses use approximations of the waveforms and do not consider unbalance in the three phases. One unbalanced three phase model uses transfer functions rather than differential equations and ignores the effect of source impedance on overlap [42] [43]. The time domain model developed in this thesis extends previous work [8] [13] to permit an analysis of the circuit under unbalanced conditions, with a constant scheduled DC load.

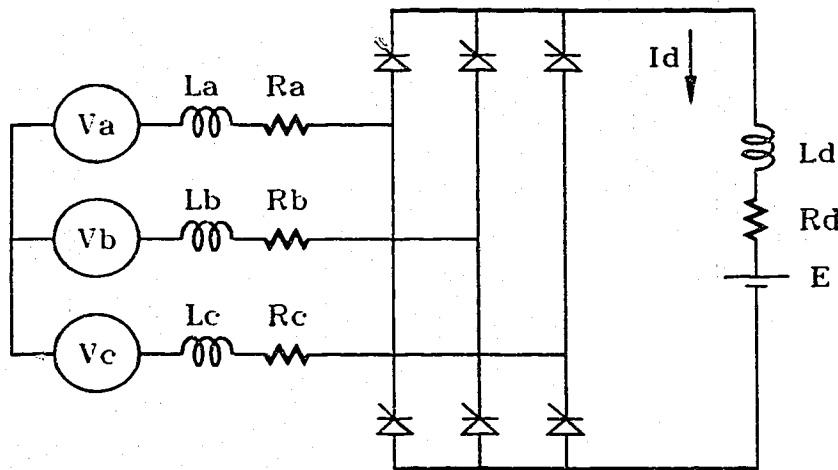


Figure 2.8.1 - Three Phase Converter Bridge

The power output of the d.c. bridge is constant for any given speed and load condition of the motor it supplies. To model this condition, the voltage "E" is adjusted until the product of DC current and voltage, $E \cdot I_d$ matches the scheduled DC power P_{dc} .

With reference to figure 2.8.1 the six pulse converter consists of six thyristors or diodes which are connected to a three phase A.C. supply and which feed a D.C. bus. The devices are fired in sequence in such a way as to apply the maximum AC line to line voltage to the DC load. Under balanced conditions this results in each AC phase supplying current for one-third of each electrical fundamental frequency cycle. At the moment that any device fires the current must divert from the device on the same DC rail through which it is flowing to the most recently fired device. These devices are said to commute during the time taken for the current to divert from one to the other. Due to circuit inductance this cannot occur instantaneously; consequently, there is an overlap period during which current is flowing through three devices. Once the current reaches zero in one of the commutated devices, it flows through two devices. In the case of thyristors the initial flow of current can be delayed by the firing circuitry. This delay is measured by the firing angle, α . The purpose of delaying the firing is usually to control the voltage of the DC rails in the bridge.

Typical circuit topologies are shown in figures 2.8.2 through 2.8.4. The equations describing these circuit topologies are classified as follows:

- a) Off state.
- b) One device firing onto each DC rail (Non overlap state). See figure 2.8.2.
- c) One device firing onto the negative rail while two devices commute on the positive rail (Positive rail overlap state). See figure 2.8.3.
- d) One device firing onto the positive rail while two devices commute on the negative rail (Negative Rail overlap state). See figure 2.8.4.

It can be observed that there are three inductances in series in the non-overlap state circuit topology, requiring one state variable, and there are three parallel inductive branches in the overlap state circuit topology, requiring three state variables.

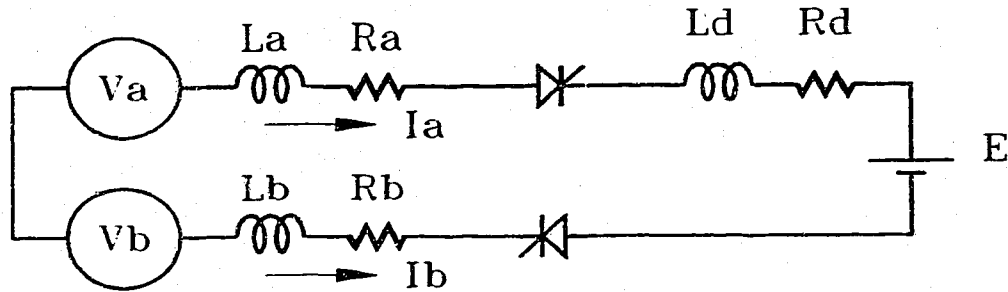


Figure 2.8.2 - Non-Overlap State

The differential equations for the non-overlap state shown in figure 2.8.2 are given by equations (2.8.1), (2.8.2) and (2.8.3) as follows,

$$\frac{di_a}{dt} = \frac{v_a - v_b - E - i_a(R_a + R_b + R_d)}{L_a + L_b + L_d} \quad (2.8.1)$$

$$\frac{di_b}{dt} = - \frac{di_a}{dt} \quad (2.8.2)$$

$$\frac{di_c}{dt} = 0 \quad (2.8.3)$$

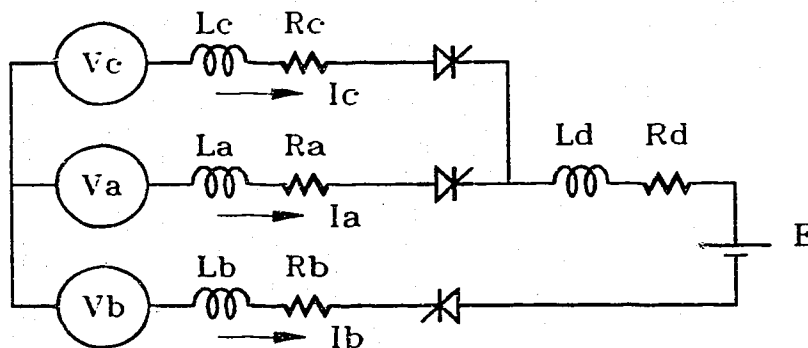


Figure 2.8.3 - Overlap State On The Positive Rail

The differential equations for the overlap state on the positive rail shown in figure 2.8.3 are given by equations (2.8.4), (2.8.5) and (2.8.6) as follows,

$$\frac{di_b}{dt} = \frac{v_b - v_c + E - i_b(R_b + R_d) + i_c R_c + \left[\frac{L_c}{L_a} \right] [v_b - v_a + E - i_b(R_b + R_d) + i_a R_a]}{L_b + L_d + \left[\frac{L_c}{L_a} \right] [L_a + L_b + L_d]} \quad (2.8.4)$$

$$\frac{di_c}{dt} = \frac{v_b - v_a + E - i_b(R_b + R_d) + i_a R_a - \frac{di_b}{dt} [L_a + L_b + L_d]}{L_a} \quad (2.8.5)$$

$$\frac{di_a}{dt} = -\frac{di_b}{dt} - \frac{di_c}{dt} \quad (2.8.6)$$

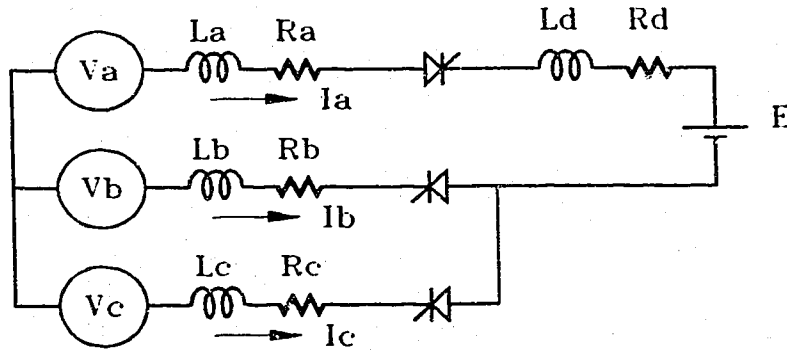


Figure 2.8.4 - Overlap State On The Negative Rail

The differential equations for the overlap state on the negative rail shown in figure 2.8.4 are given by equations (2.8.7), (2.8.8) and (2.8.9) as follows,

$$\frac{di_a}{dt} = \frac{v_a - v_c - E - i_a(R_a + R_d) + i_c R_c + \left[\frac{L_c}{L_b} \right] [v_a - v_b - E - i_a(R_a + R_d) + i_b R_b]}{L_a + L_d + \left[\frac{L_c}{L_b} \right] [L_a + L_b + L_d]} \quad (2.8.7)$$

$$\frac{di_c}{dt} = \frac{v_a - v_b - E - i_a(R_a + R_d) + i_b R_b - \frac{di_a}{dt} [L_a + L_b + L_d]}{L_b} \quad (2.8.8)$$

$$\frac{di_t}{dt} = - \frac{di_a}{dt} - \frac{di_c}{dt} \quad (2.8.9)$$

These equations are solved with a Runge-Kutta fourth order method and a time step equivalent to one-half of an electrical degree. It is observed that as voltage on all phases is lowered, the current increases approximately in inverse proportion. It is also observed that as the voltage is unbalanced, the fundamental loading of each phase varies, but not in proportion to the voltage. These two observations lead to two conclusions. The first conclusion is that the fundamental load on any phase can be modeled as constant kVA during any particular iteration, providing the voltage variation is restrained to a range of approximately 10% of nominal voltage. The second conclusion is that the per phase loads have to be recalculated between voltage iterations to achieve the correct load and current injection for a particular DC loaded bridge. Table 2.8.1 shows the fundamental kVA per phase for a 600 Volt diode bridge supplying a 200 kVA DC load when a sinusoidal, unbalanced voltage is applied. "A" phase is at rated voltage (347 V),

"B" phase is approximately 5% low (330 V), and "C" phase is approximately 10% low (312 V). All values are given in RMS.

Table 2.8.1 AC Loads on Unbalanced DC Diode Bridge Supplying VFD

Phase	AC Voltage (Sinusoidal)	AC Current (Fundamental)	kVA (Fundamental)
A	$347\angle 0^\circ$	$246.3\angle -10.9^\circ$	85.47
B	$330\angle 240^\circ$	$199.1\angle 221.9^\circ$	65.70
C	$312\angle 120^\circ$	$202.6\angle 117.6^\circ$	63.21

Table 2.8.2 demonstrates that kVA remains approximately constant for the same percentage increase in voltage on all three phases. Both tables indicate that the phase current is not proportional to phase voltage. As the fundamental kVA load on each phase remains approximately constant when voltage is varied these tables validate the constant kVA load model used for the three phase loadflow calculations.

Table 2.8.2 AC Voltage In Table 2.8.1 Increased 10% On Each Phase

Phase	AC Voltage (Sinusoidal)	AC Current (Fundamental)	kVA (Fundamental)
A	$381.7\angle 0^\circ$	$226.9\angle -10.9^\circ$	86.61
B	$363\angle 240^\circ$	$175.1\angle 221.0^\circ$	63.56
C	$343.2\angle 120^\circ$	$181.9\angle 119.9^\circ$	62.42

2.9 Conclusion To Chapter 2

Chapter 2 describes the linear modelling of the following power system components:

- a) Power Transformer
- b) Three Phase Induction Motor
- c) Power Cable
- d) Three Phase Synchronous Generator.

Nonlinear models are developed for the following:

- a) Transformer magnetizing branch
- b) Synchronous generator magnetizing branch
- c) Six Pulse Converter.

The nonlinear models are based upon the solution of differential equations to obtain time domain waveforms, then utilize Fourier techniques to calculate the harmonic currents in the frequency domain.

Skin effect increase in resistance is examined for power cable, and a separate model is developed to analyze its effect on the amortisseur bars in a generator. Skin effect decrease in flux linkages is incorporated into the cable model.

Chapter 2 provides sufficient detail to permit a functional harmonic solution program, which is described later, to be implemented. To validate the rotor heating models of Chapter 2 requires measuring nonlinear loads supplied from generators which are not synchronized to the power system. Data from the generator measurements may be obtained by asynchronously sampling with an oscilloscope. The harmonic spectra obtained by such measurements are smeared and the true underlying signal harmonics are extracted utilizing the method developed in Chapter 3.

Chapter 3

Measurement Of Nonlinear Loads

3.0 Introduction To Chapter 3

The work in this chapter is in response to difficulties encountered during laboratory measurement of VFD harmonics. Certain equipment, for example stand-alone generators, and the motors supplied from the variable frequency drives, operates at frequencies other than the power system frequency of 60 Hertz. During validation measurements of the load harmonics associated with these devices the measurement technique may lead to certain analysis errors. In this case the technique is to take measurements with an oscilloscope which is set to obtain 4000 samples over 0.5 seconds. The period of the signal is estimated from the zero crossings observed on the oscilloscope. With this technique the sampling period may not be an integer multiple of the fundamental frequency of the underlying signal. When the data is subjected to a Fourier analysis based upon the crude assessment of the fundamental period of the signal Fourier coefficients may arise for frequencies which are not integer multiples of the assumed fundamental frequency. This is an indication that there is spectral leakage between adjacent harmonic "bins".

Correct measurement of the harmonics generated by nonlinear loads is important for model validation. Taking too few data points can lead to aliasing which may exclude higher frequencies from the measured results. Measuring a sample of data with a window duration which is not an integer multiple of the period of one fundamental cycle leads to leakage and the generation of harmonics in the measurement analysis which are not present in the original power signal [39]. These types of errors are commonly referred to as "instrument artifacts". The interpolation technique described hereafter is used to recover the frequencies and magnitudes of the Fourier coefficients of the original signal from the Fourier coefficients of the sampled data.

3.1 The Relationship Between The Observed Spectrum And The Continuous Spectrum

Current and voltage are the usual signals measured in a power system. These may be practically considered as periodic and continuous in time and are given the general symbol $x_c(t)$ where the subscript "c" indicates "continuous". When measuring a signal, a window of a finite length, τ , is used to observe only a portion of the signal. The observed portion is given the symbol $x_o(t)$ where the subscript "o" indicates "observed". The window is given the symbol $w_r(t)$ where the subscript "r" refers to the rectangular nature of the window used in this method. Figure 3.1.1 illustrates the assignment of variables. The continuous signal is multiplied by the window in the time domain, and the Fourier transform of the continuous signal and the Fourier transform of the window are convolved in the frequency domain.

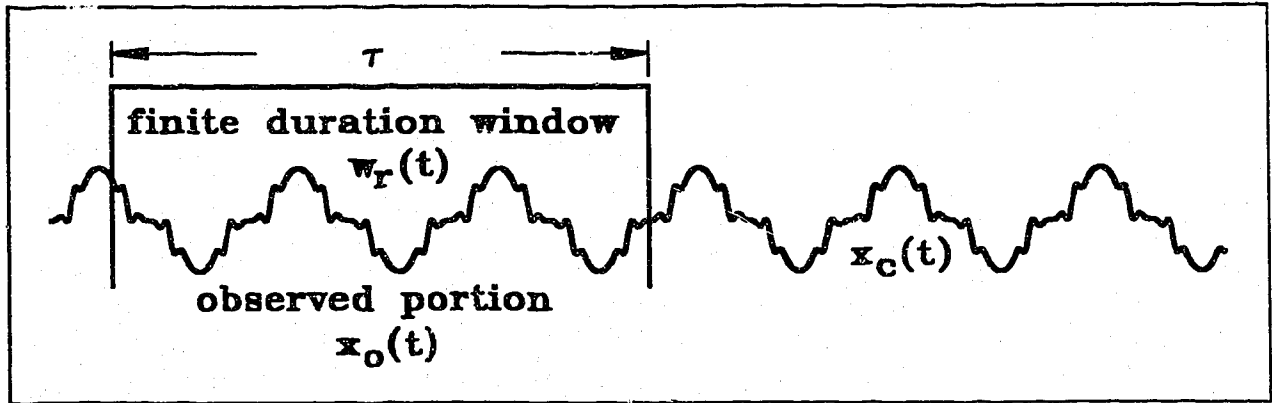


Figure 3.1.1 - Windowed Signal

The product expression is given by,

$$x_o(t) = x_c(t) \cdot w_r(t) \quad (3.1.1)$$

The Fourier transform of the rectangular window of unity magnitude and duration, τ , is

$$W_r(\omega) = \mathcal{F}\{w_r(t)\} = \int_{-\frac{\tau}{2}}^{\frac{\tau}{2}} (1) e^{-j\omega t} dt = \tau \frac{\sin\left(\frac{\tau}{2}[\omega]\right)}{\left(\frac{\tau}{2}[\omega]\right)} = \tau \text{Sa}\left(\frac{\tau}{2}[\omega]\right) \quad (3.1.2)$$

The Fourier transform of a periodic signal is an impulse sequence with impulses located at harmonic order intervals and magnitudes equal to the Fourier coefficients, $C(h)$, for each harmonic order, h . The continuous periodic signal is represented as a Fourier series given by,

$$x_c(t) = \sum_{h_c = -\infty}^{+\infty} C(h_c) e^{j h_c \omega_c t} \quad (3.1.3)$$

where ω_c is the fundamental frequency of the continuous signal and h_c is the harmonic order of a particular term in the series for the continuous signal. It is necessary to distinguish between harmonics of the continuous signal, h_c , and the harmonics of the observed signal, h_o , in the following derivation. The Fourier coefficients are defined as,

$$C(h_c) = \frac{\omega_c}{2\pi} \int_0^{\frac{2\pi}{\omega_c}} x_c(t) e^{-j h_c \omega_c t} dt \quad (3.1.4)$$

The Fourier transform of the continuous signal is,

$$X_c(\omega) = \mathcal{F}\{x_c(t)\} = \sum_{h_c = -\infty}^{+\infty} C(h_c) \mathcal{F}\{e^{j h_c \omega_c t}\} = \sum_{h_c = -\infty}^{+\infty} 2\pi C(h_c) \delta(\omega - h_c \omega_c) \quad (3.1.5)$$

Convolving the transforms in the frequency domain yields,

$$X_o(\omega) = X_c(\omega) \otimes W_r(\omega) \quad (3.1.6)$$

Applying the modulation property with the temporary variable, σ , to change the convolving operation to the integral of a product results in,

$$X_o(\omega) = \int_{\sigma = -\infty}^{+\infty} X_c(\omega - \sigma) \cdot W_r(\sigma) d\sigma \quad (3.1.7)$$

and substituting the expanded equations (3.1.2) and (3.1.5) for the Fourier transforms gives,

$$X_o(\omega) = \int_{\sigma=-\infty}^{+\infty} \sum_{h_c=-\infty}^{+\infty} 2\pi C(h_c) \delta(\omega - \sigma - h_c \omega_c) \tau \text{Sa}\left(\frac{\tau}{2}[\sigma]\right) d\sigma \quad (3.1.8)$$

Interchanging the integral and summation and applying the sifting property at $\sigma = \omega - h_c \omega_c$ results in

$$X_o(\omega) = \sum_{h_c=-\infty}^{+\infty} 2\pi C(h_c) \tau \text{Sa}\left(\frac{\tau}{2}[\omega - h_c \omega_c]\right) \quad (3.1.9)$$

Thus the spectrum of the observed portion of the signal is continuous and is described by a train of Sa functions centred on each harmonic frequency with amplitudes given by the weighting of the Fourier coefficients. Samples from $X_o(\omega)$ can be obtained using the Discrete Fourier Transform (DFT) which is given by

$$X_o(h_o \omega_o) = \sum_{n=0}^{N-1} x_o(nT) e^{-j2\pi \frac{T}{\tau} nh_o} = \sum_{n=0}^{N-1} x_o(nT) e^{-j\omega_o T nh_o} \quad (3.1.10)$$

$$\omega_o = \frac{2\pi}{\tau} \quad (3.1.11)$$

$$\tau = NT \quad (3.1.12)$$

Where τ is the length of the observed signal, N is the number of samples, T is the sampling interval and $x_o(nT)$ are samples of $x_o(t)$. The sampling frequency ($1/T$) must be at least twice the highest significant harmonic to be within the Nyquist limit.

If equation (3.1.9) is evaluated at $\omega = h_o \omega_o$ then

$$X_o(h_o \omega_o) = \sum_{h_c=-\infty}^{+\infty} 2\pi C(h_c) \tau \text{Sa}\left(\frac{\tau}{2}[h_o \omega_o - h_c \omega_c]\right) \quad (3.1.13)$$

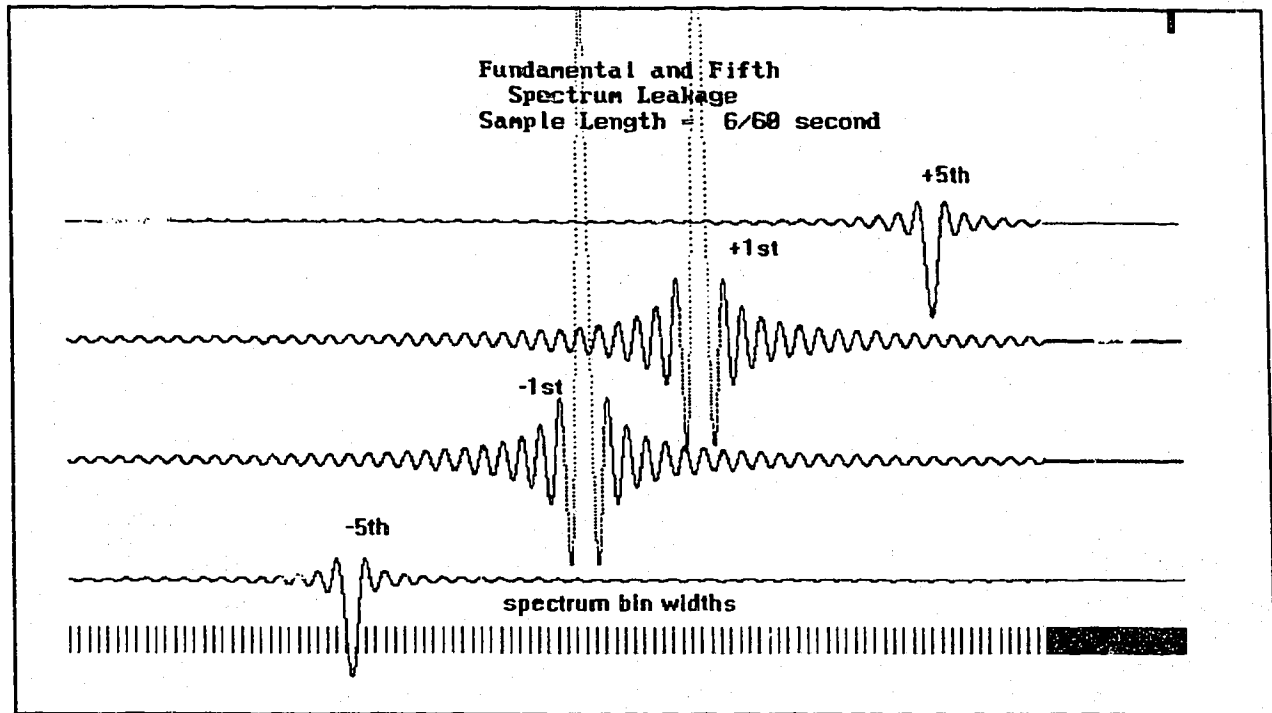


Figure 3.1.2 - Spectrum Leakage With 0.1 Second Window

Equation (3.1.13) indicates that any particular harmonic order in the observed signal is affected by all the harmonic orders in the continuous signal, subject to a weighting function which depends on the difference between the frequency of the observed harmonic and the frequency of the harmonic in the continuous signal. In other words, leakage from all h_c harmonics will affect a particular h_o harmonic. An examination of the nature of the contribution from each term in equation (3.1.13) shows that the harmonic h_c which is closest to a particular h_o of interest has a much stronger effect on h_o than other harmonics located further away. Figure 3.1.2 shows the ripple effects emanating from a fundamental and a fifth harmonic in a system where the window is 0.1 second duration and the fundamental frequency of the continuous signal is 61 Hz. Figure 3.1.3 shows the compression in the bin widths which occurs when the sampling window duration is increased to 0.33 seconds. The ripple from the harmonics in the continuous signal is reduced to a low value when it reaches its neighbouring harmonic region. The greatest magnitudes for interaction occur between the positive and negative fundamental

harmonics, or if it is present, between the DC component and the fundamental.

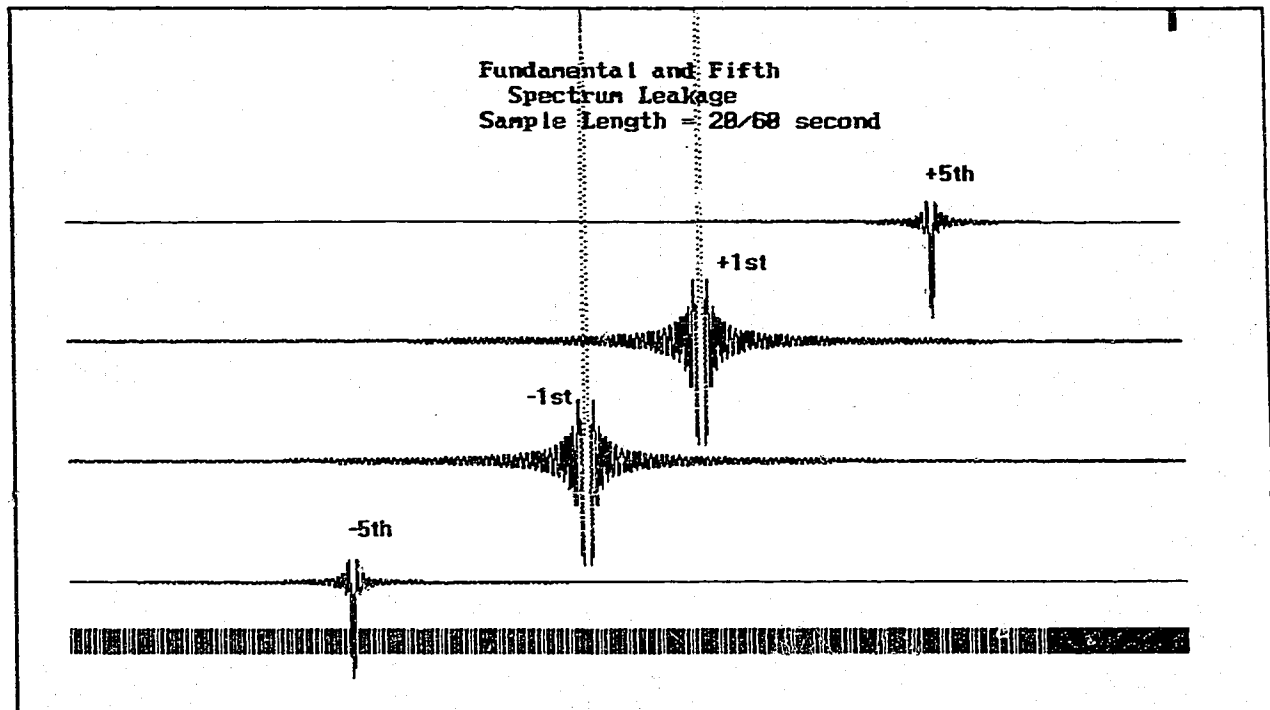


Figure 3.1.3 - Spectrum Leakage With 0.33 Second Window

Figure 3.1.4 shows that for a window of 1.0 second, the ripple may be neglected. For a one second window the fundamental positive and negative harmonic spectra are 120 bin widths apart, giving them adequate spacing for the ripple to be reduced to a negligible value (less than 1%). The spectrum bin widths are not distinguishable in the figure and appear as a black band across the bottom. This behaviour suggests that a reasonable approximation can be made to equation (3.1.13) to calculate the Fourier coefficients of those spectra in the observed signal which are in near proximity to the spectra of the continuous signal.

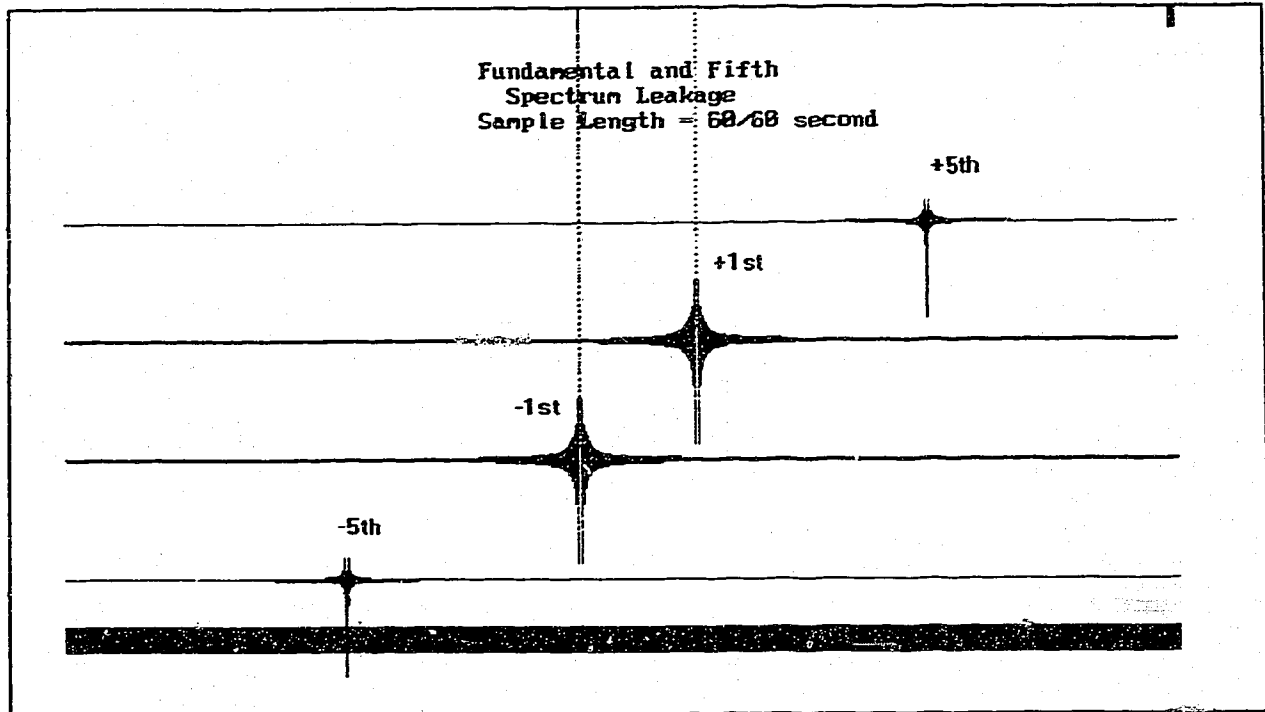


Figure 3.1.4 - Spectrum Leakage With 1.0 Second Window

To rephrase, if certain strictures are applied, that is, that the fundamental frequency of the observed signal is much smaller than the frequency of the continuous signal (ie the window has a long duration), and provided that the observed harmonic frequency of interest lies within a region, r , which is close to a harmonic frequency of the continuous signal, then the following approximation can be applied,

$$X_o(h_o \omega_o) \bigg|_{\substack{\omega_o < \omega_c \\ (h_c \omega_c - r) \leq h_o \omega_o \leq (h_c \omega_c + r)}} \approx C(h_c) Sa\left(\frac{\tau}{2} [h_o \omega_o - h_c \omega_c]\right) \quad (3.1.14)$$

3.2 Interpolation Method To Recover The Original Signal Spectrum

Equation 3.1.12 can be expressed in terms of absolute magnitudes (with the strictures dropped for clarity). The result is,

$$|X_o(h_c \omega_o)| \approx |C(h_c)| \left| \text{Sa} \left(\frac{\tau}{2} [h_o \omega_o - h_c \omega_c] \right) \right| \quad (3.2.1)$$

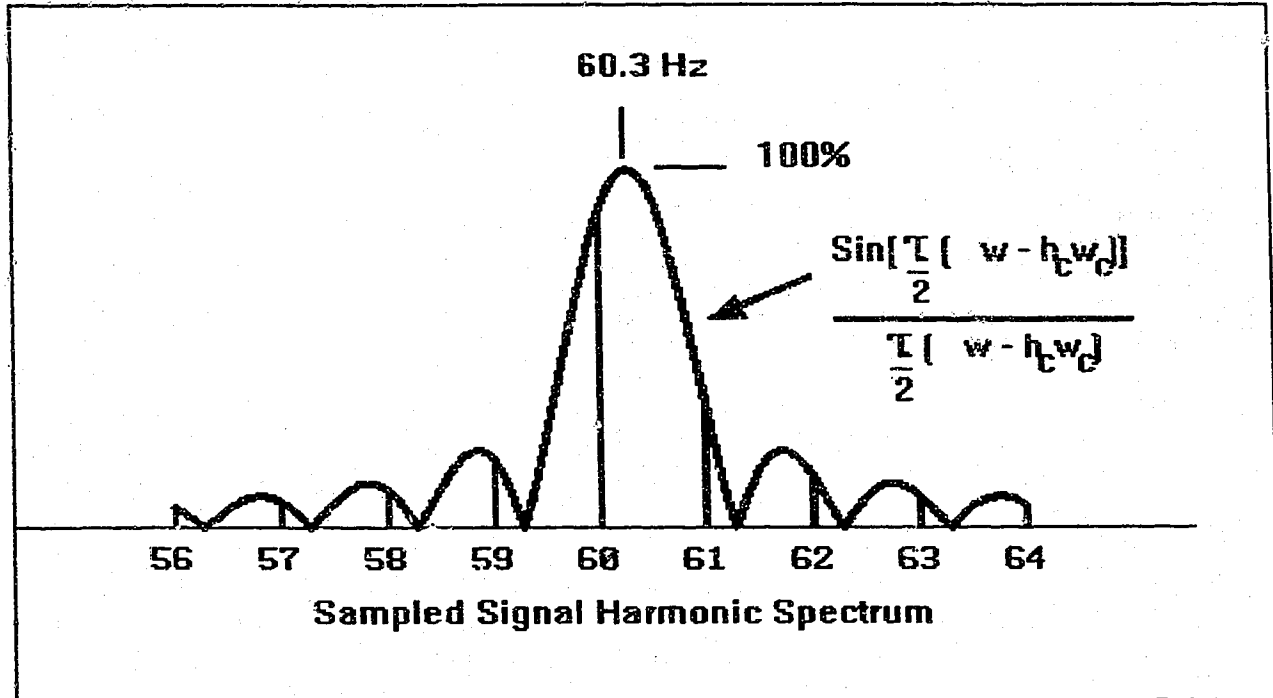


Figure 3.2.1 - Spectrum Leakage In The Vicinity Of The Fundamental

When the Sa curve of equation 3.2.1 is fitted to the measured spectrum of the observed signal in the vicinity of the fundamental the result is similar to that shown in figure 3.2.1. Once the Sa curve is fitted to the smeared spectra of the sampled signal, the harmonic magnitude and frequency of the continuous signal are established by the peak of the Sa curve. The frequency of the continuous harmonic lies between the two largest spectra measured for a given harmonic order and this shows up as leakage in the adjacent spectra of the sampled signal.

For the example in figure 3.2.1 it is estimated from the zero crossing at the time of measurement that the signal's fundamental frequency is approximately 60 Hz. with a probable variation not exceeding ± 1 Hz. The sample period is selected at one second duration to obtain sample spectra bin widths of 1 Hz., hence only the harmonic magnitudes of the sampled spectra from 56 to 64 Hz. need to be considered to obtain a useful range of values in the vicinity of the fundamental frequency of the continuous signal.

Initially the Sa curve was fitted using a method of least squares using several points on either side of the harmonic order of interest, but it was subsequently found when validating the method that sufficient accuracy can be obtained by fitting the Sa curve to the two largest sampling spectra. This allows a saving of computational effort. The computer algorithm initially locates and calculates the ratio of the magnitudes of the two largest sampled spectra in the vicinity of a harmonic order of interest. It then slides a unity magnitude Sa curve horizontally until the two largest sample spectra frequencies intersect the Sa curve with the same ratio. The Sa curve is then scaled vertically until it intersects the magnitudes of the two largest spectra. The peak of the located and scaled Sa curve then determines the magnitude and frequency of the continuous signal's harmonic.

3.3 Error Of The Interpolation Method

The error, ϵ_{ok} in any particular harmonic term, h_{ok} of the observed signal lying in close proximity to a term, h_{ck} of the continuous signal is calculated from,

$$\epsilon_{h_{ok}} = \left[\sum_{h_c = -\infty}^{+\infty} C(h_c) Sa\left(\frac{\tau}{2}[h_{ok}\omega_o - h_c\omega_c]\right) \right] - C(h_{ck}) Sa\left(\frac{\tau}{2}[h_{ok}\omega_o - h_{ck}\omega_c]\right) \quad (3.3.1)$$

For the example shown in Table 3.3.1 the infinite series error summation is restricted to the first 60 harmonics of the continuous signal. The continuous signal is a quasi-square wave (ie. a square wave with 120 degree lobes - see figure 4.4.2 in the next

chapter) with a fundamental frequency of 60.3 Hz. The observed signal is taken with a one second window. The error terms associated with the first few harmonics of the observed signal are shown in the final column of the table. Each error term is associated with that harmonic of the observed signal which is on either side of and lying closest to a particular harmonic of the continuous signal.

Table 3.3.1 - Leakage Harmonics And Associated Error Terms

h_c	f_c (actual)	h_o (f_c+/f_c-)	$ C(h_o) $ (measured)	ϵ_{ho} (per unit)
1	60.3	60	86.0841	0.00285
		61	36.5452	0.00660
5	301.5	301	12.6854	0.00372
		302	12.7793	0.00371
7	422.1	422	14.1273	0.00536
		423	1.4862	0.04794
11	663.3	663	7.8219	0.00232
		664	3.3259	0.00542

The table describes the error in the method for the fundamental and the 5th, 7th, and 11th harmonics of the continuous signal. The actual fundamental frequency of the continuous signal is 60.3 Hz, hence the frequencies tabulated in the second column are harmonic multiples of 60.3. A window of one second duration is used to observe the signal, hence the fundamental of the observed signal is 1/(one second) or 1 Hz. The frequencies lying on either side of the continuous harmonics are tabulated in the third

column. For example, at the 5th harmonic of the continuous signal the actual frequency is 301.5 Hz. The observed harmonics on either side of this frequency are $h_o = 301$ and $h_o = 302$. The magnitudes of these spectral pairs are tabulated in the fourth column. Finally, equation 3.3.1 is used, with the harmonic orders from - 60 to + 60 replacing the infinite limits in the first summation, to calculate the error.

Table 3.3.2 - Comparison Between Actual And Interpolated Signal Harmonics

h_c	f_c (actual)	$ C(h_c) $ (actual)	f_c (interpolated)	$ C(h_c) $ (interpolated)
1	60.300	100.000	60.299	100.003
5	301.500	20.000	301.488	20.001
7	422.100	14.285	422.088	14.338
11	663.300	9.091	663.282	9.125

Table 3.3.2 indicates the interpolation technique is accurate to within two one hundredths of a Hz, with a magnitude error of less than 0.4% for the least accurate harmonic.

3.4 Conclusion To Chapter 3

In conclusion a practical method is demonstrated to recover the Fourier coefficients of a continuous signal from the sampled data of power system current and voltage. It is developed in response to a need to measure accurately the harmonics of loads operating at variable frequencies. The technique is used to validate certain models. The method is a new contribution, and is derived as a variation on a well-known behaviour of digital signal processing.

Chapter 4

Mathematical Methods For Harmonic Analysis of Power Systems

4.0 Introduction To Chapter 4

This chapter introduces a variety of mathematical methods which when applied to computer modelling assist in the solution of harmonics. When a power system with nonlinear loads operates with voltage unbalanced conditions, unbalanced harmonics propagate throughout the system and appear as residual harmonics in the system neutrals. These residual harmonics behave similarly to zero sequence currents and voltages in that they cause noise which can strongly affect communications and control circuits. They also penetrate computerized control equipment through common mode noise mechanisms appearing on the ground planes. To analyze unbalanced harmonics requires solving the network on a multiphase basis.

Multiphase analysis of harmonics requires combining linear and nonlinear analysis methods into a computer algorithm. The power system is separated into linear and nonlinear portions and the two portions are analyzed with different methods. In the linear network the harmonic producing loads are replaced with frequency-domain harmonic current sources and in the nonlinear network the boundary with the linear network is modeled by time-domain voltage sources. An interactive algorithm is applied to provide an iterative solution to the voltage and current at the boundary points between the linear and nonlinear portions of the circuit [33]. As this method requires a tremendous amount of computer work, the solution method selected must be fast and efficient. The approach is to apply sparsity directed programming to the Zollenkopf bifactorization method of inverting a matrix [11].

4.1 Symmetrical Components Sequence Frame of Reference

Prior to discussing these various methods it is worth reviewing the method known as "Symmetrical Components". To increase the generality of solution it is desirable that the proposed method be able to handle systems with non-symmetrical impedances, that is, systems where the phase impedances for particular devices are not the same in each phase. Authors have shown that in such systems the sequence voltages depend upon the currents in the positive, negative, and zero symmetrical component reference frame [61]. To illustrate this concept, consider the following equations where the subscripts **a**, **b**, and **c** refer to phase quantities, and the subscripts **1**, **2**, and **0** refer to the positive, negative, and zero sequence symmetrical components. The **a** operator is defined as a 120 degree phase shifter. This is defined as,

$$a = e^{j\frac{2\pi}{3}} \quad (4.1.1)$$

The phase impedances and sequence currents are formulated to define phase voltage in equation (4.1.2) given by,

$$\begin{aligned} E_a &= Z_a I_{a0} + Z_a I_{a1} + Z_a I_{a2} \\ E_b &= Z_b I_{a0} + a^2 Z_b I_{a1} + a Z_b I_{a2} \\ E_c &= Z_c I_{a0} + a Z_c I_{a1} + a^2 Z_c I_{a2} \end{aligned} \quad (4.1.2)$$

and the sequence voltages are given by,

$$\begin{aligned} E_{a0} &= \frac{1}{3} (E_a + E_b + E_c) \\ E_{a1} &= \frac{1}{3} (E_a + a E_b + a^2 E_c) \\ E_{a2} &= \frac{1}{3} (E_a + a^2 E_b + a E_c) \end{aligned} \quad (4.1.3)$$

Substituting (4.1.2) into (4.1.3) yields,

$$\begin{aligned}
 E_{a0} &= \frac{1}{3} (Z_a + Z_b + Z_c) I_{a0} + \frac{1}{3} (Z_a + a^2 Z_b + a Z_c) I_{a1} + \frac{1}{3} (Z_a + a Z_b + a^2 Z_c) I_{a2} \\
 E_{a1} &= \frac{1}{3} (Z_a + a Z_b + a^2 Z_c) I_{a0} + \frac{1}{3} (Z_a + Z_b + Z_c) I_{a1} + \frac{1}{3} (Z_a + a^2 Z_b + a Z_c) I_{a2} \\
 E_{a2} &= \frac{1}{3} (Z_a + a^2 Z_b + a Z_c) I_{a0} + \frac{1}{3} (Z_a + a Z_b + a^2 Z_c) I_{a1} + \frac{1}{3} (Z_a + Z_b + Z_c) I_{a2}
 \end{aligned} \tag{4.1.4}$$

Since,

$$1 + a + a^2 = 0, \tag{4.1.5}$$

it can be seen that for balanced phase impedances, most of the terms in equation (4.1.4) drop out, leaving the sequence voltages dependent upon only current of the same sequence. The sequence voltages for unbalanced impedances must be computed by considering the currents in all three (zero, positive, and negative) sequences. While this is a feasible computation, it would not save any computer work as compared to retaining a phase frame of reference. From this reasoning it was elected to develop a method which retained the phase frame of reference.

4.2 Applying Zollenkopf's Bifactorization Method

When a power system has its components interconnected, the busses are directly joined together by relatively few branches. This results in a matrix of the admittances containing a large number of zeros. Computer programmers have utilized this fact for decades to reduce the storage requirements for data. Mathematicians like Zollenkopf have devised sparsity directed methods of Gauss elimination for solving matrices which avoid generation and storage of matrices containing a large number of elements. Thus the zero elements (which essentially contain no data but are of topological interest) have incurred a fair amount of thought and interest as to how to best use them. To solve

power problems it is useful to invert admittance matrices to obtain impedance matrices.

The inverse of the bus admittance matrix is given by,

$$Z_{BUS} = [Y_{BUS}]^{-1} = \begin{bmatrix} z_{11} & z_{12} & \cdots & z_{1n} \\ z_{21} & z_{22} & \cdots & z_{2n} \\ \vdots & \vdots & \ddots & \vdots \\ z_{n1} & z_{n2} & \cdots & z_{nn} \end{bmatrix} \quad (4.2.1)$$

A number of ways are available to achieve this inversion, several of them being based on Gauss elimination. A comparison of three methods in Table 4.2.1 indicates there is little difference in computational effort between Triangularization and Bifactorization to invert a matrix. However, when the Bifactorization method is modified to improve the order of factorization and to invert Z Bus one column at a time, the number of operations and storage requirements decrease significantly as shown in Table 4.2.2.

Table 4.2.1 - Comparison Among Gauss Elimination Methods (n Bus Network)

METHOD	OPERATIONS	STORAGE
Pivotal Gauss Elimination	$\approx n^3$	$\approx n^2$
LDH Triangularization	$\approx \frac{n^3}{3}$	$\approx n^2$
Zollenkopf's Bifactorization	$\approx \frac{n^3}{3}$	$\approx n^2$

Table 4.2.2 - Operations and Storage Requirements For The Modified Bifactorization

METHOD	OPERATIONS	STORAGE
Modified Bifactorization applied to sparse harmonic load busses (n_h)	$\approx \frac{n^3}{3} \frac{n_h}{n} \approx \frac{n^2}{3} n_h$	$\approx n n_h$
Modified Bifactorization applied to sparse harmonic loads and taking advantage of improved ordering	$\approx \frac{n^2}{3} \frac{n_h}{2} \approx \frac{n^2 n_h}{6}$	$\approx n n_h$

One notable difference between the methods is that combining the triangularization factors forms the original Y_{BUS} whereas combining the bifactorization factors forms the inverse. Advantage is taken of the Zollenkopf method to reduce the work required to solve a network which contains only a few harmonic load busses. A modified bifactorization method has been developed by the author [19] which permits formulation of the Z_{BUS} one column at a time, thus avoiding much of the work required for a full matrix inversion and the storage of a full Z_{BUS} . Advantage is taken of the order in which the factorization matrices are created to store results for only those busses supplying nonlinear loads. In a typical power system this achieves a considerable saving in computational effort.

Showing the factorization steps by means of superscripts, the Zollenkopf method uses the fact that any matrix can be reduced one row and one column at a time by factoring out row and column factorization matrices. This is given by,

$$\begin{aligned}
C^{(1)} Y_{BUS}^{(0)} R^{(1)} &= Y^{(1)} \\
C^{(2)} Y_{BUS}^{(1)} R^{(2)} &= Y^{(2)} \\
&\vdots \\
C^{(n)} Y_{BUS}^{(n-1)} R^{(n)} &= Y^{(n)}
\end{aligned} \tag{4.2.2}$$

At step n (corresponding to the number of columns in the matrix) we obtain the unity matrix, given by,

$$Y^{(n)} = U \tag{4.2.3}$$

where,

$$Y^{(n)} = C^{(n)} \dots C^{(k)} \dots C^{(1)} Y_{BUS} R^{(1)} \dots R^{(k)} \dots R^{(n)} = U \tag{4.2.4}$$

Pre-multiplying by the inverses of the column factors, then post-multiplying by the column factors in reverse order gives,

$$Y_{BUS} R^{(1)} \dots R^{(k)} \dots R^{(n)} C^{(n)} \dots C^{(k)} \dots C^{(1)} = U \tag{4.2.5}$$

Pre-multiplying both sides by Y_{BUS}^{-1} yields the inverse matrix,

$$R^{(1)} \dots R^{(k)} \dots R^{(n)} C^{(n)} \dots C^{(k)} \dots C^{(1)} = Y_{BUS}^{-1} \tag{4.2.6}$$

where the factorization matrices for step " k " are given by,

$$C^{[K]} = \begin{bmatrix} 1 & . & . & C_{1K} & . & . \\ . & 1 & . & C_{JK} & . & . \\ . & . & 1 & \vdots & . & . \\ . & . & . & C_{KK} & . & . \\ . & . & . & \vdots & 1 & . \\ . & . & . & C_{NK} & . & 1 \end{bmatrix} \quad R^{[K]} = \begin{bmatrix} 1 & . & . & . & . & . \\ . & 1 & . & . & . & . \\ . & . & 1 & . & . & . \\ R_{KI} & \dots & R_{KJ} & 1 & \dots & R_{KN} \\ . & . & . & . & 1 & . \\ . & . & . & . & . & 1 \end{bmatrix} \tag{4.2.7}$$

The column factor elements are given by,

$$C_{JK}^{[K]} = \frac{-Y_{JK}^{[K-1]}}{Y_{KK}^{[K-1]}} \quad C_{KK}^{[K]} = \frac{1}{Y_{KK}^{[K-1]}} \quad (4.2.8)$$

The row factor elements for a symmetrical matrix are,

$$R_{KJ}^{[K]} = C_{JK}^{[K]} \quad , \quad K \neq J \quad , \quad R_{KK} = 1 \quad (4.2.9)$$

and the reduced matrix elements are given by,

$$Y_{IJ}^{[K]} = Y_{IJ}^{[K-1]} - \frac{Y_{IK}^{[K-1]} Y_{KJ}^{[K-1]}}{Y_{KK}^{[K-1]}} \quad (4.2.10)$$

Zollenkopf's method stops at this point and yields a fast method of computing the inverse, but requires storing a very large Z_{BUS} matrix. In the next section a Z Bus algorithm is developed which permits formulation of the Z Bus one column at a time. The Z Bus is a key element in the development of the proposed method. The linear portion of the system is modelled by an admittance network at all harmonic orders greater than the fundamental. In addition all active loads are replaced either by passive circuit elements or by injected current sources. This permits the direct solution of the network voltages without having to resort to iterative loadflow solutions. The motivating factors for using Z Bus are:

- a) It can be obtained directly from the Y Bus admittance matrix.
- b) It is directly suited for solution when the nonlinear portions of the network are modelled as injected current sources.
- c) With sparsity directed programming and the application of an advanced Gauss elimination technique, it is fast.

4.3 Modified Bifactorization Algorithm

An examination of an industrial power system will often reveal that there are very few busses supplying harmonic loads hence there are few points at which harmonic current is injected into the system. One bus is the connection to the utility. Other points are the large rectifier loads and variable frequency drives. To assist the reader, the modified bifactorization algorithm is described using an example power system with only four busses where harmonic currents are injected. These busses are the incoming bus (1) and three other busses (L), (J), and (K) supplying harmonic loads. For this example we need concern ourselves with finding only four columns of the Z_{BUS} matrix, namely column 1, column L, column J, and column K, and further require only the injected harmonic currents I_1 , I_L , I_J , and I_K to solve all the bus voltages.

Z_{BUS} is found one column at a time by multiplying the factors of the inverse in equation 4.2.7 times the appropriate column of the unity matrix U. For example the k^{th} column of Z Bus is given by,

$$\begin{bmatrix} Z_{1K} \\ \vdots \\ Z_{KK} \\ \vdots \\ Z_{NK} \end{bmatrix} = R^{(1)} \dots R^{(k)} \dots R^{(n)} C^{(n)} \dots C^{(k)} \dots C^{(1)} \begin{bmatrix} 0 \\ \vdots \\ 0 \\ 1 \\ 0 \\ \vdots \\ 0 \end{bmatrix} \quad (4.3.1)$$

where the factors are multiplied by the k^{th} column of the unity matrix.

In implementing the above, a dynamic ordering technique is employed in which at each step of factorization the reduced matrix is searched for the unfactorized column containing the fewest elements, and this column is then factorized next. This method

keeps the reduced matrix sparse. Modifying this procedure to factorize the harmonic load busses last eliminates all the column factors in equation (4.3.1) except those for the harmonic busses. In the example only column factors for the harmonic load busses 1, J, K, & L need be considered, provided these busses are factorized as steps N-3, N-2, N-1, and N. This is made possible because multiplying a column factorization matrix of the "J" column by the "K" column of U results in the "K" column of U. The row factors have a different topology and all of them must be included. Placing the harmonic load bus factors last modifies equation (4.3.1) to give,

$$\begin{bmatrix} Z_{1K} \\ \vdots \\ Z_{KK} \\ \vdots \\ Z_{NK} \end{bmatrix} = R^{(1)} \dots R^{(K)} \dots R^{(N)} C^{(N)} C^{(N-1)} C^{(N-2)} C^{(N-3)} \begin{bmatrix} 0 \\ \vdots \\ 0 \\ 1 \\ 0 \\ \vdots \\ 0 \end{bmatrix} \quad (4.3.2)$$

To solve the particular example, the Z_{BUS} columns created in (4.3.2) for the four busses 1, J, K, and L, are injected with current, as shown by,

$$\begin{bmatrix} V_1 \\ V_2 \\ \vdots \\ \vdots \\ V_N \end{bmatrix} = \begin{bmatrix} Z_{11} \\ Z_{21} \\ \vdots \\ \vdots \\ Z_{N1} \end{bmatrix} \cdot I_1 + \begin{bmatrix} Z_{1J} \\ Z_{2J} \\ \vdots \\ \vdots \\ Z_{NJ} \end{bmatrix} \cdot I_J + \begin{bmatrix} Z_{1K} \\ Z_{2K} \\ \vdots \\ \vdots \\ Z_{NK} \end{bmatrix} \cdot I_K + \begin{bmatrix} Z_{1L} \\ Z_{2L} \\ \vdots \\ \vdots \\ Z_{NL} \end{bmatrix} \cdot I_L \quad (4.3.3)$$

Since this process has to be repeated for each harmonic of interest, preserving sparsity is important. The first 80 harmonics must be solved to comply with the utility

regulations and this requires storing the contents of eighty voltage vectors.

4.4 Establishing The Relative Angle For a Harmonic At a Particular Bus

It is necessary to establish the phase angle of the fundamental current at a bus to provide the reference phase angles at that bus for the injected current harmonics. In the frequency domain the angle of a harmonic component depends upon two variables. The first is the relative phase angle of its fundamental with respect to some arbitrary system reference and the second is its own angular displacement at the harmonic frequency. A phasor method suitable for balanced systems [15] is extended in this chapter to multiphase unbalanced systems. In this section a method is developed to provide correct phase shifting for harmonic currents injected at harmonic load busses.

To develop this concept consider a time domain real valued signal comprising harmonic components based upon a standard Fourier summation. This is given by,

$$f(t) = C_{dc} + \sum_{h=1}^{\infty} \left[a_h \cos\left(\frac{2h\pi t}{T}\right) + b_h \sin\left(\frac{2h\pi t}{T}\right) \right] \quad (4.4.1)$$

where,

$$C_{dc} = \frac{1}{T} \int_0^T f(t) dt \quad (4.4.2)$$

$$a_h = \frac{2}{T} \int_0^T f(t) \cos\left(\frac{2h\pi t}{T}\right) dt \quad (4.4.3)$$

$$b_h = \frac{2}{T} \int_0^T f(t) \sin\left(\frac{2h\pi t}{T}\right) dt \quad (4.4.4)$$

The same harmonic series expressed in terms of the magnitude and phase angle for a real valued signal is developed by other authors [50] as,

$$f(t) = C_{dc} + \sum_{h=1}^{\infty} C_h \cos[h(\omega_1 t) + \phi_h] \quad (4.4.5)$$

where,

C_{dc} = magnitude of the direct current component

$C_h = \sqrt{a_h^2 + b_h^2}$ = peak magnitude of the harmonic term,

h = harmonic order,

$\omega_1 = \frac{2\pi}{T}$ = fundamental frequency, and

ϕ_h = harmonic phase shift, $\tan^{-1} \frac{b}{a}$

As current flows through a network it is phase shifted by various mechanisms, a typical one being the vector addition of winding currents in the lines supplying the delta windings of the delta-wye transformers. This phase shift can be expressed as a time shift t_0 , which when substituted into equation (4.4.5) becomes,

$$f(t - t_0) = C_{dc} + \sum_{h=1}^{\infty} C_h \cos[h(\omega_1 t - \omega_1 t_0) + \psi_h] \quad (4.4.6)$$

where it is understood that ψ_h is the characteristic angle associated with harmonic h for a particular shape of waveform required by a specific load, when t_0 equals zero. The fundamental phase shift is measured in this thesis relative to the A phase voltage at the swing bus. A load bus has a voltage angle δ with respect to the swing bus voltage and its current injected into a bus is related to the bus voltage by the angle θ . This is given by,

$$\omega_1 t_0 = \delta + \theta \quad (4.4.7)$$

For thyristor loads this latter angle depends upon the firing angle α and the overlap angle μ , which can be approximated by the relationship,

$$\theta \approx \alpha + \frac{\mu}{2} \quad (4.4.8)$$

The relationship between the injected angle ϕ_h , the characteristic harmonic angle ψ_h , the fundamental current power factor angle θ_1 , and the fundamental bus voltage angle δ_1 , is shown in equation (4.4.9),

$$\phi_h = \psi_h - h(\delta_1 + \theta_1) \quad (4.4.9)$$

The reason for casting the equations into this form is to permit an analysis of the network to be performed for each harmonic of interest, and then to recombine the signals at each bus of interest. To recombine the harmonics properly necessitates incorporating the phase shift of the fundamental into the calculation of the phase angle of each harmonic.

It is necessary to run a three phase loadflow at the fundamental frequency to establish the fundamental phase shift of voltage and current on each bus. Linear loads may be modeled in the traditional fashion of specifying the watts and vars at each bus. The nonsinusoidal loads have to be subjected to a preliminary Fourier analysis to estimate the current and voltage at the fundamental frequency and from this the resulting watts and vars at the fundamental frequency are estimated. Losses can be neglected for nonsinusoidal loads to obtain a starting value for the study. The characteristic harmonic magnitudes and angles must also be established for the load waveforms.

Having thus established the relative angles of current and voltage at each bus,

subsequent harmonic calculations may proceed. To develop this concept, consider a system in which it is desired to find the relative phase angle of a harmonic on the primary and secondary of a particular phase of a three phase delta-wye transformer. It is known that under balanced conditions the fundamental will shift 30 degrees across the machine. Under unbalanced conditions the phase shift will differ on each phase and will be a function of the addition of the winding current vectors at each vertex of the delta.

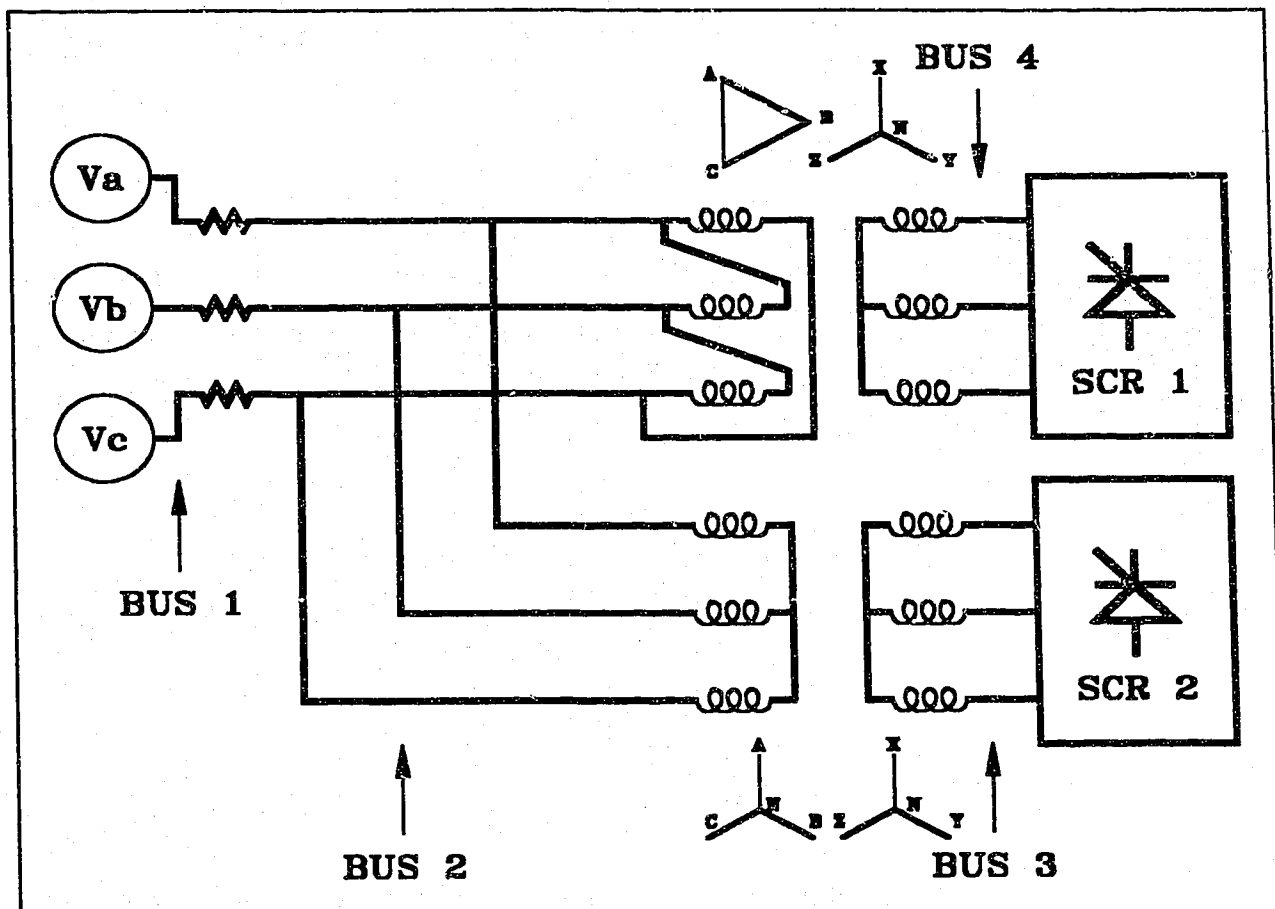


Figure 4.4.1 - Example Network To Demonstrate Shifted Harmonic Angles

With reference to Figure 4.4.1, assume that a balanced condition loadflow has established the Table 4.4.1 voltages and currents at the A phase buses. The SCR loads have equal magnitudes, firing angles, and overlap angles such that their current lags their voltage by 25 degrees.

Table 4.4.1 Fundamental Phase A Current & Voltage (Balanced Conditions)

	Bus 1	Bus 2	Bus 3	Bus 4
V 1 angle	0	-10	-10	-40
I 1 angle	-35	-35	-35	-65

To determine the characteristic harmonic and magnitudes of the load current, a Fourier analysis is made of the load current with assumed zero phase shift. In this example the load waveforms were assumed to be quasi-square waves (square waves with 120 degree lobes) as shown in Figure 4.4.2 and of equal magnitude for each SCR load. Taking fundamental phase shifts into account, the harmonic angles can be established for the harmonic currents injected by each SCR. The first few harmonic orders are tabulated in Table 4.4.2.

Table 4.4.2 Fourier Analysis of Load Current (No Phase Shift)

Harmonic Order	Relative Magnitude	Characteristic Angle ψ
1	100%	0 degrees
5	20.0%	180 degrees
7	14.3%	0 degrees
11	9.1%	180 degrees
13	7.7%	0 degrees

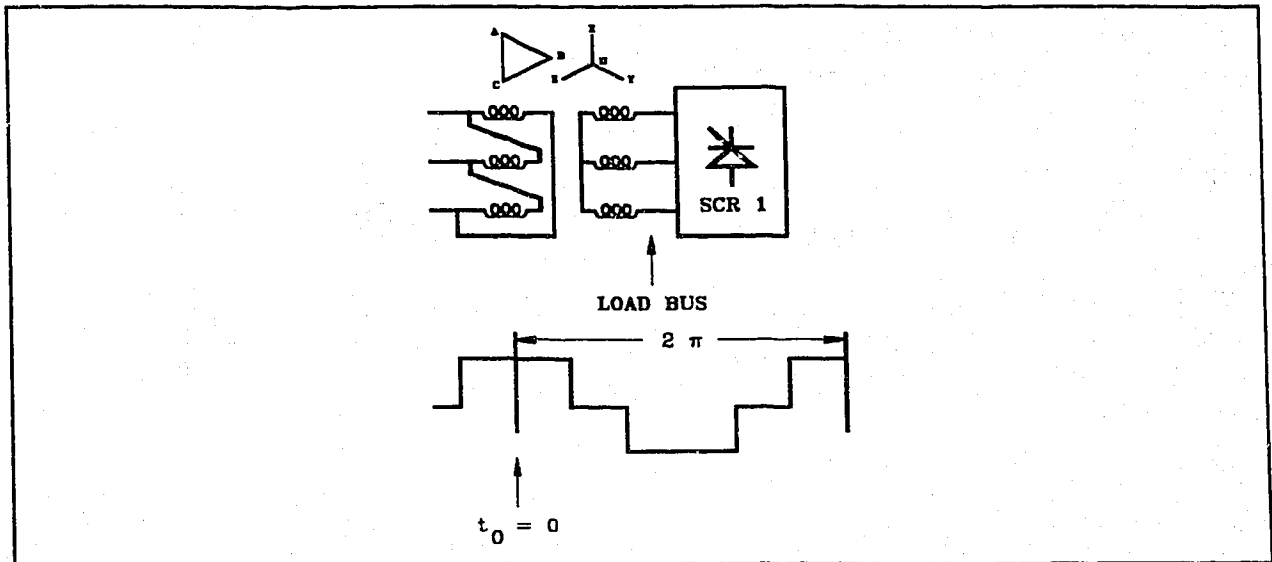


Figure 4.4.2 - Example Quasi-Square Wave Loads - ψ_h Established When $t_0 = 0$

Table 4.4.3 compares the phase angles of current injected by the converters. The harmonic currents injected at Bus 4 are phase shifted by the Delta Wye transformer. The 1st, 7th, and 13th are positive sequence hence undergo a shift of +30 degrees, while the 5th, and 11th are negative sequence hence undergo a shift of -30 degrees. The harmonic currents injected at Bus 3 undergo no phase shift when passing through the Wye Wye transformer. Table 4.4.4 compares the inverter currents after they have been shifted by the transformers.

Table 4.4.3 - Harmonic Angles of Currents Injected by SCR 1 and SCR 2

Harmonic Order	Bus 3 ϕ_h	Bus 4 ϕ_h
1	-35	-65
5	+5	-145
7	+115	-95
11	+155	+185
13	-95	-125

Table 4.4.4 - Harmonic Angles of Currents at Transformer Primaries

Harmonic Order	Wye Wye Primary ϕ_h	Delta Wye Primary ϕ_h
1	-35	-35
5	+5	-175
7	+115	-65
11	+155	+155
13	-95	-95

Note that the transformer primary 5th and 7th harmonic currents are 180 degrees out of phase and will cancel one another at Bus 2. The 11th and 13th transformer current harmonics are in phase and will be additive at Bus 2. This behaviour gives rise to the use of 30 degree phase shifting transformers to provide 6 pulse harmonic cancellation. It is only successful if the two 6 pulse group loads are equivalent in magnitude and if they have similar firing angles.

4.5 Three Phase Loadflow

The standard loadflow equations need to be extended to formulate solutions for A, B, and C phases as well as the neutral buses. In a three phase loadflow there are four bus types of primary interest referred to as:

"Load Busses"	power and vars held constant, and
"Generator Busses"	power and voltage magnitude held constant, provided the generator is operating within a certain +/- var range,
"Swing Busses"	voltage and angle held constant,
"Neutral Busses"	voltage dependent upon the voltages of electrically attached busses.

Utilizing a Gauss-Siedel formulation of the nodal admittance equations one can define the key parameters at each of the bus types as follows:

$$\text{Load Busses} \quad V_K = \frac{1}{Y_{KK}} \left(\frac{P_K - jQ_K}{V_K^*} - \sum_{J=1}^N Y_{KJ} V_J \right) \quad J \neq K \quad (4.5.1)$$

$$\text{Generator Busses} \quad Q_K = -\text{Imaginary} \left[\left(Y_{KK} V_K + \sum_{J=1}^N Y_{KJ} V_J \right) V_K^* \right] \quad J \neq K \quad (4.5.2)$$

$$\text{Swing Busses} \quad P_K - jQ_K = \left(\sum_{J=1}^N Y_{KJ} V_J \right) V_K^* \quad J \neq K \quad (4.5.3)$$

$$\text{Neutral Busses} \quad V_K = \frac{1}{Y_{KK}} \left(- \sum_{J=1}^N Y_{KJ} V_J \right) \quad J \neq K \quad (4.5.4)$$

Note that the neutral bus is a special case of a load bus with no current injected. It is formulated to avoid dividing by the bus voltage which in most systems will be zero or a small value close to zero. The equations are established on a per phase basis, hence

all voltages are expressed as line to neutral, all complex power is expressed as watts and vars per phase, and current is per phase.

The following worked example assumes the supply voltage in the system depicted in Figure 4.4.1 to be unbalanced 600 V with phase "A" and "C" at nominal (347 V line to neutral) and phase "B" 2% low (340 V), but with their phasors 120 degrees apart, and also assumes the following system characteristics:

Source impedance	$z = j\ 0.1$, $y = -j\ 10$ per unit on 750 kVA base
Transformers	$z = j\ 0.05$, $y = -j\ 20$ per unit, 1 to 1 voltage ratio, 750 kVA each
SCR 1	600 kVA load, apparent power factor 0.8 ($160 + j\ 120$ per phase)
SCR 2	450 kVA load, apparent power factor 0.7 ($105 + j\ 107$ per phase)

With this information we are able to construct the Y Bus admittance matrix which describes the system. This matrix is assembled from the sub matrixes describing major components. The SCR transformers are of particular interest as they contain ungrounded neutrals. In formulating a solution each transformer matrix may therefore be constructed in accordance with the method in Chapter 2 to either retain or eliminate the neutral busses. Removal of the neutral by matrix reduction is shown on the following pages.

The Delta-Wye transformer shown in figure 4.5.1 is expressed as an admittance matrix described by equation (4.5.5).

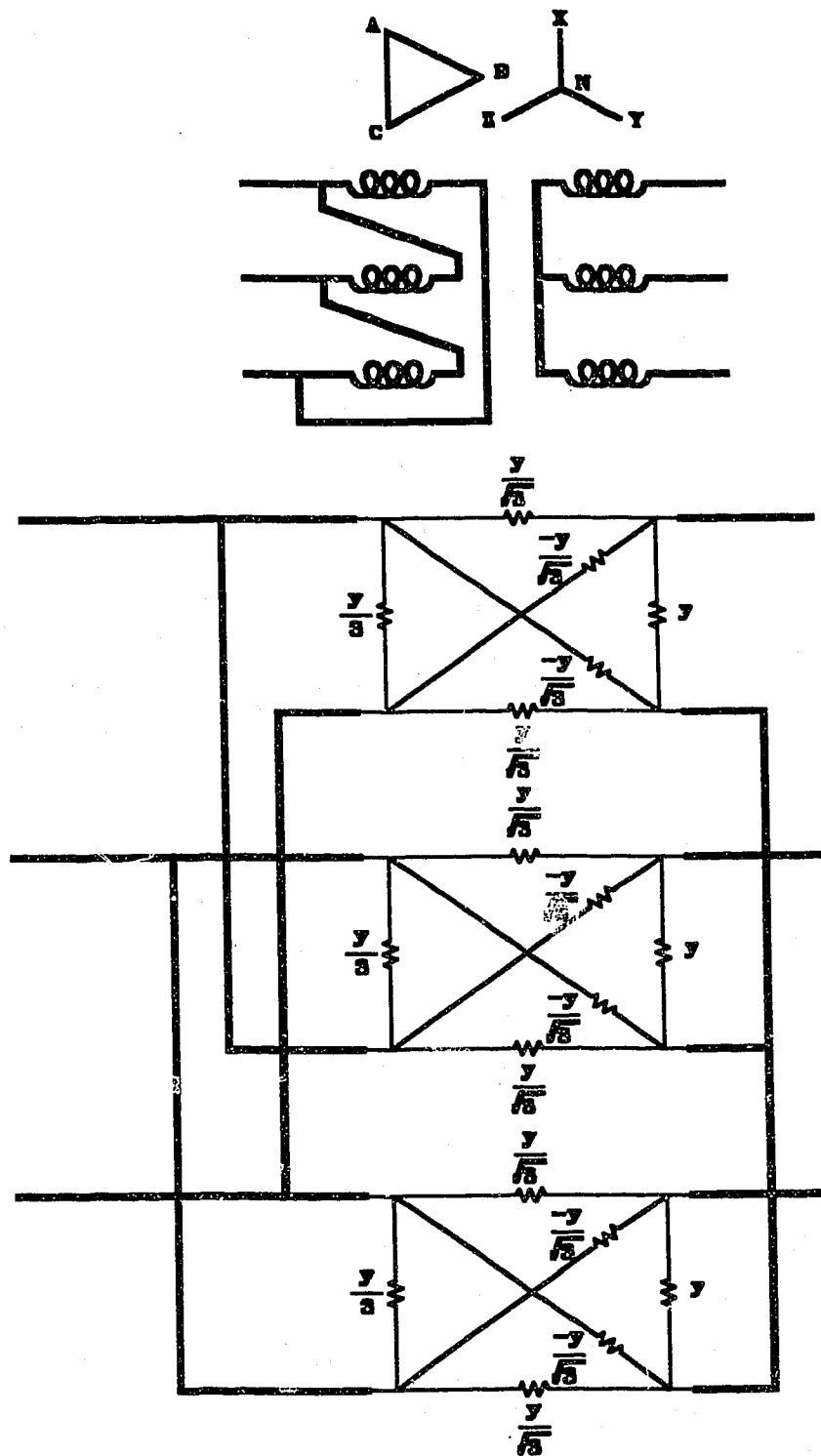


Figure 4.5.1 - Transformer Core Matrices Connected in Delta Ungrounded Wye

The admittance matrix for the delta-ungrounded wye transformer in figure 4.5.1 is given by,

$$Y_{DY} = \begin{matrix} & \begin{matrix} 2a & 2b & 2c & 4a & 4b & 4c & 4n \end{matrix} \\ \begin{matrix} 2a \\ 2b \\ 2c \\ 4a \\ 4b \\ 4c \\ 4n \end{matrix} & \begin{bmatrix} \frac{2y}{3} & -\frac{y}{3} & -\frac{y}{3} & -\frac{y}{\sqrt{3}} & \frac{y}{\sqrt{3}} & \cdot & \cdot \\ -\frac{y}{3} & \frac{2y}{3} & \frac{y}{3} & \cdot & -\frac{y}{\sqrt{3}} & \frac{y}{\sqrt{3}} & \cdot \\ -\frac{y}{3} & -\frac{y}{3} & \frac{2y}{3} & \frac{y}{\sqrt{3}} & \cdot & -\frac{y}{\sqrt{3}} & \cdot \\ -\frac{y}{\sqrt{3}} & \frac{y}{\sqrt{3}} & \cdot & y & \cdot & \cdot & -y \\ \cdot & -\frac{y}{\sqrt{3}} & \frac{y}{\sqrt{3}} & \cdot & y & \cdot & -y \\ \frac{y}{\sqrt{3}} & \cdot & -\frac{y}{\sqrt{3}} & \cdot & \cdot & y & -y \\ \cdot & \cdot & \cdot & -y & -y & -y & 3y \end{bmatrix} \end{matrix} \quad (4.5.5)$$

By partitioning the matrix and reducing to eliminate the neutral bus this becomes,

$$Y_{DY} = \begin{matrix} & \begin{matrix} 2a & 2b & 2c & 4a & 4b & 4c \end{matrix} \\ \begin{matrix} 2a \\ 2b \\ 2c \\ 4a \\ 4b \\ 4c \end{matrix} & \begin{bmatrix} \frac{2y}{3} & -\frac{y}{3} & -\frac{y}{3} & -\frac{y}{\sqrt{3}} & \frac{y}{\sqrt{3}} & \cdot \\ -\frac{y}{3} & \frac{2y}{3} & \frac{y}{3} & \cdot & -\frac{y}{\sqrt{3}} & \frac{y}{\sqrt{3}} \\ -\frac{y}{3} & -\frac{y}{3} & \frac{2y}{3} & \frac{y}{\sqrt{3}} & \cdot & -\frac{y}{\sqrt{3}} \\ -\frac{y}{\sqrt{3}} & \frac{y}{\sqrt{3}} & \cdot & \frac{2y}{3} & -\frac{y}{3} & -\frac{y}{3} \\ \cdot & -\frac{y}{\sqrt{3}} & \frac{y}{\sqrt{3}} & -\frac{y}{3} & \frac{2y}{3} & -\frac{y}{3} \\ \frac{y}{\sqrt{3}} & \cdot & -\frac{y}{\sqrt{3}} & -\frac{y}{3} & -\frac{y}{3} & \frac{2y}{3} \end{bmatrix} \end{matrix} = \begin{bmatrix} Y_{DY22} & Y_{DY24} \\ Y_{DY42} & Y_{DY44} \end{bmatrix} \quad (4.5.6)$$

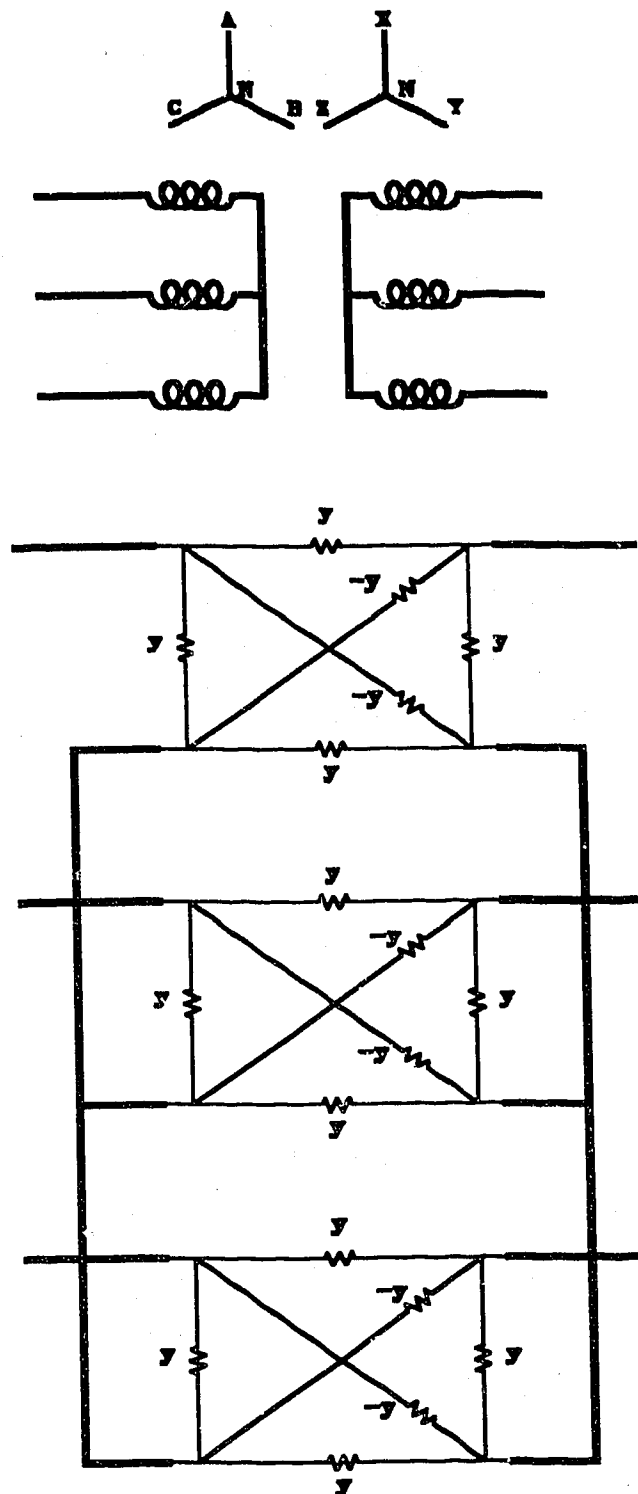


Figure 4.5.2 - Transformer Core Matrices Connected in Ungrounded Wye - Wye

The ungrounded wye-wye transformer shown in figure 4.5.2 is described by an admittance matrix given by,

$$Y_{YY} = \begin{matrix} & \begin{matrix} 2a & 2b & 2c & 2n & 3a & 3b & 3c & 3n \end{matrix} \\ \begin{matrix} 2a \\ 2b \\ 2c \\ 2n \\ 3a \\ 3b \\ 3c \\ 3n \end{matrix} & \begin{bmatrix} y & \cdot & \cdot & -y & -y & \cdot & \cdot & y \\ \cdot & y & \cdot & -y & \cdot & -y & \cdot & y \\ \cdot & \cdot & y & -y & \cdot & \cdot & -y & y \\ -y & -y & -y & 3y & y & y & y & -3y \\ -y & \cdot & \cdot & y & y & \cdot & \cdot & -y \\ \cdot & -y & \cdot & y & \cdot & y & \cdot & -y \\ \cdot & \cdot & -y & y & \cdot & \cdot & y & -y \\ y & y & y & -3y & -y & -y & -y & 3y \end{bmatrix} \end{matrix} \quad (4.5.7)$$

By partitioning the matrix and reducing to eliminate the neutral busses this becomes,

$$Y_{YY} = \begin{matrix} & \begin{matrix} 2a & 2b & 2c & 3a & 3b & 3c \end{matrix} \\ \begin{matrix} 2a \\ 2b \\ 2c \\ 3a \\ 3b \\ 3c \end{matrix} & \begin{bmatrix} \frac{2y}{3} & -\frac{y}{3} & -\frac{y}{3} & -\frac{2y}{3} & \frac{y}{3} & \frac{y}{3} \\ -\frac{y}{3} & \frac{2y}{3} & -\frac{y}{3} & \frac{y}{3} & -\frac{2y}{3} & \frac{y}{3} \\ -\frac{y}{3} & -\frac{y}{3} & \frac{2y}{3} & \frac{y}{3} & \frac{y}{3} & -\frac{2y}{3} \\ -\frac{2y}{3} & \frac{y}{3} & \frac{y}{3} & \frac{2y}{3} & -\frac{y}{3} & -\frac{y}{3} \\ \frac{y}{3} & -\frac{2y}{3} & \frac{y}{3} & -\frac{y}{3} & \frac{2y}{3} & -\frac{y}{3} \\ \frac{y}{3} & \frac{y}{3} & -\frac{2y}{3} & -\frac{y}{3} & -\frac{y}{3} & \frac{2y}{3} \end{bmatrix} \end{matrix} = \begin{bmatrix} Y_{YY22} & Y_{YY23} \\ Y_{YY32} & Y_{YY33} \end{bmatrix} \quad (4.5.8)$$

The assumption that in this example the source impedance has no mutual coupling from

The assumption that in this example the source impedance has no mutual coupling from phase to phase results in

$$Y_{SOURCE} = \begin{matrix} & \begin{matrix} 1a & 1b & 1c & 2a & 2b & 2c \end{matrix} \\ \begin{matrix} 1a \\ 1b \\ 1c \\ 2a \\ 2b \\ 2c \end{matrix} & \begin{bmatrix} y & \cdot & \cdot & -y & \cdot & \cdot \\ \cdot & y & \cdot & \cdot & -y & \cdot \\ \cdot & \cdot & y & \cdot & \cdot & -y \\ -y & \cdot & \cdot & y & \cdot & \cdot \\ \cdot & -y & \cdot & \cdot & y & \cdot \\ \cdot & \cdot & -y & \cdot & \cdot & y \end{bmatrix} \end{matrix} = \begin{bmatrix} Y_{S11} & Y_{S12} \\ Y_{S21} & Y_{S22} \end{bmatrix} \quad (4.5.9)$$

The source admittance matrix and the transformer admittance matrices can be added together to form the system admittance matrix. Note that the column and row positions of the sub-matrices require adjusting to conform to the bus topology of the system. The result is,

$$Y_{BUS} = \begin{bmatrix} Y_{S11} & Y_{S12} & \cdot & \cdot \\ Y_{S21} & (Y_{S22} + Y_{YY22} + Y_{DY22}) & Y_{YY23} & Y_{YD24} \\ \cdot & Y_{YY32} & Y_{YY33} & \cdot \\ \cdot & Y_{DY42} & \cdot & Y_{DY44} \end{bmatrix} \quad (4.5.10)$$

Substituting the numerical values for the example results in,

$$Y_{BUS} = -j \begin{bmatrix} 10 & \cdot & \cdot & -10 & \cdot & \cdot & \cdot & \cdot & \cdot & \cdot & \cdot & \cdot \\ \cdot & 10 & \cdot & \cdot & -10 & \cdot & \cdot & \cdot & \cdot & \cdot & \cdot & \cdot \\ \cdot & \cdot & 10 & \cdot & \cdot & -10 & \cdot & \cdot & \cdot & \cdot & \cdot & \cdot \\ -10 & \cdot & \cdot & \frac{110}{3} & -\frac{40}{3} & -\frac{40}{3} & -\frac{40}{3} & \frac{20}{3} & \frac{20}{3} & -\frac{20}{\sqrt{3}} & \frac{20}{\sqrt{3}} & \cdot \\ \cdot & -10 & \cdot & -\frac{40}{3} & \frac{110}{3} & -\frac{40}{3} & \frac{20}{3} & -\frac{40}{3} & \frac{20}{3} & \cdot & -\frac{20}{\sqrt{3}} & \frac{20}{\sqrt{3}} \\ \cdot & \cdot & -10 & -\frac{40}{3} & -\frac{40}{3} & \frac{110}{3} & \frac{20}{3} & \frac{20}{3} & -\frac{40}{3} & \frac{20}{\sqrt{3}} & \cdot & -\frac{20}{\sqrt{3}} \\ \cdot & \cdot & \cdot & -\frac{40}{3} & \frac{20}{3} & \frac{20}{3} & \frac{40}{3} & -\frac{20}{3} & -\frac{20}{3} & \cdot & \cdot & \cdot \\ \cdot & \cdot & \cdot & \frac{20}{3} & -\frac{40}{3} & \frac{20}{3} & -\frac{20}{3} & \frac{40}{3} & -\frac{20}{3} & \cdot & \cdot & \cdot \\ \cdot & \cdot & \cdot & \frac{20}{3} & \frac{20}{3} & -\frac{40}{3} & -\frac{20}{3} & -\frac{20}{3} & \frac{40}{3} & \cdot & \cdot & \cdot \\ \cdot & \cdot & \cdot & -\frac{20}{3} & \cdot & \frac{20}{3} & \cdot & \cdot & \cdot & \frac{40}{3} & -\frac{20}{3} & -\frac{20}{3} \\ \cdot & \cdot & \cdot & \frac{20}{3} & -\frac{20}{3} & \cdot & \cdot & \cdot & \cdot & -\frac{20}{3} & \frac{40}{3} & -\frac{20}{3} \\ \cdot & \cdot & \cdot & \cdot & \frac{20}{3} & -\frac{20}{3} & \cdot & \cdot & \cdot & -\frac{20}{3} & -\frac{20}{3} & \frac{40}{3} \end{bmatrix} \quad (4.5.11)$$

Using a computer to solve the loadflow to a voltage mismatch of less than 10^{-8} per unit results in the voltages and currents shown in Tables 4.5.2 and 4.5.3 for the example system. The bus identification cross references are tabulated in Table 4.5.1. As the secondary nodal voltages of the transformer are otherwise indeterminate, it was elected to set the secondary neutral of the delta-wye transformer to zero voltage and to let the secondary voltage of the wye-wye neutral match the primary neutral voltage.

To conclude, the three phase loadflow is used to establish the magnitude and phase angle of the fundamental component of the load currents at the load busses. Reference voltages must be set for floating neutrals.

Table 4.5.1 - Bus Cross Reference Identification For Example

Bus	Matrix Node Numbers
1a, 1b, 1c	1, 2, 3
2a, 2b, 2c	4, 5, 6
3a, 3b, 3c	7, 8, 9
4a, 4b, 4c	10, 11, 12
2n (Wye Wye Primary Neutral)	13
3n (Wye Wye Secondary Neutral)	14
4n (Delta Wye Secondary Neutral)	15

Table 4.5.2 - Fundamental Load Currents For Loads In Example System

Node	Load Current (Amps)	Load Angle (Degrees Relative To Bus 1 Voltage)
7	676.17	313.76
8	694.82	193.36
9	676.17	73.76
10	504.69	275.93
11	510.74	155.35
12	512.20	36.18

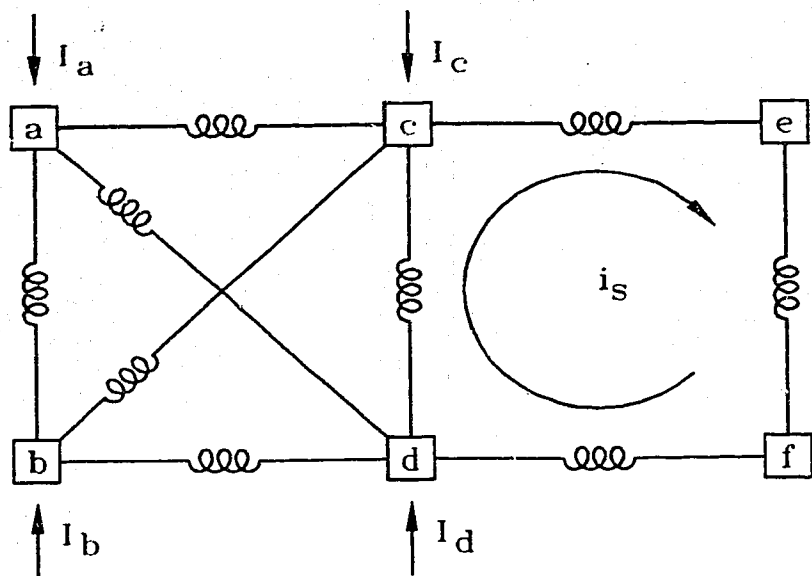
Table 4.5.3 - Fundamental Voltages For Example System

Node No.	V (per unit)	Angle (Degrees)
1	1.0000	0.00
2	0.9800	240.00
3	1.0000	120.00
4	0.8813	353.07
5	0.8593	232.80
6	0.8813	113.07
7	0.8523	350.63
8	0.8295	230.23
9	0.8523	110.63
10	0.8560	321.47
11	0.8458	200.89
12	0.8434	81.72
13	0.007457	63.35
14	0.007860	64.77
15	0	0

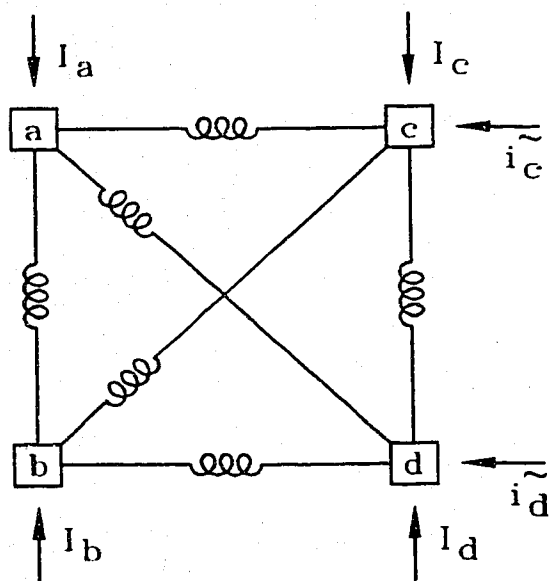
4.6 Applying Diakoptic Methods

From a computational perspective using time domain state space methods is slower than using frequency domain matrix inversion techniques to solve linear networks of comparable size. On the other hand, certain nonlinear elements and loads which are intractable to frequency domain techniques can be solved by time domain methods. It is advantageous to divide the network into linear and nonlinear portions so that each portion may be solved by the most applicable method. This division may be accomplished by tearing the network at the busses supplying nonlinear loads. Diakoptic equations may be applied to either mesh or nodal methods of analysis for linear networks [12]. By making certain approximations and solving with an iterative calculation the method is extended in this section to accommodate nonlinear portions of the network.

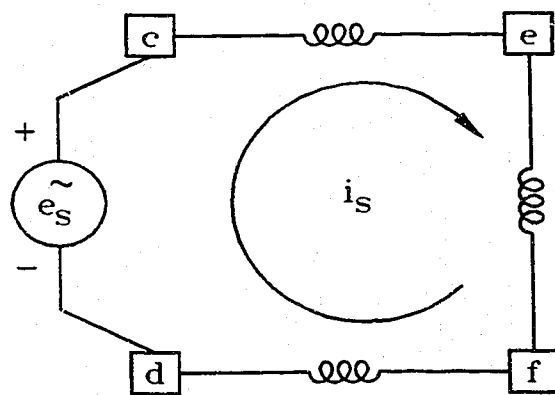
Figure 4.6.1 illustrates an example network which has been torn into two portions, one portion which is amenable to solution by nodal analysis and the other portion which is amenable to mesh analysis. The mesh portion will replace its connections to the original network with hypothetical voltage sources, \tilde{e}_β ; and the nodal portion will replace its connections to the original network with hypothetical current sources, \tilde{i}_α . The nodal portion of the network may also contain known current sources, I_α and known voltage sources E_α ; and the mesh portion of the network may also contain known current sources, I_β and known voltage sources, E_β . The problem is to evaluate all branch currents i_β in the mesh portion and all nodal voltages v_α in the nodal portion. In this development lowercase variables are used for the unknown voltages and currents and uppercase variables are used for the known voltages and currents. The subscript α will refer to the nodal network variables and the subscript β to the mesh network variables. Single subscripts designate vectors and double subscripts designate matrices.



a) Original Network



b) Nodal Network



c) Mesh Network

Figure 4.6.1 - Network Torn Into Nodal and Mesh Portions

The first step is to define the hypothetical current and voltage in terms of the unknown loop currents and node voltages. The loop currents are given by,

$$\begin{aligned}\tilde{i}_c &= -i_s \\ \tilde{i}_d &= +i_s\end{aligned}\tag{4.6.1}$$

and the nodal voltages are given by,

$$\tilde{e}_s = v_c - v_d\tag{4.6.2}$$

This is expressed in matrix form by using connection matrices, defined as,

$$\tilde{i}_\alpha = C_{\alpha\beta} i_\beta\tag{4.6.3}$$

$$\tilde{e}_\beta = -C_{\beta\alpha}^T v_\alpha\tag{4.6.4}$$

where the subscripts denote "nodal" and "mesh" connections rather than rows and columns, hence,

$$C_{\beta\alpha} = C_{\alpha\beta}\tag{4.6.5}$$

For the mesh network,

$$Z_{\beta\beta} i_\beta = E_\beta + \tilde{e}_\beta\tag{4.6.6}$$

And for the nodal network,

$$Y_{\alpha\alpha} v_\alpha = I_\alpha + \tilde{i}_\alpha\tag{4.6.7}$$

Substituting for \tilde{e}_β in (4.6.6) and \tilde{i}_α in (4.6.7) yields,

$$Y_{\alpha\alpha} v_{\alpha} = I_{\alpha} + C_{\alpha\beta} i_{\beta} \quad (4.6.8)$$

$$Z_{\beta\beta} i_{\beta} = E_{\beta} - C_{\beta\alpha}^T v_{\alpha} \quad (4.6.9)$$

Placing these in compound matrix form results in the fundamental equations of diakoptics:

$$\begin{bmatrix} Y_{\alpha\alpha} & -C_{\alpha\beta} \\ C_{\beta\alpha}^T & Z_{\beta\beta} \end{bmatrix} \begin{bmatrix} v_{\alpha} \\ i_{\beta} \end{bmatrix} = \begin{bmatrix} I_{\alpha} \\ E_{\beta} \end{bmatrix} \quad (4.6.10)$$

Premultiplying equation (4.6.8) by the inverse of admittance yields,

$$v_{\alpha} = Y_{\alpha\alpha}^{-1} (I_{\alpha} + C_{\alpha\beta} i_{\beta}) \quad (4.6.11)$$

Substituting for v_{α} in equation (4.6.9) results in,

$$(Z_{\beta\beta} + C_{\beta\alpha}^T Y_{\alpha\alpha}^{-1} C_{\alpha\beta}) i_{\beta} + C_{\beta\alpha}^T Y_{\alpha\alpha}^{-1} I_{\alpha} = E_{\beta} \quad (4.6.12)$$

Let,

$$\tilde{Z}_{\beta\beta} = Z_{\beta\beta} + C_{\beta\alpha}^T Y_{\alpha\alpha}^{-1} C_{\alpha\beta} \quad (4.6.13)$$

Then i_{β} can be expressed completely in terms of known quantities.

$$i_{\beta} = \tilde{Z}_{\beta\beta}^{-1} E_{\beta} - \tilde{Z}_{\beta\beta}^{-1} C_{\beta\alpha}^T Y_{\alpha\alpha}^{-1} I_{\alpha} \quad (4.6.14)$$

Substituting (4.6.14) into (4.6.11) solves the unknown nodal voltages.

The above described procedure works for linear networks. In this thesis the mesh

portion of the torn network is known to be nonlinear. As a result any expression which attempts to formulate or invert an impedance matrix for the mesh network must contain linearized values for the branch impedances. The direct solution of the diakoptic equations using linearized values will not give correct results. However, if equation (4.6.6) is extended to include differential equations in the time domain it becomes,

$$R_{\beta\beta} i_{\beta} + L_{\beta\beta} \left(\frac{di_{\beta}}{dt} \right) = E_{\beta} + \tilde{e}_{\beta} \quad (4.6.15)$$

where $L_{\beta\beta}$ is nonlinear for the magnetizing branches, varying as a function of flux linkages as described in Chapter 2. By recasting the equation as,

$$\left(\frac{di_{\beta}}{dt} \right) = \frac{1}{L_{\beta\beta}} [E_{\beta} + \tilde{e}_{\beta} - R_{\beta\beta} i_{\beta}] \quad (4.6.16)$$

to solve for the time differential of current, and by taking small time steps, the recursive relationship,

$$i_{\beta}^{(k+1)} \approx i_{\beta}^{(k)} + \left(\frac{di_{\beta}}{dt} \right) \Delta t \quad (4.6.17)$$

solves for the unknown currents.

If equation (4.6.7) is extended to include harmonic currents in the frequency domain, it becomes the summation,

$$\sum_{h=1}^N Y_{\alpha\alpha(h)} v_{\alpha(h)} = \sum_{h=1}^N I_{\alpha(h)} + \sum_{h=1}^N \tilde{i}_{\alpha(h)} \quad (4.6.18)$$

which can be reformulated as

$$\sum_{h=1}^N v_{\alpha(h)} = \sum_{h=1}^N \left[(Y_{\alpha\alpha(h)})^{-1} (I_{\alpha(h)} + \tilde{i}_{\alpha(h)}) \right] \quad (4.6.19)$$

to solve for the unknown voltage.

It then is possible to obtain a solution using iterative methods. The nodal matrix can be

solved directly with a Z bus Gauss elimination method provided the \tilde{i}_α values are held constant during any one iteration, and a method is implemented to update them between iterations. The method devised was to solve the differential equations of the mesh network in the time domain and to calculate the injected currents by a Fourier analysis of the resulting current waveform. These currents were injected into the nodal network to solve the nodal voltages. The voltage source \tilde{e}_p is expressed in the time domain after all harmonics in the nodal network have been solved for a particular iteration. These voltage values are then used to obtain an updated solution of the mesh network. In this fashion the iterative solution proceeds until convergence to the desired accuracy is obtained.

4.7 Conclusion To Chapter 4

In summary, several mathematical methods are developed, then synthesized to obtain a harmonic solution algorithm. The symmetrical components frame of reference does not have any computational advantage over the phase frame of reference for solving large unbalanced networks, although it is used in chapter 2 for the derivation of models for rotating machines which have balanced impedance. Zollenkopf's bifactorization method is adopted for Gauss elimination and is modified to permit solving Z Bus one column at a time with a preferred order of factorization which reduces computational effort. A three phase Gauss-Siedel loadflow algorithm is implemented to permit the solution of the correct phase angles for voltage and current at the fundamental frequency. This is combined with the shifting theorem utilized in digital signal processing to obtain the correct phase angle of injected harmonic load currents into the nodal admittance matrix for each harmonic order. Finally, the diakoptic equations for linear networks are developed and extended to an iterative method for solving networks containing nonlinear components.

Chapter 5

Synthesis of a Harmonic Solution Algorithm

5.0 Introduction To Chapter 5

The problem of calculating power system harmonics cannot be solved without the speed and accuracy of the computer. The importance of implementing mathematical and numerical methods as computer programming code cannot be overstated. No results will be obtained without this crucial step. A description of the computer program and relevant details of the algorithms are included here to provide a picture of the solution technique. The models described in the preceding chapters have been incorporated into program subroutines, which have been combined to solve the harmonic voltages and currents in the unbalanced, three phase network.

To achieve computational speed and reduce storage, a sparsity directed programming technique is used. The sparse storage scheme and the method of adding elements to it is described in the next section. The Zollenkopf bifactorization is implemented with a semi-optimal ordering scheme to minimize the number of new elements created during matrix reduction. The search strategy used during the reduction step of the matrix factorization is also described.

The three phase load flow subroutine and the nodal network solution require two distinct Y Bus formulations. The Y Bus for the load flow excludes the impedance of the motors and generators as these devices are modelled by injected current in the form of scheduled complex power. The load flow also requires reformulating the Y Bus in the solution of the neutral bus voltages. In formulating the nodal network harmonic Y Bus, the matrix is singular unless at least one bus on each side of a transformer is connected to the reference bus. The problem does not occur if motors, generators, or shunt admittances are present, or the neutrals of the transformers are earthed. The problem arises in the case of a harmonic producing load supplied from an ungrounded isolating transformer where the load is modeled solely by injected currents. One possible solution

is to model the load with a Norton equivalent circuit which places a shunt reactance across the injection current source. This approach has been described for a static var compensator [67] and for the magnetizing branch of an isolating transformer supplying a six pulse bridge [40].

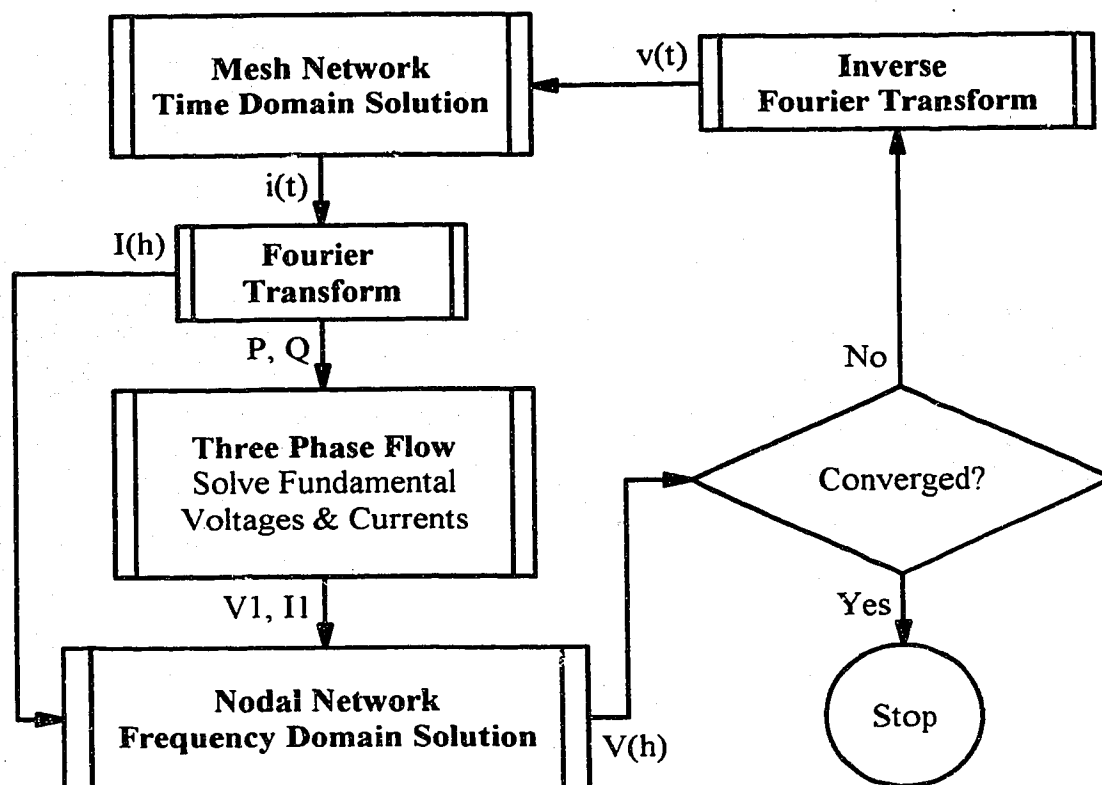


Figure 5.0.1 - Flow Chart For Harmonic Solution Algorithm

Figure 5.0.1 shows the interaction between the three phase loadflow and the solutions of the nonlinear mesh and linear nodal networks. The process begins with an initial three phase load flow which is used to establish the angles of the injected fundamental current at each bus. The mesh network is solved to determine $i(t)$ the current waveforms in the time domain. These are converted to the harmonic frequency domain currents by Fourier analysis. The fundamental power, P , and reactive power, Q , are also calculated for the six pulse converter loads. A three phase loadflow is calculated to

establish the fundamental voltage, $V(1)$, and its angle, δ , relative to the A phase swing bus, and the fundamental current, $I(1)$, and its power factor angle, θ , at each bus relative to the voltage at each bus. The harmonic currents, $I(h)$, are then injected into the nodal network to calculate the harmonic voltages, $V(h)$. The harmonic voltages are combined with an inverse Fourier transformation to establish the time domain voltage waveform, $v(t)$, which is used in the solution of the mesh network differential equations. The iterative process is stopped when convergence is obtained.

A balanced test case is run to validate the program and the results are compared to results from the Micromatrix Research "Software for Power Systems" (SPS) program.

5.1 Matrix Sparsity Storage Scheme

The linked list storage scheme is similar to that described by Brameller, Allan, & Haman [11]. The nodal network and three phase loadflow admittance matrices contain diagonal elements and off-diagonal elements. The diagonal is full but the off-diagonal positions contain many zero elements in a typical power system. Computational storage can be decreased and computational speed can be increased if a typical matrix is stored in a series of linked lists. Such a matrix is given by,

$$\begin{bmatrix} Y_{dp} & Y_t \\ Y_t & Y_{dp} \end{bmatrix} \quad (5.1.1)$$

where the subscript "dp" refers to the "driving point" diagonal elements and the subscript "t" refers to the "transfer" off-diagonal elements. The admittance, Y is stored as conductance, G and susceptance, B . The diagonal elements of Y Bus are associated with a counter "NUM" which tracks the number of off-diagonal elements associated with a particular column, and with a pointer "ICOL" which directs the program flow to the location in the off-diagonal storage scheme where the first off-diagonal element associated with a particular column is stored. If there are no off-diagonal elements, "ICOL" is set to zero to act as a flag.

The diagonal lists,

$$\begin{bmatrix} Gdp \\ \vdots \end{bmatrix} \begin{bmatrix} Bdp \\ \vdots \end{bmatrix} \begin{bmatrix} NUM \\ \vdots \end{bmatrix} \begin{bmatrix} ICOL \\ \vdots \end{bmatrix} \quad (5.3.2)$$

are stored as vector arrays, and have a dimension equal to the number of busses plus one. In the diagonal element storage scheme the array subscript refers to the particular column hence no column index is required.

The off-diagonal elements are associated with a matrix position index, "IROW" which tracks the row position, and a pointer "NXT" which directs the program flow to the location in the off-diagonal storage scheme where the next off-diagonal element associated with a particular column is stored. If there is no other element, the "NXT" pointer is set to zero to act as a flag. The off-diagonal lists,

$$\begin{bmatrix} Gt \\ \vdots \end{bmatrix} \begin{bmatrix} Bt \\ \vdots \end{bmatrix} \begin{bmatrix} IROW \\ \vdots \end{bmatrix} \begin{bmatrix} NXT \\ \vdots \end{bmatrix} \quad (5.1.3)$$

are stored as vector arrays, and have a dimension which is dynamic and limited only by the storage capacity of the computer or the ability of the software to allocate storage. In the off-diagonal lists, the subscripts of the "GT", "BT", "IROW" & "NXT" arrays are the same for any particular element stored, hence the subscripts act as links between the lists.

A program flow pointer "L" is used to tell the program where the next available storage space is located. As each matrix element is calculated, it is either placed in the "driving point" lists (if on a diagonal) or is placed in "transfer" lists (if it is an off diagonal of the matrix) and L is incremented accordingly. Once all elements of a column have been stored, the NXT value of the final element is set arbitrarily to zero to serve as a flag to alert the program that it has come to the end of a particular column. Figure 5.1.1 illustrates some of the pointers and links utilized in the sparse storage scheme.

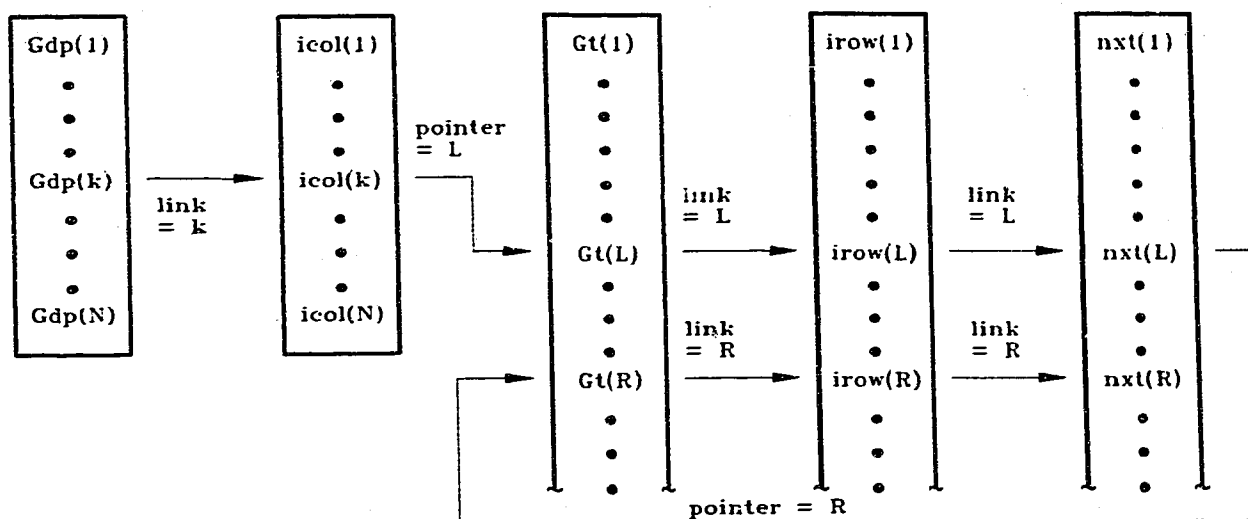


Figure 5.1.1 - Typical Pointers and Links In Sparse Storage Lists

The elements for column k are stored as follows: The driving point conductance is stored in location $Gdp(k)$ which is linked to $ICOL(k)$ by the array subscripts. The contents of $ICOL(k) = L$, which points to the location of the first transfer conductance stored in $Gt(L)$. This array is linked to $IROW(L)$, whose contents indicate the row of the original matrix associated with the transfer conductance. The contents of $NXT(L) = R$, which points to the location of the next transfer conductance element stored in $Gt(R)$. The susceptance values are stored in the Bdp array linked to Gdp , and in the Bt array linked to Gt .

The "Add" subroutine described in figure 5.1.2 illustrates the bookkeeping associated with the HYBus subroutine. There are three cases for adding an element. The first case occurs if the element is to be added to the matrix diagonal admittance. The second case is if the element is to be added to an existing element on the matrix off-diagonal. The third case is if the element is a new off-diagonal matrix element. The first two cases are straightforward as the storage lists and pointers do not change in length or position. The third case requires the lists' pointers and counters to be updated.

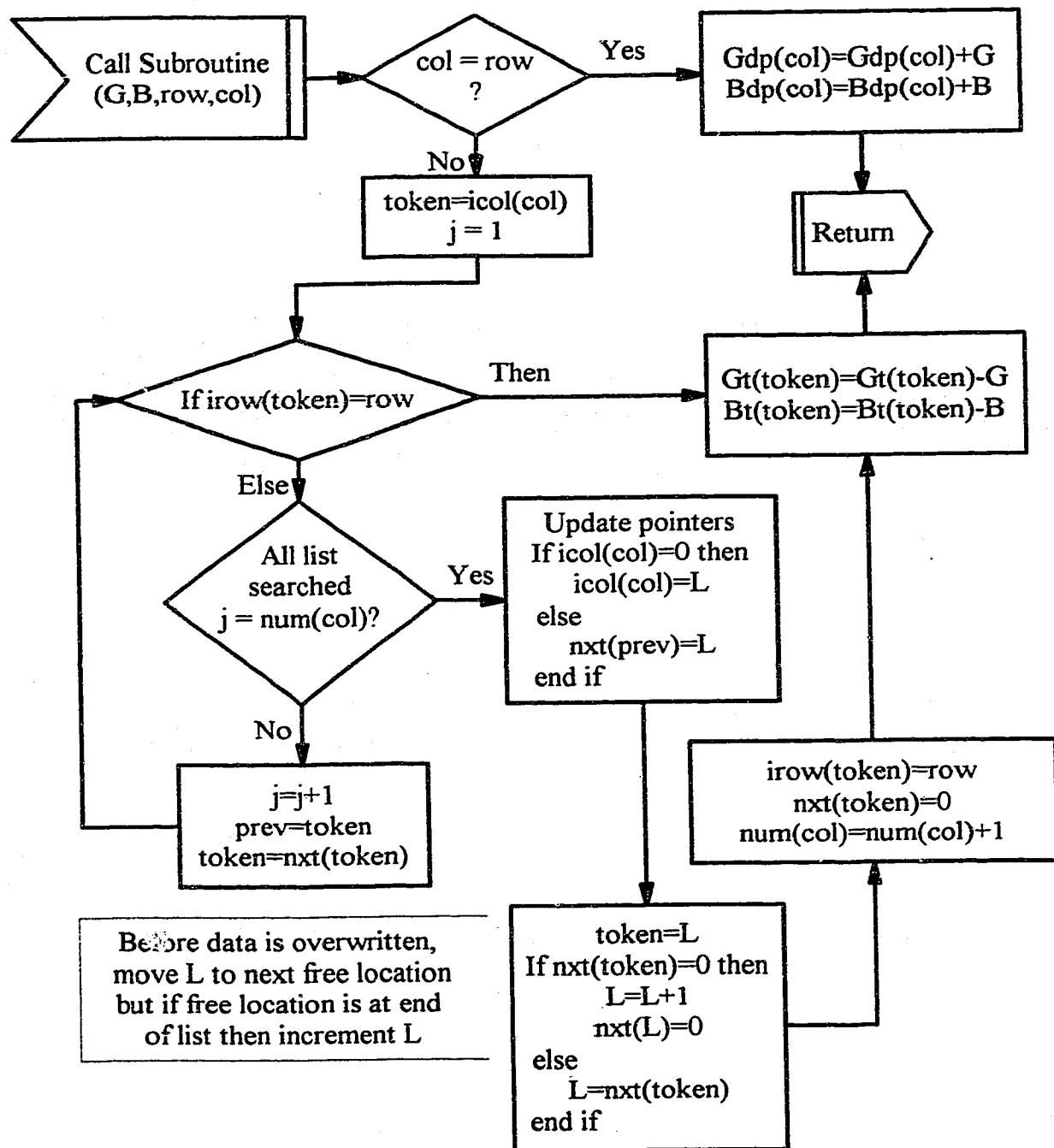


Figure 5.1.2 - Flow Chart For The Add Algorithm In The HYBUS Subroutine

5.2 Bifactorization With Semi-optimal Ordering

Semi-optimal ordering is defined as a process in which, at each step of factorization, the busses are searched to find the bus with the fewest number of transfer admittances connected to it. This tends to minimize the number of elements contained in the resulting row and column factors. This method is adopted in the "Order" and "Factor" subroutines, and gives good results for the radial topology power systems investigated. A description of the ordering algorithm is shown in figure 5.2.1. The order of factorization is stored in ORD to permit a subsequent algorithm to extract the column and row factors in the correct sequence. As each column is factored a flag is set so the column will be skipped during subsequent factorization searches.

In bifactorization, a reduced matrix is formed from the old matrix as the factors are calculated. Each new element in the reduced matrix,

$$Y_{ij(new)} = Y_{ij(old)} + Y_{ik} \frac{Y_{kj}}{Y_{kk}} \quad (5.2.1)$$

is changed from its old value only if the remaining terms in the formula are non-zero. In the matrix, the diagonal (or pivot) term Y_{kk} always exists and is non-zero due to the way the matrix was formed from the Y Bus matrix. This algorithm therefore first identifies the "k"th column as the one to be factored. It identifies Y_{kk} from Gdp(k) and Bdp(k) in the storage scheme and calculates the column factor diagonal element,

$$C_{kk} = \frac{1}{Y_{dp(k)}} \quad (5.2.2)$$

The row factor elements, R_{kj} , are then calculated by searching all other columns, skipping any column already factored, to search for elements Y_{kj} in ROW "k". If an Y_{kj} is found, the row factor element,

$$R_{kj} = -Y_{kj} C_{kk} \quad (5.2.3)$$

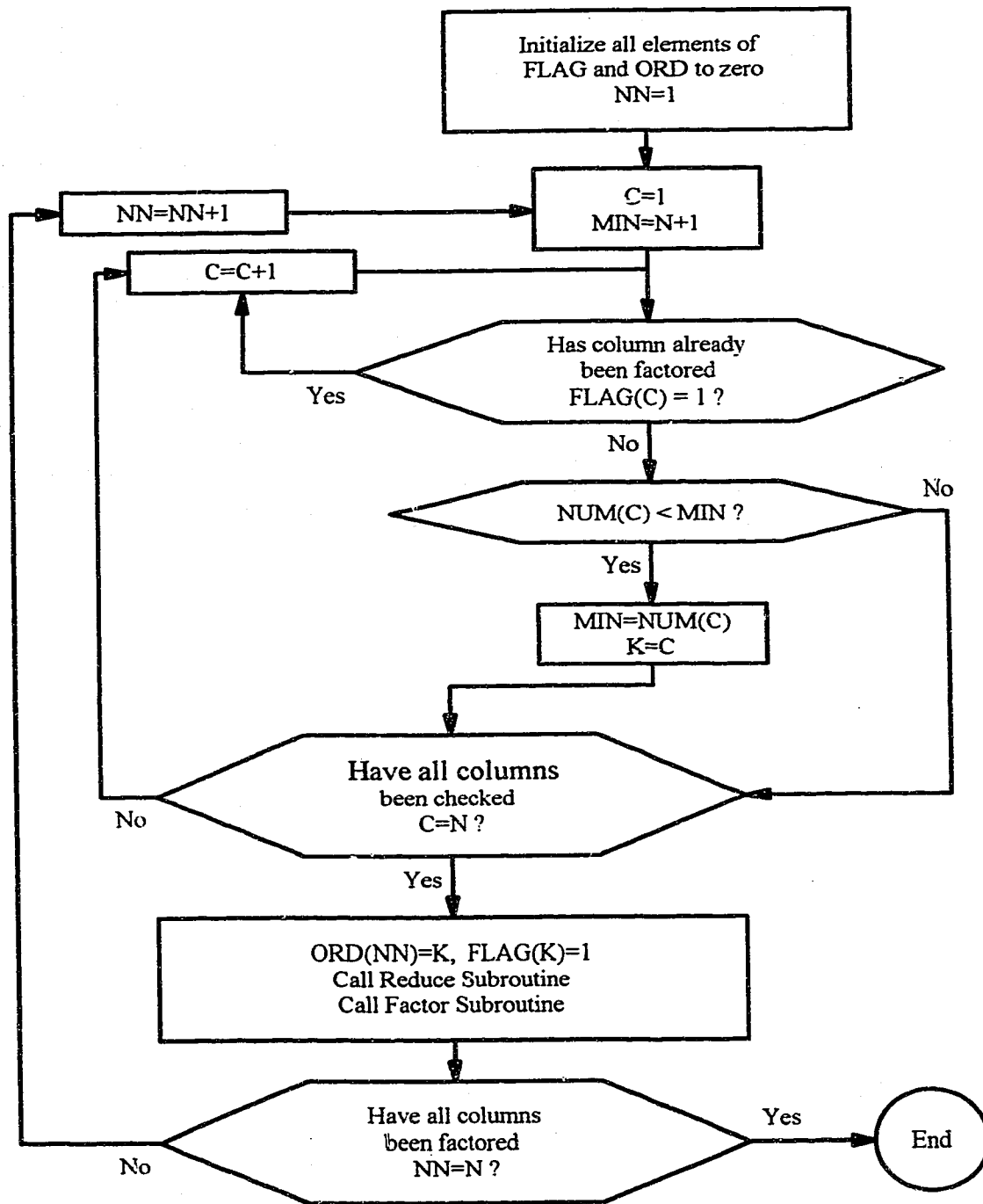


Figure 5.2.1 - Flow Chart For Order Algorithm

is stored temporarily in scratchpad COLUMN "N+1". This avoids over-writing data in the storage scheme which will be required for various remaining calculations. Element Y_{kj} is then deleted from COLUMN "j" and column "k" is scanned for the off-diagonal elements, Y_{ik} .

Figure 5.2.2 forms the basis for the search logic of the algorithm. As each Y_{ik} is found, its ROW location is recorded as "i". Next column "j" is scanned to see if it contains an element Y_{ij} in row "i". This scan must include the diagonal as well as the off-diagonal elements in column "j" due to the relationship of Y_{ij} to Y_{ik} and Y_{kj} , namely that the "i" in Y_{ik} and the "j" in Y_{kj} determine the address of Y_{ij} .

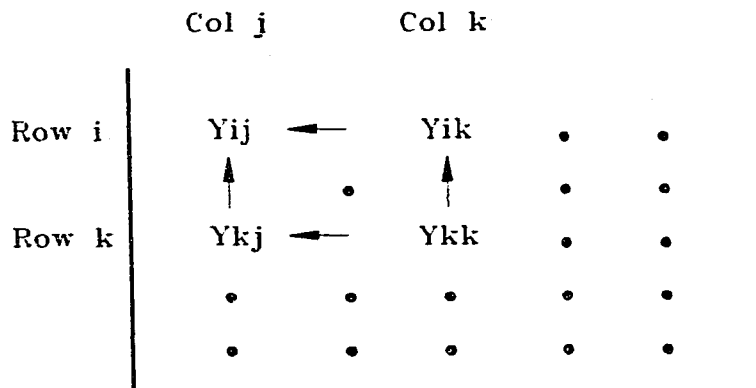


Figure 5.2.2 - Bifactorization Search Scheme For The Factor Subroutine

This process is continued until a new Y_{ij} in column "j" has been calculated which corresponds to every Y_{ik} in column "k". The algorithm then continues its search of columns looking for the next Y_{kj} in row "k" and the process of calculating the Y_{ij} terms is repeated. The column factor elements,

$$C_{ik} = -Y_{ik} C_{kk} \quad (5.2.4)$$

are computed and at the same time the associated Y_{ik} terms are deleted from column "k".

The row factor elements, R_{kj} , are then transferred from temporary storage in the temporary column N+1 to permanent storage in column "k", and the N+1 column is emptied, ready for the next factorization. A new column is then selected for factorization and so on, until all columns have been factored. Once all the row factor elements, R_{kj} ,

have been calculated and all the elements, Y_{ij} , of the matrix have been reduced, the C_{kk} real and imaginary parts are stored in the G_{dp} and B_{dp} linked lists, and the real and imaginary parts of the R_{kj} row factor elements are stored in the G_t and B_t linked lists. The original harmonic Y Bus matrix elements are overwritten to save storage space. The C_{kj} elements are the transpose of the R_{jk} elements and need not be stored.

5.3 Inverting The Matrix One Column At A Time

A review of the pertinent equations provides a starting point for describing the Invert subroutine. It is desired to solve the voltage in the equation,

$$YV=I \quad (5.3.1)$$

by premultiplying by the inverse of Y to obtain the form,

$$V = Y^{-1}I \quad (5.3.2)$$

This is directly calculated by substituting the row and column factors which results in,

$$V = \{ R^{(1)} \dots R^{(k)} \dots R^{(n)} C^{(n)} \dots C^{(k)} \dots C^{(1)} \} I \quad (5.3.3)$$

where the numbers in brackets refer to the order of factorization. One column of the inverted matrix,

$$\begin{bmatrix} Z_{1K} \\ \vdots \\ Z_{KK} \\ \vdots \\ Z_{NK} \end{bmatrix} = R^{(1)} \dots R^{(K)} \dots R^{(N)} C^{(N)} C^{(N-1)} C^{(N-2)} C^{(N-3)} \begin{bmatrix} 0 \\ \vdots \\ 0 \\ 1 \\ 0 \\ \vdots \\ 0 \end{bmatrix} \quad (5.3.4)$$

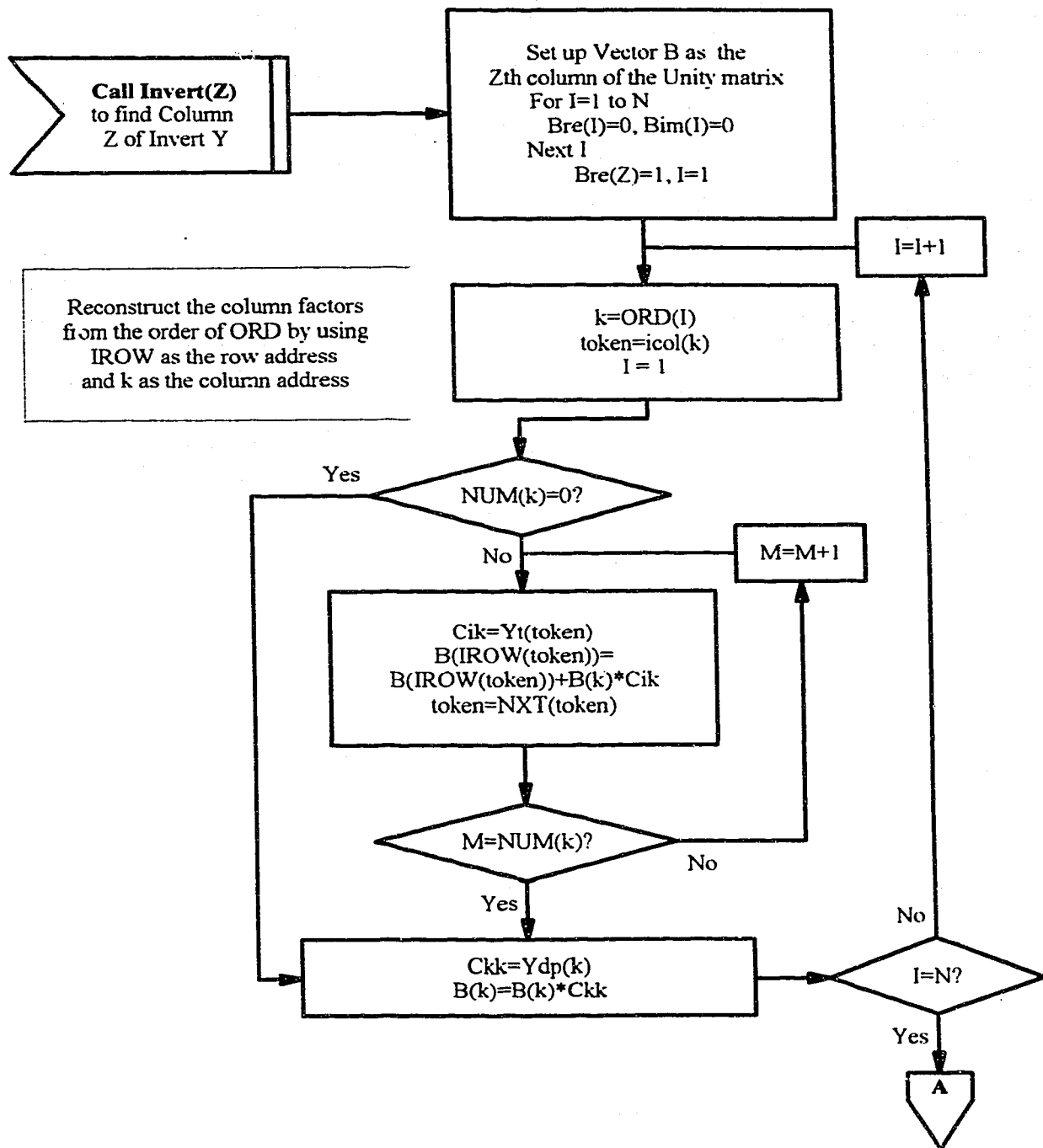


Figure 5.3.1 - Flow Chart -Invert Subroutine - a) Reconstructing the Column Factors

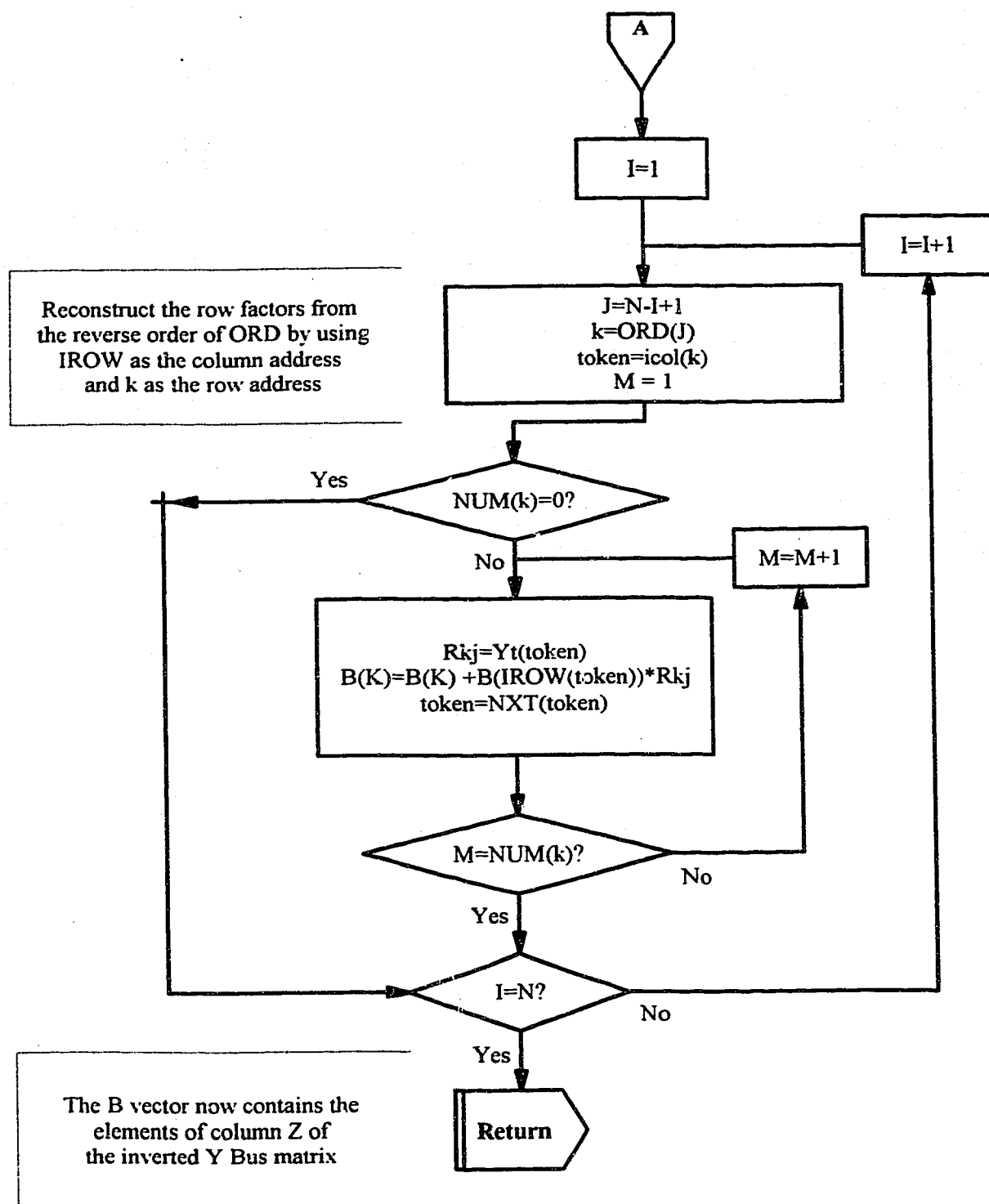


Figure 5.3.2 - Flow Chart -Invert Subroutine - b) Reconstructing the Row Factors

is all that is required to find the component of voltage,

$$\begin{bmatrix} V_{1(K)} \\ V_{2(K)} \\ \vdots \\ \vdots \\ V_{N(K)} \end{bmatrix} = R^{(1)} \dots R^{(K)} \dots R^{(N)} C^{(N)} C^{(N-1)} C^{(N-2)} C^{(N-3)} \begin{bmatrix} 0 \\ \vdots \\ 0 \\ 1 \\ 0 \\ \vdots \\ 0 \end{bmatrix} \cdot I_K \quad (5.3.5)$$

at each bus contributed by the current at one particular bus. This is implemented in the flow chart for the Invert algorithm in figure 5.3.1. First the subroutine sets up a column of the unity matrix in the **b** vector, then it reconstructs the column factors from the order of ORD by treating IROW as the row address and k as the column address. The **b** vector accumulates the sum of the **Cik*b** products and the sum of the **Ckk*b** products. The flow chart continues in figure 5.3.2 where the subroutine reconstructs the row factors from the reverse order of ORD by treating IROW as the column address and k as the row address. Only off-diagonal elements exist in row factors hence the **b** vector accumulates the sum of **Rkj*b** products. When the subroutine finishes the **b** vector contains the elements of column z of the inverted Y Bus matrix.

5.4 Three Phase Loadflow Subroutine

The flow chart for the three phase loadflow subroutine is shown in figure 5.4.1. The routine accepts data from two sources, the data file which contains the linear elements and fundamental power for the motors and generators, and an input from the mesh network solution which provides the fundamental power of the converter loads. The Y Bus is assembled for the fundamental frequency. It contains the neutral busses, but does not contain shunt branches for the motor loads and generator supplies. The magnetizing branches of motors, generators and transformers are included as linear elements to model their contribution to the fundamental frequency Y Bus. The loadflow is calculated using a straight forward Gauss Siedel method. This method is well documented elsewhere and, except for the neutral bus voltages, will not be discussed here. The purpose of running the loadflow is to provide the correct angular relationships, δ , for fundamental voltage with reference to the A phase swing bus, and the power factor angle, θ , for fundamental current with respect to the phase voltage at each bus, together with the magnitudes of fundamental current and voltage. The neutral bus voltage is formulated with a summation term given by,

$$V_K = \frac{1}{Y_{KK}} \left(- \sum_{J=1}^N Y_{KJ} V_J \right) \quad J \neq K \quad (5.4.1)$$

This is incorporated into the "Neutral" algorithm as shown in figure 5.4.2.

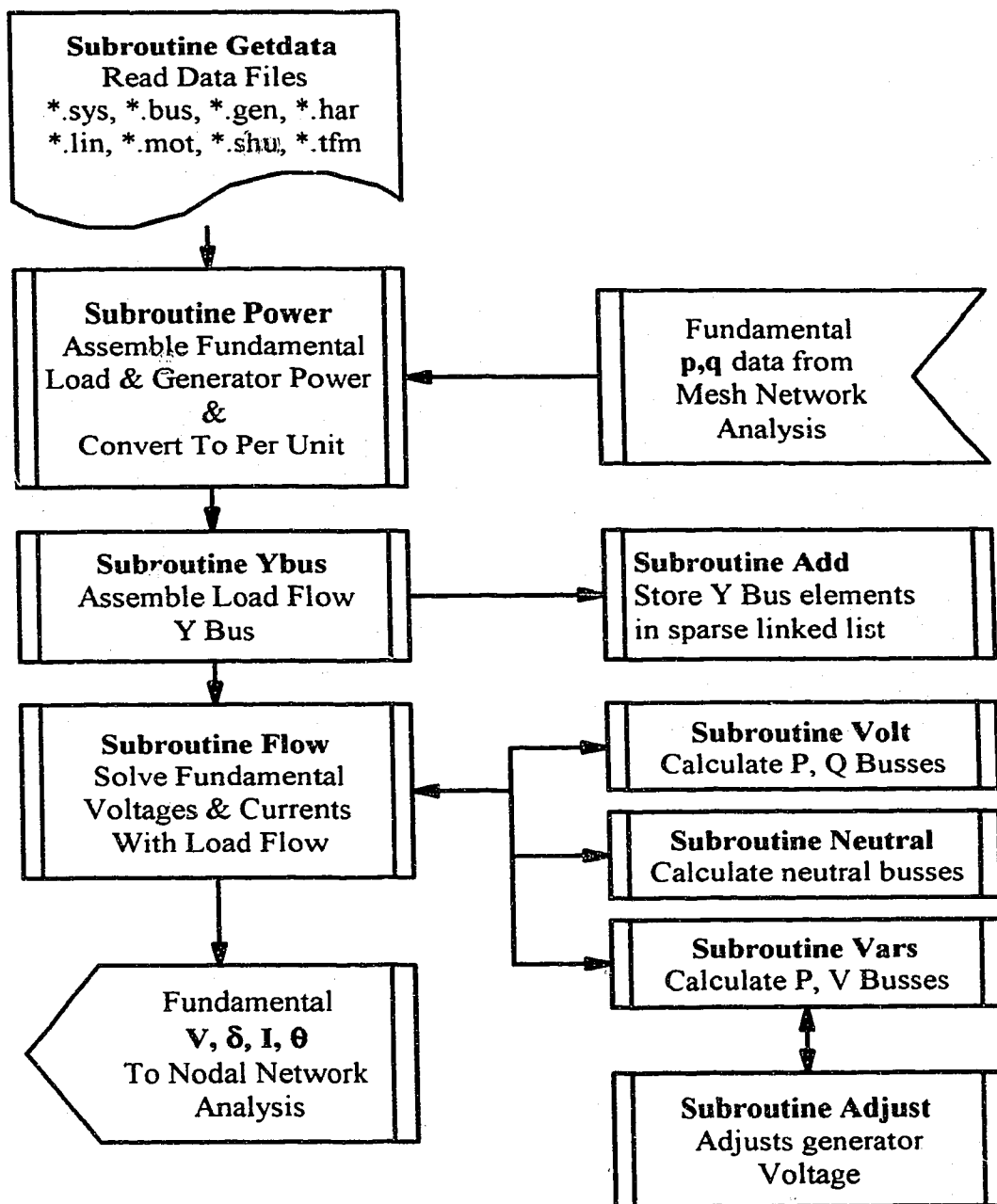


Figure 5.4.1 - Flow Chart For Three Phase Loadflow Algorithm

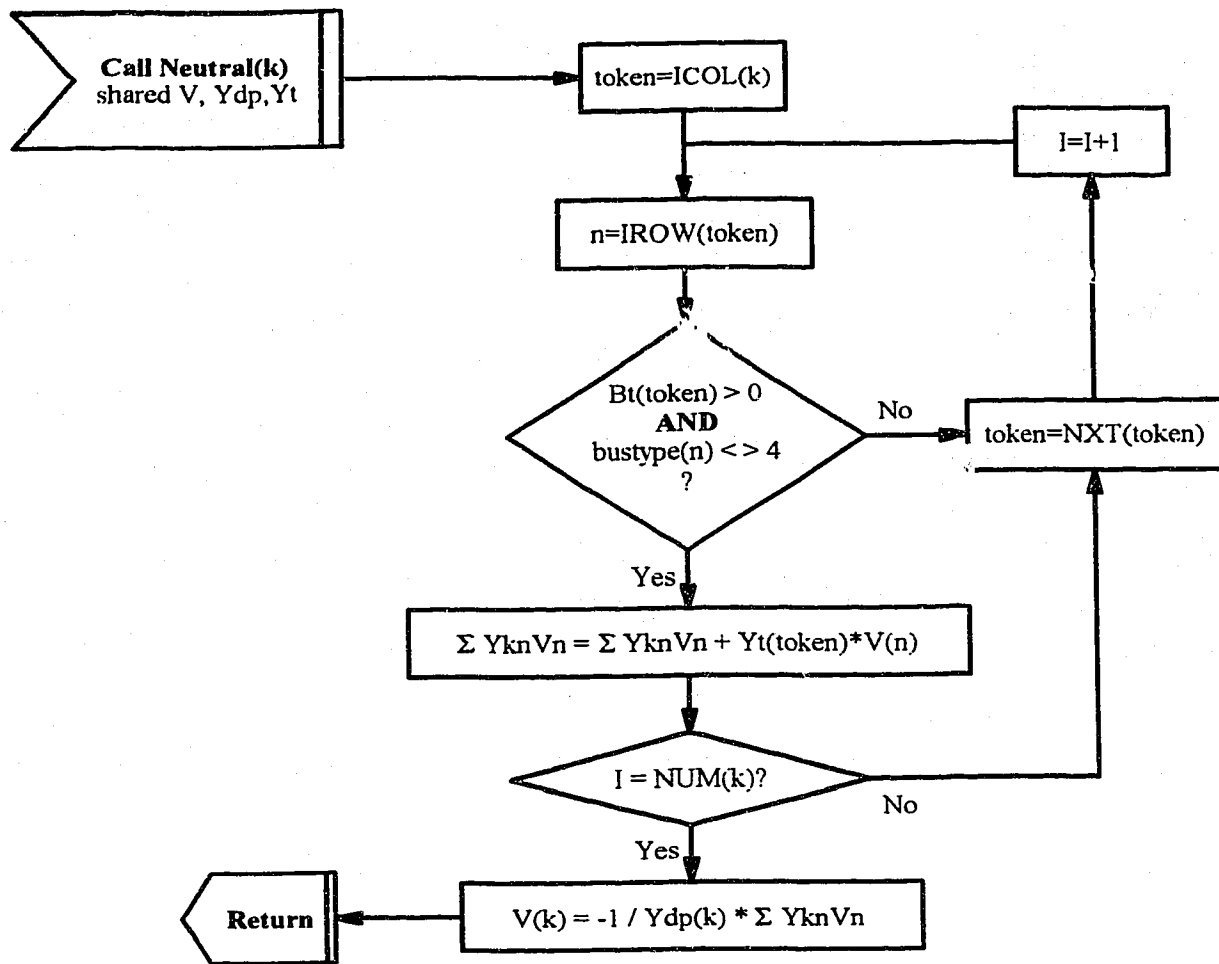


Figure 5.4.2 - Flow Chart For Neutral Bus Loadflow Algorithm

The "Neutral" algorithm accesses the most recently calculated bus voltages and the network admittances from the storage lists, and is passed the variable "k" which identifies the neutral bus number. It accumulates the sum of the product of the off-diagonal transfer admittances and their associated bus voltages, and divides by the negative of the driving point admittance to obtain the neutral bus "k" voltage.

With reference to figure 4.5.1 in chapter 4 it is seen that the neutral bus in a delta-wye transformer is connected to each primary and secondary phase by the model. The delta winding connections may be excluded from the summation term in equation (5.4.1) because they add to zero. This is shown by the first six terms of the summation given by,

$$V_n = -\frac{1}{Y_{nn}} \left(V_A \frac{y}{\sqrt{3}} - V_A \frac{y}{\sqrt{3}} + V_B \frac{y}{\sqrt{3}} - V_B \frac{y}{\sqrt{3}} + V_C \frac{y}{\sqrt{3}} + V_C \frac{y}{\sqrt{3}} + (V_X + V_Y + V_Z) y \right) \quad (5.4.2)$$

For the wye-wye transformer model shown in figure 4.5.2 in chapter 4, equation (5.4.1) can be solved using the model connections for the primary neutral "n" of the transformer to yield,

$$V_n = -\frac{1}{Y_{nn}} \left[(V_N - V_X) y + (V_N - V_Y) y + (V_N - V_Z) y + (V_A + V_B + V_C) y \right] \quad (5.4.3)$$

where "N" is the neutral of the secondary winding and "X", "Y", and "Z" are the secondary winding terminals. The first three terms of the summation in equation (5.4.3) describe the currents in the branches of the secondary wye winding and these must always add to zero for an unconnected neutral. This justifies omitting these terms when calculating the primary neutral bus voltage of a transformer with an unconnected secondary neutral in situations where it is desired to retain the secondary neutral terminal in the model. By making these simplifications, the speed and numerical stability of the algorithm is enhanced.

5.5 Mesh Network Subroutines

There are two subroutines used to solve the differential equations in the mesh network. The first is the six pulse converter algorithm shown in figure 5.5.1.

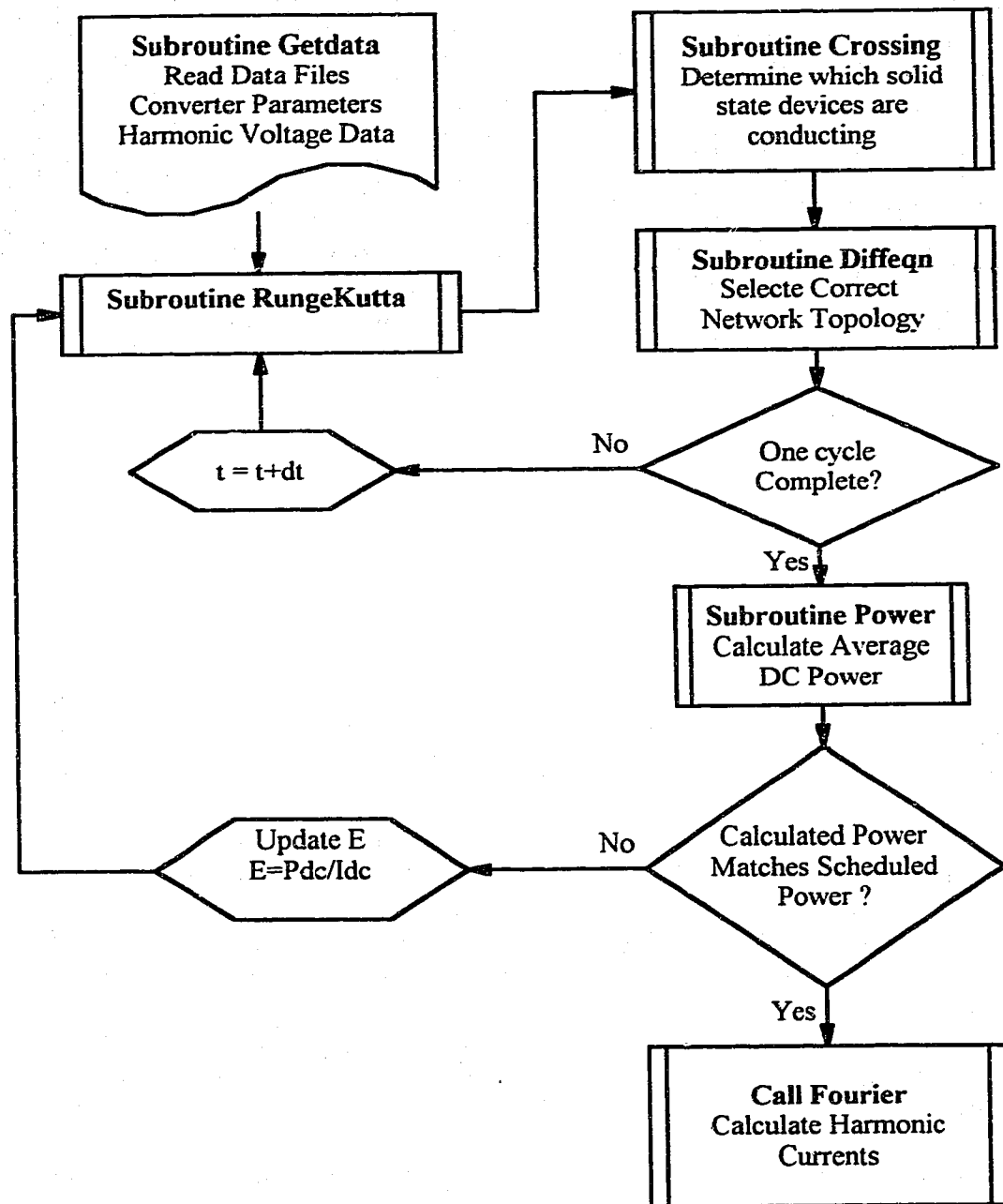


Figure 5.5.1 - Flow Chart For Six Pulse Converter Algorithm

Care must be taken when establishing the parameters for the differential equations to avoid "divide by zero" errors in the program run time module. The derivative of current,

$$\frac{dI_c}{dt} = \frac{V_a - V_b - E - I_a(R_a + R_d) + I_b R_b - \frac{dI_a}{dt} [L_a + L_b + L_d]}{L_b} \quad (5.5.1)$$

on the negative rail overlap condition illustrates this point. The denominator of the equation is the AC inductance L_b , which must have a non-zero value if the equation is not to "blow up". When formulating the nonlinear mesh network, some AC inductance must be included to obtain satisfactory results. The question arises as to what should be used for this inductance. If AC line reactors are present on the converter their inductance is the best choice. If there is a long cable run supplying the converter, its inductance may be a satisfactory choice, but if the cable inductance is small then the numerical accuracy of the procedure will be inherently poor. If there are no line reactors and the cable reactance is small the inductance must be chosen arbitrarily. The difficulty with this is that the mesh voltage must be established at the diakoptic bus between the nodal network and the mesh network. A method is devised which corrects the transformer secondary voltage,

$$\tilde{V}_{(h)} = V_{sec(h)} + I_{sec(h)} x_{leakage(h)} \quad (5.5.2)$$

to permit an approximation of tearing the mesh network at the transformer primary while tearing the nodal network at the transformer secondary.

The second subroutine for solving the mesh network is that shown in figure 5.5.2 for magnetizing branches. The input data is used to construct an hyperbolic model of the magnetization curve neglecting hysteresis. The AC voltage is integrated to calculate the AC flux linkages and added to the DC flux linkage, and at each step of integration the magnetizing current is calculated. One complete fundamental cycle of voltage has to be

integrated to determine the magnetizing current waveform.

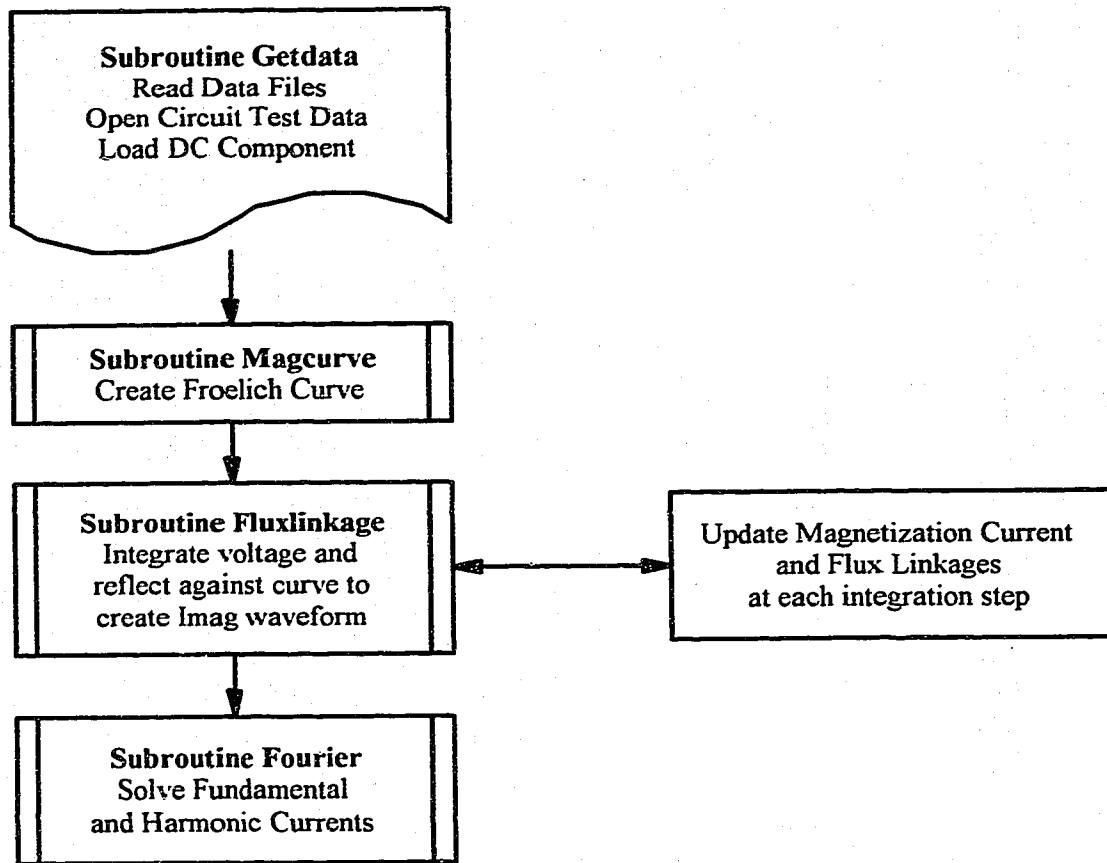


Figure 5.5.2 - Flow Chart of Transformer Magnetizing Branch Algorithm

5.6 Nodal Network Subroutine

The nodal network subroutine is shown in figure 5.6.1. It combines several routines described earlier in this chapter, namely "Hybus", "Order", "Factor", and "Invert". The "Hybus" subroutine assembles the nodal admittance matrix for a particular harmonic. It is then factored, inverted, and injected with harmonic currents at a particular harmonic frequency to calculate the harmonic components of voltage at that frequency. The voltage components are stored and recombined by an inverse Fourier analysis to formulate the time domain waveforms at the diakoptic busses. It is designed to be interactive with the mesh network routines to converge on a solution of voltage at the diakoptic busses.

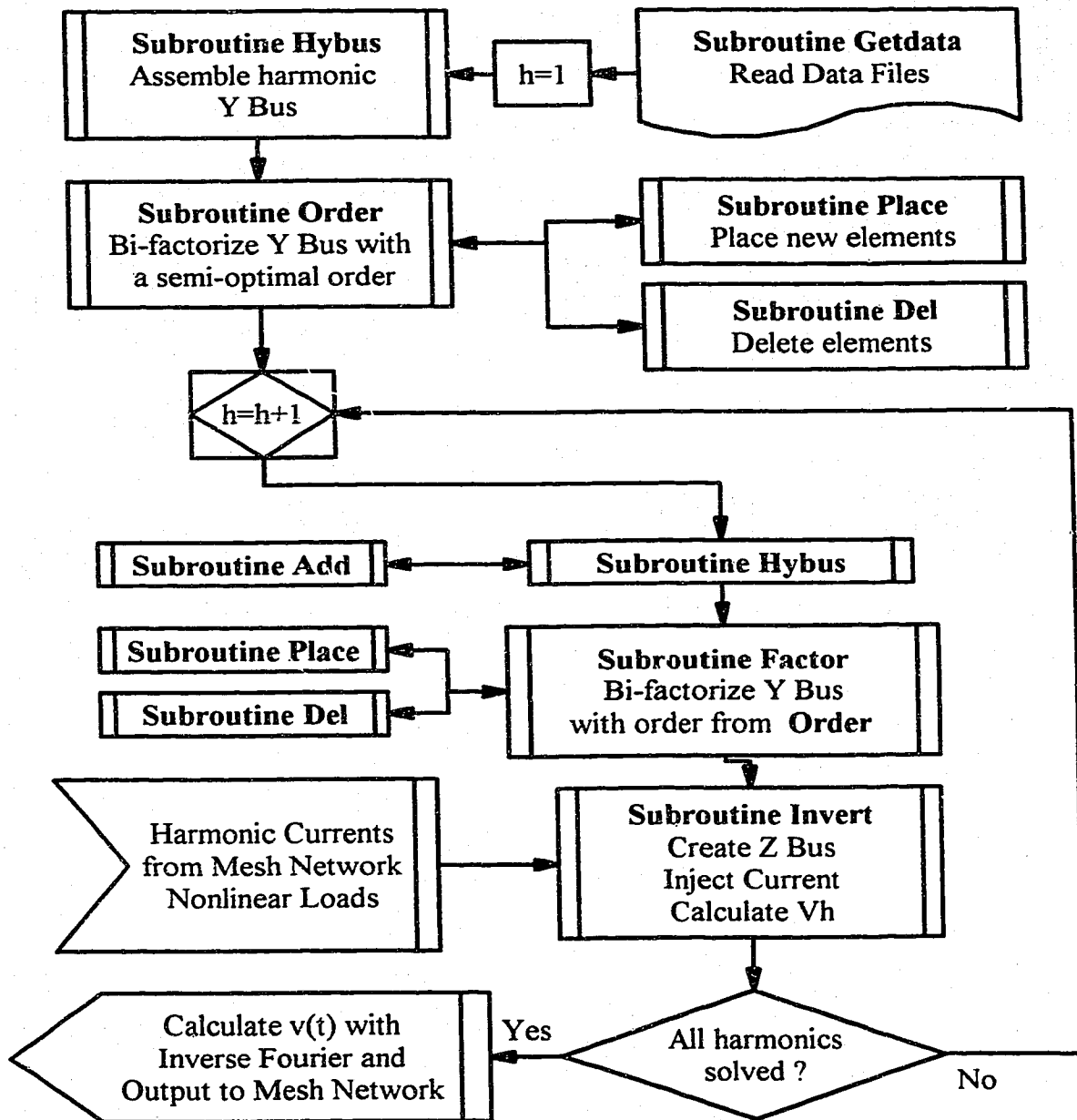


Figure 5.6.1 - Flow Chart of Nodal Network Harmonic Solution Algorithm

5.7 Program Validation

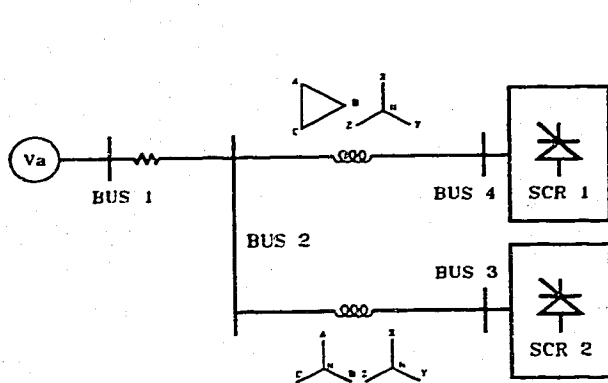


Figure 5.7.1a - "SPS" 1 Line Diagram

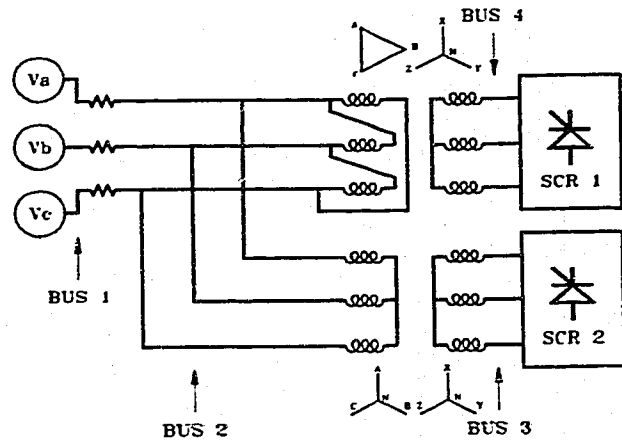


Figure 5.7.1b - "Solver" 3 Line Diagram

To validate the program, a balanced 4 bus network, shown in figure 5.7.1a, is prepared for "SPS", and a 12 bus network, shown in figure 5.7.1b, is prepared for the "SOLVER" program developed in this thesis. The "SPS" program is commercially available software which takes a single phase (as opposed to a three phase) approach to formulating networks but which includes the phase shifts which occur on delta-wye transformers for balanced loads and network elements. The network solutions are compared in Table 5.7.1. For this balanced case the "SPS" and "SOLVER" harmonic voltages agree to within 6 parts in 100,000 (0.006 %). From these results it is concluded that the harmonic solution algorithm synthesized in this thesis is successful.

Table 5.7.2 shows the results when the same network is subjected to a 2% voltage unbalance on "B" phase, and this is combined with load unbalance and firing angle unbalance. The combined unbalanced conditions increase the magnitudes of the fifth and seventh harmonic voltages, and reduce the magnitudes of the eleventh and thirteenth harmonic voltages. Because the SPS software cannot solve an unbalanced system no comparison with it was made for the unbalanced case.

Table 5.7.1 - Comparison of Harmonic Voltages For The Balanced Case

Bus	SPS - % V (by harmonic order)			SOLVER - % V (by harmonic order)		
	1	5,7	11,13	1	5,7	11,13
1	100.000	0	28.623	100.000	0	28.651
2	86.797	0	47.706	86.798	0	47.510
3	83.847	4.771	52.476	83.852	4.775	52.526
4	83.847	4.771	52.476	83.852	4.775	52.526

5.8 Conclusion To Chapter 5

In chapter 5 the various harmonic solution methods are implemented as computer algorithms which form the constituent parts of the harmonic solution program

The matrix elements' sparse storage lists are described. It is shown how these lists are used in the bifactorization algorithm and the three phase loadflow algorithm. The mesh and nodal solution program flow charts are described and the interactions between the various modules are identified in terms of the diakoptic equations. The resulting program is successfully validated for a balanced test network. A calculation for the example network with multiple unbalanced conditions shows such unbalanced conditions can have a major impact on harmonic magnitudes. Development of the multiphase harmonic analysis software achieves the specific purpose of the research project.

Table 5.7.2 - Harmonic Voltages For The Unbalanced Case

Bus	1st		5th		7th		11th		13th	
	Mag %	Ang deg.	Mag %	Ang deg.	Mag %	Ang deg.	Mag %	Ang deg.	Mag %	Ang deg.
1a	100.0	0	9.2	140	12.1	174	17.5	139	15.4	166
1b	98.0	240	8.9	259	11.7	48	19.2	255	16.3	46
1c	100.0	120	8.7	20	11.7	294	18.3	20	16.1	288
2a	88.1	353	15.3	140	20.3	174	29.1	139	25.7	166
2b	85.9	233	14.9	259	19.5	49	32.0	255	27.2	46
2c	88.1	113	14.6	20	19.5	294	30.6	20	26.8	288
3a	85.2	351	18.8	129	23.7	166	33.1	143	29.2	172
3b	82.9	230	18.4	247	23.2	40	36.1	260	31.1	52
3c	85.2	111	18.0	9	22.9	285	34.5	24	30.6	294
4a	85.6	321	15.1	183	21.0	154	32.0	165	28.5	130
4b	84.6	201	15.4	303	21.5	30	32.3	280	27.9	10
4c	84.3	82	15.0	63	19.7	272	34.6	44	28.9	251

Chapter 6

Summary And Recommendations For Further Research

6.1 Recommendations For Further Research

Studies of the transformer have shown that further research into modelling the magnetizing branch is advisable. While the behaviour under sinusoidal load current conditions is well known there is evidence that minor hysteresis loops may be a significant factor when the energizing voltage is distorted. If this is the case, the open circuit test data based on sinusoidal voltage may not be extendable to the harmonic model. One possibility is to develop an open circuit test where the voltage is distorted by the equivalent of a nearby six pulse converter load to see if this creates second order effects of significant magnitude.

Harmonic models for earth return circuits need to be developed. The soils models used in power system substation ground grid step and touch voltage calculations provide an entry point. Validation of these models by field measurement requires an instrument capable of injecting large harmonic current into the ground grid. One avenue for research is the development of such an instrument.

It was noted when investigating the generator failures that there was evidence one machine may have failed due to insulation breakdown as opposed to overheating. Research is needed to determine if low voltage windings (480 V) which are random wound and coated with contaminants (salt spray and oil) are subject to partial discharge failures when supplying SCR front end drives. These drives create relatively high dV/dt due to line-to-line voltage notching when the thyristors commute.

6.2 Summary

The main objective of this research project is to develop a three phase harmonic solution algorithm to solve unbalanced systems. Several key models are developed, the underlying mathematical procedures are extended and written into software algorithms, and the goal is achieved.

The Zollenkopf bifactorization method is extended to efficiently invert a matrix one column at a time. This permits a minimum expenditure of computational effort when injecting harmonic currents to solve harmonic voltages. The importance of resolving a power system into linear and nonlinear portions is demonstrated and the diakoptic equations are extended to permit treatment of the nonlinear portion as mesh network differential equations and the linear portion as a superposed series of harmonic nodal networks. By using such a division methods pertinent to each network solution can be employed. The nodal network is solved in the frequency domain by inverting Y Bus to obtain Z Bus, and the mesh network is solved in the time domain by solving differential equations. The time domain current solution from the mesh network is converted to harmonic current by a Fourier transformation and the harmonic voltage solution from the nodal network is converted to a time domain waveform by an inverse Fourier transform. The currents and voltages at the diakoptic bus boundaries between the nodal and mesh networks are solved by iteratively using the harmonic currents from the mesh solution as input to the nodal network and the voltage waveforms from the nodal solution as input to the mesh network.

A number of models of power system components are developed in Chapter 2. The underlying requirements for the models used in the nodal network is firstly that they correctly implement mutual coupling between phases, and secondly that they are linear to within reasonable engineering approximation. This research project is concerned with the frequency range of interest for power system harmonic analysis as defined in the IEEE 519 standard, namely 50 to 5000 Hertz. The transformer is a key component; hence, it is modelled in detail and its behaviour is verified by laboratory measurements to validate the use of simplifying assumptions.

Transformers which supply converters are often subjected to loading conditions in which there is a significant DC component in the load current. As a consequence, harmonic currents are created by the magnetizing branch. This is modelled and the model is checked by laboratory measurements. The results are promising, but the accuracy of the model is on the order of $\pm 25\%$. This is an area which needs further refinement.

Heating effects on a generator rotor when the machine is supplying non-sinusoidal loads may damage the machine. A model is developed to permit analysis of the harmonic currents induced into the rotor by synthesizing known methods. The model includes skin effect and thus accommodates variations in the diameter of the amortisseur bars. More VFD load measurements are required to validate this model.

A technique is developed in Chapter 3 to interpolate the underlying operating frequency of measured waveforms from the measured spectra when the sampling is performed asynchronously.

Chapters 4 and 5 describe the synthesis of several methods and models into a network harmonic analysis program which permits the solution of harmonics in a three phase frame of reference, including neutral busses, for unbalanced loads, unbalanced sources, and unbalanced network components. The program is validated by comparing a balanced multiphase network, using the program, with a balanced single phase network, using a commercially available program, SPS. The results compare to within a 0.006 % tolerance. An unbalanced case is also calculated to show that combined unbalance conditions in the network can have a major effect on system harmonics.

One important result of this research project is that it provides power system designers with a computer program capable of harmonic analysis within the multiphase frame of reference. This allows them to verify that their designs meet the utility standards. Of equal importance it allows designers to investigate the effect of unbalanced supply voltage on various phase-shifting harmonic cancellation schemes. Many of these designs depend on balanced voltage and balanced loading conditions to obtain good results and do not provide the desired results when systems are unbalanced.

The contribution of the research presented in this thesis is summarized as follows:

- 1 The Zollenkopf bifactorization method is extended to invert one bus at a time and the order of factorization is modified to factor harmonic load busses last which minimizes the required computational effort.
- 2 The diakoptic equations are modified to describe the mesh portion of the network in the time domain and to describe the nodal portion of the network in the frequency domain allowing the linear and nonlinear portions of the network each to be solved by well-suited methods.
- 3 A model is synthesized which predicts generator rotor heating due to harmonic loads when using different diameters of amortisseur bars.
- 4 A technique is developed to accurately interpolate the frequency of measured repetitive waveforms from asynchronously sampled data.
- 5 A computer program is created which calculates harmonic voltages and currents in an unbalanced multiphase power system.

Bibliography

- [1] Acha, E., Arrillaga, J., Medina, A., Semlyn, A. "General Frame of Reference for Analysis of Harmonic Distortion in Systems With Multiple Transformer Nonlinearities", IEE Proc¹, Vol 136, Pt C, No. 5, Sept, 1989, p. 271.
- [2] Alberta Power "Harmonic Specification For Harmonic Producing Customers Connected To The Alberta Power System (Rev Mar. 1988)".
- [3] Anderson, P. M., Fouad, A. A., "Power System Control and Stability", Chapter 4 - "The Synchronous Machine", IEEE Press, New York, 1994.
- [4] Arrillaga, J., Arnold, C. P. (1983) "Computer Analysis of Power Systems", John Wiley & Sons, New York.
- [5] Arrillaga, J., Arnold, C. P. (1990) "Computer Modelling of Electrical Power Systems", John Wiley & Sons, New York.
- [6] Arrillaga, J., Bradley, D. A., Bodger, P.S. (1985) "Power System Harmonics", John Wiley & Sons, Toronto.
- [7] Arrillaga, J., Callaghan, C. D. "Double-Iterative Algorithm for the Analysis of Power and Harmonic Flows at AC/DC Convertor Terminals", IEE Proc, Vol 136, Pt C, No. 6, Nov, 1989, p.319.
- [8] Baghzouz, Y. "An Accurate Solution To Line Harmonic Distortion Produced By AC/DC Converters With Overlap And DC Ripple", IA-29, No. 3, May/June, 1993, p. 536.

¹ The following abbreviations and acronyms are used throughout the bibliography:

IEE - British Institute of Electrical Engineers
IEEE - Institute of Electrical and Electronic Engineers
IA - IEEE Transactions on Industry Applications
IASC - IEEE Industry Applications Society Annual Conference
ICHPS - IEEE International Conference on Harmonics in Power Systems
IGA - IEEE Transactions on Industry & General Applications
PAS - IEEE Transactions on Power Apparatus & Systems
PCIC - IEEE Petroleum and Chemical Industry Conference
PWRS - IEEE Transactions on Power Systems

- [9] Bedford, R. E., Nene, V. D. "Complex Frequency-Domain Analysis of Inverter-Fed Machines", IA-8, No. 3, May/June, 1972, p. 269.
- [10] Blackburn, J. L., "Protective Relaying Principles and Applications", Chapter 11 - Motor Protection, Marcel Dekker Inc., New York, 1987.
- [11] Brameller, A., Allan, R. N., Haman, Y. M. (1976) "Sparsity Its Practical Application To System Analysis", Pitman Publishing, Toronto.
- [12] Brameller, A., John, M. N., Scott, M. R. (1969) "Practical Diakoptics for Electrical Networks", Chapman & Hall Ltd., London.
- [13] Crnosija, P., Kmetec, M. "Determination of Network Voltage Distortion Factor by Digital Computer Simulation", IEE Proc, Vol 127, Pt B, No. 6, November, 1980, p. 358.
- [14] DeWinter, F. A., Grainger, L. G. "A Practical Approach To Solving Large Drive Harmonic Problems At The Design Stage", IA-26, 5, Nov/Dec 1990, p.1095.
- [15] Dortort, I. K. "Phase Shifting of Harmonics in AC Circuits of Rectifiers", IGA-4, No. 6, Nov/Dec, 1968, p. 655.
- [16] Duffey, C. K., Stratford, R. P. "Update of Harmonic Standard IEEE-519: IEEE Recommended Practices and Requirements for Harmonic Control in Electric Power Systems" Paper No. PCIC-88-7 Conference Record of PCIC, September, 1988.
- [17] Emanuel, A. E., Orr, J. A., Cyganski, D. "Review of Harmonics Fundamentals and Proposal for a Standard Terminology", Proceedings of Third ICHPS, September, 1987, p. 1.
- [18] Graham, A. D., Schonholzer, E. T. "Line Harmonics of Converters With DC Motor Loads", IA-19, No. 1, Jan/Feb 1983, p. 84.
- [19] Grainger, L. G., Spencer, R. C. "Residual Harmonics in Voltage Unbalanced Power Systems", IA-30, No. 5, Sep/Oct 1994, p. 1398.
- [20] Greene, J. D., Gross, C. A. "Nonlinear Modelling of Transformers", IA-24, No. 3, May/June 1988, p. 434.
- [21] Gorman, J., Grainger, J. J. "Transformer Modelling for Distribution System Studies Part I - Linear Modelling Basics", IEEE PES Proc. Dallas Transmission and Distribution Conf. Sept. 22-27, 1991, p.539.

- [22] Gorman, J., Grainger, J. J. "Transformer Modelling for Distribution System Studies Part II - Addition of Models to YBus and ZBus", IEEE PES Proc. Dallas Transmission and Distribution Conf. Sept. 22-27, 1991, p.547.
- [23] Gunther, E. W., McGranaghan, M. F. "A P-C Based Simulation Program for Power System Harmonic Analysis", Proceedings of Second ICHPS, October, 1986, p. 175.
- [24] Hassan, M. M., Stanek, E. K. "Analysis Techniques in AC/DC Power Systems", IA-17, No. 5, Sept/Oct 1981, p. 473.
- [25] IEEE 84 TH 0115-6 PWR (1984) "Sine-Wave Distortions in Power Systems and the Impact on Protective Relaying" a report prepared by the Power System Relaying Committee of the IEEE Power Engineering Society, IEEE Press, New York.
- [26] IEEE Standard 519 (1981) "IEEE Guide for Harmonic Control and Reactive Compensation of Static Power Converters", IEEE Press, New York.
- [27] IEEE Standard 597 (1983) "Practices and Requirements for General Purpose Thyristor DC Drives", IEEE Press, New York.
- [28] IEEE Standard 936 (1987) "IEEE Guide for Self-Commutated Converters", IEEE Press, New York.
- [29] IEEE Power System Harmonics Working Group Report, "Bibliography of Power System Harmonics - Part I", PAS-103, No. 9, Sept., 1984, p. 2460.
- [30] IEEE Power System Harmonics Working Group Report, "Bibliography of Power System Harmonics - Part II", PAS-103, No. 9, Sept., 1984, p. 2470.
- [31] Kimbark, E. W. (1956) "Power System Stability - Volume III" Chapter 14, Damper Windings and Damping, John Wiley & Sons, New York.
- [32] Kimbark, E. W. (1971) "Direct Current Transmission - Volume 1" Wiley-Interscience, John Wiley & Sons, New York.
- [33] Kitchin, R. H. "New Method For Digital Computer Evaluation of Converter Harmonics in Power Systems Using State Variable Analysis", IEE Proc, Vol 128, Pt C, No. 4, July, 1981, p. 196.
- [34] Kron, G. "Diakoptics" 1963, MacDonald, London.

- [35] Liew, A. "Excessive Neutral Currents in Three-Phase Fluorescent Lighting Circuits", IA-25, No.4, July/August 1989, p. 776.
- [36] Mahmoud, A. A., Shultz, R. D. "A Method for Analyzing Harmonic Distribution in A.C. Power Systems", PAS-101, No. 6, June, 1982, p. 1815.
- [37] Marinos, Z. A., Pereira, J. L. R., Carneiro Jr., S. "Fast harmonic power flow calculation using parallel processing", IEE Proc Gener. Transm. Distrib., Vol 141, No. 1, Jan 1994, p. 27.
- [38] Neves, W. L., Dommel, H. W. "On Modelling Iron Core Nonlinearities", PWRS-8, No. 2, May 1993, p. 417.
- [39] Oppenheim, A. V., Schafer, R. W. (1989) "Discrete-Time Signal Processing", Chapter 3 - Sampling of Continuous Time Signals and Chapter 11 - Fourier Analysis of Signals Using the Discrete Fourier Transform, Prentice-Hall, New Jersey.
- [40] Pillegi, D. J., Chandra, N. H., Emanuel, A. E. "Prediction of Harmonic Voltages in Distribution Systems", PAS-100, No. 3, Mar., 1981, p. 1307.
- [41] Prusty, S., Rao, M. V. S. "New Method for Predetermination of True Saturation Characteristics of Transformers and Nonlinear Reactors" IEE Proc, Vol 127, Pt C, No. 2, March, 1980, p. 106.
- [42] Rashid, M. H., Maswood, A. I. "Analysis of Three-Phase AC-DC Converters Under Unbalanced Supply Conditions", IA-24, No. 3, May/June 1988, p. 449.
- [43] Rashid, M. H., Maswood, A. I. "A Novel Method of Harmonic Assessment Generated by Three-Phase AC-DC Converters Under Unbalanced Supply Conditions", IA-24, No. 4, July/August 1988, p. 590.
- [44] Rice, D. E. "Adjustable Speed Drive and Power Rectifier Harmonics - Their Effect on Power Systems Components", IA-22, No. 1, Jan/Feb, 1986, p. 161.
- [45] Rice, D. E. "A Detailed Analysis of Six-Pulse Converter Harmonic Currents", IA-30, No. 2, Mar/Apr 1994, p. 294.
- [46] Semlyen, A., Acha, A., Arrillaga, J. "Harmonic Norton Equivalent for the Magnetising Branch of a Transformer", IEE Proc, Vol 134, Pt C, No. 2, March, 1987, p.162.

- [47] Semlyen, A., Eggleston, J. F., Arrillaga, J. "Admittance Matrix Model of a Synchronous Machine for Harmonic Analysis", PWRs-2, No. 4, November 1987, p. 333.
- [48] Sharma, V. K., Fleming, R. J. "Harmonic Analysis of Power Transmission Network in the Frequency Domain", Proceedings of Second ICHPS, October, 1986, p. 148.
- [49] Shipp, D. "Harmonic Analysis and Suppression for Electrical Systems Supplying Static Power Converters and Other Nonlinear Loads" IA-15, No. 5, Sept/Oct, 1979, p. 453.
- [50] Soliman, S. S., Srinath, M. D., (1990) "Continuous and Discrete Signals and Systems", Chapter 3 - Fourier Series, Prentice Hall, New Jersey.
- [51] Stagg, G. W., El-Abiad, A. H. (1968) "Computer Methods In Power System Analysis", McGraw-Hill, London.
- [52] Steeper, D. E., Stratford, R. P. "Reactive Compensation and Harmonic Suppression for Industrial Power Systems Using Thyristor Converters", IA-12, No. 3, May/June, 1976, p. 232.
- [53] Stevenson, W. D. (1962) "Elements of Power System Analysis - Second Edition", Chapter 4 - "Resistance And Skin Effect", McGraw-Hill, New York.
- [54] Stevenson, W. D., Grainger, J. J. (1994) "Power System Analysis", Chapter 7 - "The Admittance Model and Network Calculations", McGraw-Hill, New York.
- [55] Stratford, R. P. "Harmonic Pollution on Power Systems - A Change in Philosophy", IA-16, No. 5, Sept/Oct, 1980, p. 617.
- [56] Stratford, R. P. "Analysis of Harmonic Current in Systems with Static Power Converters" IA-17, No. 1, Jan/Feb, 1981, p. 71.
- [57] Szabados, B. "On the Interaction Between Power System Configuration and Industrial Rectifier Harmonic Interference: A Practical Case Study", PAS-101, No. 8, August, 1982, p. 2762.
- [58] Tamby, J. P., John, V. I. "Q'Harm - A Harmonic Program For Small Power Systems" PWRs-3, No. 3, Aug 1988, p. 949.
- [59] TransAlta Utilities Corporation "1991 - 09 - 30 Standard - Harmonic Specification For Harmonic Producing Customers Connected To The TransAlta Utilities Corporation System".

- [60] Vivani, G. L., Li, L. "A Transformer Model for Investigating the Effect of Harmonics", Proceedings of Third ICHPS, September, 1987, p. 271.
- [61] Wagner, C. F., Evans, R. D. "Symmetrical Components", Chapter XVII - "Induction Motors" and Chapter XVIII - "Unsymmetrical Systems and Phase Balancers", McGraw-Hill, New York, 1933.
- [62] Xia, D., Heydt, G. T. "Harmonic Power Flow Studies Part I - Formulation and Solution", PAS-101, No. 6, June 1982, p. 1257.
- [63] Xia, D., Heydt, G. T. "Harmonic Power Flow Studies Part II - Implementation and Practical Application", PAS-101, No. 6, June 1982, p. 1266.
- [64] Xia, D., Shen, Z., Zhu, Z. "Unified Fundamental Frequency and Characteristic Harmonic Load Flow Solution in AC/DC Power Systems" Proceedings of Third ICHPS, September, 1987, p. 15.
- [65] Xia, D., Shen, Z., Liao, Q. "Solution of Non-Characteristic Harmonics Caused by Multiple Factors in HVDC Transmission System", Proceedings of Third ICHPS, September, 1987, p. 222.
- [66] Xu, W., Marti, J. R., Dommel, H. W. "A Multiphase Harmonic Load Flow Solution Technique", PWRS-6, No. 1, Feb., 1991, p.174.
- [67] Xu, W., Marti, J. R., Dommel, H. W. "Harmonic Analysis of Systems With Static Compensators", PWRS-6, No. 1, Feb., 1991, p.183.
- [68] Xu, W., Marti, J. R., Dommel, H. W. "A Synchronous Machine Model For Three Phase Harmonic Analysis and EMPT Initialization", PWRS-6, No. 4, Nov., 1991, p.1530.
- [69] Yacamini, R., Oliveira, J. C. "Harmonics Produced by Direct Current in Converter Transformers", IEE Proc, Vol 125, No. 9, Sept 1978, p. 873.
- [70] Yacamini, R., Oliveira, J. C. "Core Saturation Transients Caused by Converter Firing Unbalance", IEE Proc, Vol 126, No. 3, March 1979, p. 233.
- [71] Yacamini, R., Oliveira, J. C. "Harmonics in Multiple Converter Systems: A Generalized Approach", IEE Proc, Vol 127, Pt B, No. 2, March, 1980, p. 96.
- [72] Yacamini, R., Oliveira, J. C. "Comprehensive Calculation of Converter Harmonics With System Impedance and Control Representation", IEE Proc, Vol 133, Pt B, No. 2, March, 1986, p. 95.

- [73] Yan, Y. H., Chen, C. S., Moo, C. S., Hsu, C. T. "Harmonic Analysis For Industrial Customers", IA-3-, No. 2, Mar/Apr, 1994, p. 462.